Coordinated directional outgrowth and pattern formation by integration of Wnt5a and Fgf signaling in planar cell polarity

Bo Gao[1,3 *], Rieko Ajima[4,Δ], Wei Yang[1], Chunyu Li[3,5], Hai Song[3,#], Matthew J. Anderson[4], Robert R. Liu[3], Mark B. Lewandoski[4], Terry P. Yamaguchi[4], Yingzi Yang[2,3 *]

1. School of Biomedical Sciences, Li Ka Shing Faculty of Medicine, The University of Hong Kong, Pokfulam, Hong Kong, China

2. Department of Developmental Biology, Harvard School of Dental Medicine, 188 Longwood Ave., Boston, MA 02115, USA

3. Developmental Genetics Section, Genetic Disease Research Branch, National Human Genome Research Institute, NIH, Bethesda, MD 20892, USA

4. Cancer and Developmental Biology Laboratory, Center for Cancer Research, National Cancer Institute-Frederick, NIH, Frederick, MD 21702, USA

5. China-Japan Union Hospital of Jilin University, Changchun, Jilin 130033, China

***Corresponding author**

Yingzi Yang
Department of Developmental Biology
Harvard School of Dental Medicine
188 Longwood Ave, Boston, MA 02115
Tel: (617)432-8304
Fax: (617)432-3246
Email: yingzi_yang@hsdm.harvard.edu

Bo Gao
School of Biomedical Sciences
Li Ka Shing Faculty of Medicine
The University of Hong Kong
21 Sassoon Road, Pokfulam, Hong Kong, China
Tel: +852 3917-6809
Fax: +852 2855-1254
Email: gaobo@hku.hk

∆ Current address:
National Institute of Genetics,
1111 Yata, Mishima,
Shizuoka 411-8540, JAPAN

Current address:
Life Sciences Institute
Zhejiang University
866 Yuhangtang Road
Hangzhou, Zhejiang Province
P.R.China 310058

Keywords: Fgf; Wnt; Vangl2; Planar cell polarity; PCP; morphogenesis.

Summary Statement: During limb morphogenesis, Wnt5a plays both instructive and permissive roles in regulating planar cell polarity. While Wnt5a itself can orient PCP, Wnt5a signaling also allows AER-derived Fgfs to orient PCP.

Abstract

Embryonic morphogenesis of a complex organism requires proper regulation of patterning and directional growth. The Planar Cell Polarity (PCP) signaling is emerging as a critical evolutionarily conserved mechanism whereby directional information is conveyed. PCP is thought to be established by global cues, and recent studies have revealed an instructive role of Wnt signaling gradient in epithelia tissues of both invertebrates and vertebrates. However, it remains unclear whether Wnt/PCP signaling is coordinately regulated with embryonic patterning during morphogenesis. Here in the mammalian developing limbs, we find that the AER-derived Fgfs required for limb patterning regulates PCP along the proximal-distal axis in a Wnt5a-dependent manner. We demonstrate with genetic evidence that Wnt5a gradient acts as a global cue that is instructive in establishing PCP in the limb mesenchyme, while Wnt5a also plays a permissive role to allow Fgf signaling to orient PCP. Our results indicate that limb morphogenesis is critically regulated by coordination of directional growth and patterning through integrating Wnt5a and Fgf signaling in PCP regulation.

Introduction

Planar Cell Polarity (PCP), which originally refers to the coordinated alignment of epithelial cells within a plane perpendicular to their apical-basal axis, is an essential mechanism underlying coordinately polarized cellular and tissue behaviors (*Wang and Nathans, 2007, Simons and Mlodzik, 2008, Gray et al., 2011, Yang and Mlodzik, 2015*). PCP is required in many symmetry-breaking morphogenetic events in vertebrate development, for instance, left-right patterning, sensory hair cell orientation in the inner ear, skin hair orientation and neural tube closure (*Montcouquiol et al., 2003, Wang and Nathans, 2007, Devenport and Fuchs, 2008, Song et al., 2010, Hashimoto et al., 2010*). Establishment of PCP is first evidenced molecularly by uniform asymmetric distribution of core PCP proteins, which are Frizzled, Dishevelled, Van Gogh, Prickle and Flamingo identified first in *Drosophila*, throughout the polarized tissue *(Goodrich and Strutt, 2011, Adler, 2012, Singh and Mlodzik, 2012)*. Such uniform asymmetric localization is a result of both intracellular and intercellular interactions of the core PCP proteins that amplify and coordinate the initial polarizing signals provided by global cues (*Simons and Mlodzik, 2008, Vladar et al., 2009, Goodrich and Strutt, 2011, Wu and Mlodzik, 2009, Yang and Mlodzik, 2015*). Several mechanisms have been proposed to regulate PCP establishment by global cues, including cell adhesion gradients, morphogenetic forces and Wnt signaling gradients (*Lawrence et al., 1996, Casal et al., 2002, Lawrence et al., 2007, Aigouy et al., 2010, Matis and Axelrod, 2013, Wu et al., 2013, Chu and Sokol, 2016, Minegishi et al., 2017, Humphries and Mlodzik, 2017*). Secreted Wnt molecules have been shown to regulate PCP by binding to Wnt receptors, Frizzled (*Adler et al., 1997, Tomlinson et al., 1997, Lawrence et al., 2004, Dabdoub and Kelley, 2005, Wu and Mlodzik, 2008, Wu and Mlodzik, 2009, Wu et al., 2013*) and Ror2 (*Gao et al., 2011, Wang et al., 2011*). In vertebrates, Wnt ligands are required to regulate PCP (*Rauch et al., 1997, Heisenberg et al., 2000, Kilian et al., 2003, Gros et al., 2009*) and Wnt5a genetically interact with a core PCP protein, Vangl2, in multiple developmental processes (*Qian et al., 2007,*

Wang et al., 2011). Recent studies in *Drosophila* wing, *Xenopus* ectoderm and mouse node epithelium also provide evidence for an instructive role of Wnts in establishing PCP *(Wu et al., 2013, Chu and Sokol, 2016, Minegishi et al., 2017, Humphries and Mlodzik, 2017)*.

Embryonic morphogenesis is a complex process that requires proper regulation of both patterning and tissue polarity. While morphogen gradients are well known for their roles in pattern formation and Wnt5a signaling is critical for PCP regulation, it remains to be elucidated whether there is an intrinsic coordination between tissue patterning and Wnt5a-regulated PCP establishment to ensure proper morphogenesis. Limb is an ideal experimental system to tackle these questions as early limb patterning is controlled by well-defined signaling centers (*Zeller et al., 2009*) and we have shown previously that Wnt5a signaling is required for PCP establishment along the proximal-distal (P-D) limb axis in the forming chondrocytes (*Gao et al., 2011*). Wnt5a and Fgfs are both required for limb elongation along the P-D axis. *Wnt5a* is expressed in a P-D gradient in the limb mesoderm and *Wnt5a* null limb is truncated with distal digits missing (*Parr et al., 1993, Yamaguchi et al., 1999, Fisher et al., 2008*). It is well known that Fgfs (fibroblast growth factors) secreted from the apical ectoderm ridge (AER) play an instructive role in early limb patterning along the P-D axis (*Lewandoski et al., 2000, Sun et al., 2002, Mariani et al., 2008*). Before chondrogenic mesenchymal condensation occurs, Fgfs induce multiple responses such as maintaining the progenitor cell pool, regulating mesenchymal differentiation, promoting proliferation, inhibiting apoptosis, acting as chemoattractants or stimulating random cell movements in early limb bud (*Niswander et al., 1993, Li and Muneoka, 1999, Sun et al., 2002, Yu and Ornitz, 2008, Benazeraf et al., 2010, Gros et al., 2010*). When *Fgf4* and *Fgf8* are specifically removed from the AER by *Msx2-Cre*, the distal limb cartilage is much shortened, but cell death is only restricted to the proximal limb mesenchyme and cell proliferation is largely unchanged (*Sun et al., 2002, Mariani et al., 2008*), suggesting that Fgf signaling may also regulate elongation of cartilage in the distal limb independently of cell

proliferation or survival. We therefore hypothesized that AER-derived FGF signals may play a role in P-D limb elongation by interacting with Wnt5a/PCP signaling during chondrogenesis.

Vangl2 and Vangl1 are core PCP proteins that show uniform asymmetric localization in a field of planar polarized cells and they are required for limb cartilage elongation (*Song et al., 2010, Gao et al., 2011, Wang et al., 2011*). Vangl2 is randomly present on the membrane of pre-chondrogenic mesenchymal cells before E11.5, but quickly becomes asymmetrically localized along the P-D axis in newly differentiated chondrocytes at E12.5. *Wnt5a* is required for Vangl2 asymmetric localization and it dose-dependently induces Vangl2 phosphorylation (*Gao et al., 2011*). As *Wnt5a* is the only *Wnt* expressed in a gradient along the P-D axis in the limb mesoderm and required for cartilage elongation (*Parr et al., 1993, Yamaguchi et al., 1999, Fisher et al., 2008, Witte et al., 2009, Gao et al., 2011, Zhu et al., 2012*), it is likely that Wnt5a plays an instructive role in the limb mesenchyme to planar polarize the differentiating chondrocytes along the P-D axis.

In this study, we found a previously unappreciated role of AER-derived Fgf signaling in regulating Wn5a/PCP signaling during limb morphogenesis, though *Wnt5a* and *Fgf8* did not regulate each other's expression in the developing limb bud. We also showed with genetic approaches that Wnt5a signaling played both instructive and permissive roles in orienting PCP during limb morphogenesis. Our results suggest that PCP and patterning are intrinsically linked during morphogenesis, and multiple cues regulate PCP in the limb mesoderm.

Results

AER-derived *Fgf*s are required to regulate PCP, but not *Wnt5a* expression

As a first attempt to test the possible interaction between Fgf and Wn5a/PCP signaling, we determined whether *Wnt5a* and *Fgfs* regulated expression of each other. In the wild type embryo, *Fgf8* expression starts in the forming AER at E9.0-E9.5 (*Crossley and Martin, 1995, Sun et al., 2002*) and is weakened first in the regressing AER overlying the interdigital region at E12.5 after chondrogenesis starts (*Pajni-Underwood et al., 2007*) (*Fig. 1A*). In the *Wnt5a*$^{-/-}$ embryo, *Fgf8* expression was indistinguishable to that in the wild type control until E12.5 (*Fig. 1A*) (*Yamaguchi et al., 1999*), at which time *Wnt5a*$^{-/-}$ limb phenotype is already apparent (*Fig. 1A*). *Fgf8* expression was weakened after E12.5 and then completely disappeared at E13.5 when distal chondrogenesis failed in the *Wnt5a*$^{-/-}$ embryos (*Yamaguchi et al., 1999, Topol et al., 2003*) (*Fig. 1A*). But in the wild type embryo at E13.5, *Fgf8* expression was still detected in the AER overlying the elongating digit (*Fig. 1A*). We therefore concluded that *Wnt5a* does not directly regulate *Fgf8* expression. Earlier cessation of *Fgf8* expression in the *Wnt5a*$^{-/-}$ embryos is likely a result of loss of distal chondrogenesis, not a cause. Loss of distal chondrogenesis in the *Wnt5a*$^{-/-}$ limb bud likely disrupted the feedback between the phalanx-forming region and *Fgf8* expressed in the AER. Moreover, as loss of *Fgf8* expression in the *Wnt5a*$^{-/-}$ limb bud occurred after the normal PCP establishment time E12.5 (*Gao et al., 2011*), it is unlikely that loss of PCP is solely due to precocious weakening or loss of *Fgf8* expression in the AER. We next determined whether *Fgfs* expressed from the AER regulated *Wnt5a* expression using the *Msx2-Cre;Fgf4*$^{c/-}$*;Fgf8*$^{c/-}$ embryo (*Fig. S1A*). We found that removal of *Fgf4* and *Fgf8* from the AER in these mutant embryo did not change *Wnt5a* expression pattern, though the limb bud was much smaller, indicating that *Fgf4/8* does not regulate *Wnt5a* expression either.

As cell death in *Msx2-Cre;Fgf4$^{c/-}$;Fgf8$^{c/-}$* embryo is only restricted to the proximal limb mesenchyme and cell proliferation is largely unchanged in both early and late limb bud (*Sun et al., 2002, Mariani et al., 2008*) *(Fig. S1B)*, we reasoned that besides regulating progenitor cell pool (*Sun et al., 2002*), AER-Fgfs may also regulate limb elongation through PCP without affecting *Wnt5a* expression. Loss or reduced PCP signaling in mouse embryos has been found to cause shortened limb and digits in *Vangl1$^{-/-}$;Vangl2$^{-/-}$* (*Fig. S1C*) (*Song et al., 2010*) or *Prickle1$^{-/-}$* embryos (*Yang et al., 2013)*. To test whether Fgfs regulate PCP in the limb mesenchyme, we first examined Vangl2 localization, a functional PCP readout (*Wang and Nathans, 2007, Gray et al., 2011, Yang and Mlodzik, 2015*), in the newly formed distal digit cartilage where its asymmetric localization is most pronounced (*Gao et al., 2011*). Two features of Vangl2 localization were measured: percentage of cells showing asymmetric Vangl2 and orientation angles of Vangl2 proteins in these cells (See details in Materials and Methods). Changes in one or both of these features alter PCP. We found that the number of cells with discernable asymmetric Vangl2 was significantly reduced in the digit of the *Msx2-Cre;Fgf4$^{c/-}$;Fgf8$^{c/-}$* embryos compared to that of the littermate controls (*Fig. 1B,C*), but there was no statistically significant change of Vangl2 orientation angles in the *Msx2-Cre;Fgf4$^{c/-}$;Fgf8$^{c/-}$* mutant (*Fig. 1D*). As PCP signaling induces polarized cellular responses including chondrocyte polarity and arrangement (*Li and Dudley, 2009, Wallingford, 2012, Yang and Mlodzik, 2015, Li et al., 2017*), we then examined cell shapes and the alignment of distal chondrocytes. The results were shown as ratio of length to width (LWR) and orientation angles, respectively (See details in Materials and Methods). Indeed, we found that loss of *Fgf4* and *8* from the AER altered the cell shape in the limb mesenchyme. In control embryos, distal chondrocytes were elongated with an average LWR of 2 *(Fig. S2A)*. Control chondrocytes were oriented mostly along the x axis (-20° to +20°) *(Fig. S2B)*. In the mutant, chondrocytes were more round with reduced LWR. The average LWR was close to 1.5. The orientation angles were also increased *(Fig. S2)*. Therefore, a reduction in the proportion of chondrocytes with appropriately biased Vangl2 altered shape and orientation of chondrocytes,

suggesting that Fgf signaling may be required for proper PCP signaling in distal limb chondrocytes. Weakened PCP signaling due to absence of *Fgf4/8* may lead to weakened intercellular interaction between PCP components such as Vangl2 and Fzd in neighboring cells, which is required to strengthen uniform cell orientation (*Yang and Mlodzik, 2015*). The shortened digits resulting from loss of AER-Fgf signals may be a combined consequence of reduced progenitor cell pool and directional outgrowth regulated by PCP (*Sun et al., 2002, Gao and Yang, 2013*).

Fgf signaling plays an instructive role in PCP

To directly test whether Fgfs play a permissive or an instructive role in regulating PCP in the distal limb, we altered the direction of Fgf signaling gradient in the distal limb. Beads that were soaked in either PBS or Fgf8 protein were inserted into the interdigital mesenchyme at E11.5 when digital condensations were forming and Vangl2 asymmetric localization had not been established yet. We cultured the limb buds with bead implantation for two days under an optimized condition in a rolling tube that allows good digit morphogenesis and proper PCP establishment in the wild type control limb (*Fig. 2A and Fig. S3*). The cultured limbs implanted with PBS beads showed normal expression of *Sox9,* a chondrocyte/chondrogenic progenitor marker, *Col2a1*, a chondrocyte marker, and *Msx1* that marks distal and interdigital limb mesenchyme (*Fig. S3B*). These data indicate that the *ex utero* limb culturing system supports normal limb growth and morphogenesis for least 2 days. In contrast to PBS beads, Fgf8 beads inhibited overall limb chondrogenesis, a known effect of Fgf signaling (*Moftah et al., 2002*), and more interestingly, it also caused bending of nearby digits towards the beads (*Fig. 2A and Fig. S3A, B*). It is unlikely that such bending is due to distorted digit outgrowth as the apoptosis and proliferation patterns in distal limb induced by PBS beads and Fgf8 beads were similar (*Fig. S3C*). Furthermore, we found that Fgf8 beads did not bend the digit by inducing *Wnt5a* expression around the bead (*Fig. S4A, B*). As control, we confirmed that Fgf8 beads did

strongly induce expression of *Msx1* and *Sprouty4*, two transcriptional targets of Fgf signaling (*Furthauer et al., 2001*) (*Fig. S3B, S4A*).

To determine whether the digit bending effects of Fgf8 beads are caused by altered PCP, we first examined and quantified Vangl2 localization in the chondrocytes around the beads (*Fig. 2A-C*). First, the percentage of cells with discernable asymmetric Vangl2 were comparable in PBS and Fgf8 beads implanted limbs (*Fig. 2B*). While most of the cells around the PBS bead exhibited a Vangl2 localization pattern along the y axis (orientation angle -45° to +45° with reference to the x axis), not towards the bead, the number of cells with reoriented Vangl2 localization towards the Fgf8 bead was significantly increased (orientation angle <-45° or >45° with reference to the x axis) (*Fig. 2A, C*). In a control experiment, Shh-soaked beads were similarly inserted to the interdigital region, which caused a significant change in digit growth, but PCP was not altered. Most of cells lateral to the Shh beads were still oriented along the original P-D axis (*Fig. S4C*), indicating that growth distortion is not sufficient to cause the observed Vangl2 reorientation. Importantly, if Fgf8 caused digit bending independent of PCP, the direction of Vangl2 orientation is unlikely to be changed (explained in *Fig. S5)*. Interestingly, we observed higher Vangl2 levels and more clearly reoriented Vangl2 localization in cells slightly away from (not adjacent to) the Fgf8 bead (*Fig. 2A*), probably due to Fgf8-mediated inhibition of chondrogenesis in adjacent cells. Vangl2 asymmetric localization only occurs in chondrocytes with high *Sox9* expression (*Gao et al., 2011*). At cellular level, we found that while Fgf8 beads did not change the shape of the cells (*Fig. S6A*), cell orientation was altered significantly (*Fig. S6B*). More cells around the Fgf8 beads were oriented along y axis (<-45° or >45° with reference to the x axis) instead of x axis, indicating that altering direction of Fgf signaling gradient reoriented chondrocytes without significantly changing cell shape. These results indicate that Fgf8 can act as an instructive cue to regulate PCP when limb mesenchymal cells are differentiating into chondrocytes. If the Fgf8 beads were implanted at later stage

after PCP establishment, no digit bending was observed (*Montero et al., 2001, Hernandez-Martinez et al., 2009*).

We then tested whether the role of Fgf in regulating PCP requires Wnt5a signaling by implanting Fgf8 beads in the distal limb bud of the *Wnt5a*$^{-/-}$ embryos. Although the implanted Fgf8 beads induced *Sprouty4* expression (*Fig. S4A*), they failed to rescue limb outgrowth or restore Vangl2 asymmetric localization in Sox9^{+} chondrogenic cells (*Fig. 2D*). These results indicate that Fgf8 cannot exert its instructive role on PCP in the absence of Wnt5a signaling.

We then investigated the molecular mechanism whereby PCP is regulated by Fgf signaling. As we have shown previously that Wnt5a induces Vangl2 phosphorylation and we and others found that Vangl2 activities depend on its levels of phosphorylation in multiple organisms, including *Drosophila*, Zebrafish, *Xenopus* and mouse (*Gao et al., 2011, Ossipova et al., 2015, Kelly et al., 2016, Yang et al., 2017*), we tested whether Fgf could also regulate Vangl2 phosphorylation in limb bud mesenchymal cells. We isolated mouse E10.5~E11.5 limb bud mesenchymal cells and treated them with recombinant Fgf8 and/or Wnt5a proteins. While Wnt5a protein induced Vangl2 phosphorylation as shown by gel mobility shift, Fgf8 protein by itself did not induce obvious gel mobility shift of Vangl2 (*Fig. S7A*). When applied simultaneously, Fgf8 dose-dependently enhanced Vangl2 phosphorylation induced by a lower Wnt5a dosage (*Fig. S7A, B*). In addition, at higher doses, Fgf8 also appeared to upregulate Vangl2 protein levels (*Fig. S7B*). These *in vitro* data are consistent with the notion that Fgf's role in PCP is instructive by promoting Wnt5a-induced Vangl2 phosphorylation and/or protein levels, and in this regard, Wnt5a's function can be permissive to allow Fgf signaling to regulate PCP and an instructive Wnt5a gradient may not be absolutely required for this purpose.

PCP is partially restored by non-graded Wnt5a expression in the limb

We then asked whether Wnt5a signaling is indeed instructive in limb PCP as shown in different model systems (*Wu et al., 2013, Chu and Sokol, 2016, Minegishi et al., 2017*) or only permissive to allow other cues, such as Fgf signaling, to orient PCP. Earlier studies also suggested a permissive role of Wnt5a (*Heisenberg et al., 2000, Witze et al., 2008*). To answer these questions, we replaced the endogenous graded *Wnt5a* expression with non-graded *Wnt5a* expression by employing an inducible *Wnt5a* expression approach (*Fig. 3A, B*). As the instructive model indicates that graded *Wnt5a* expression is required for Wnt5a's function in the limb, such replacement should not rescue the PCP defects of *Wnt5a* null mutant at all. Conversely, if Wnt5a signaling is solely permissive for PCP, the proposed strategy should completely rescue the PCP defects of the *Wnt5a* mutant. We used the *Prx1-Cre* and *Sox2-Cre* mouse lines to activate even *Wnt5a* expression in the early limb bud mesenchymal cells (*Fig. 3C*). *Prx1-Cre* is expressed at E9.5 and *Sox2-Cre* is expressed in all epiblast cells at E6.5 (*Logan et al., 2002, Hayashi et al., 2002*). *Wnt5a* expressions in the *Prx1-Cre;Rosa*$^{5a/+}$*;Wnt5a*$^{-/-}$ and *Sox2-Cre;Rosa*$^{5a/+}$*;Wnt5a*$^{-/-}$ embryos were driven by the *Rosa26* promoter that is not graded in the developing limbs (*Soriano, 1999*). We found that graded *Wnt5a* expression pattern along the P-D axis of the limb bud was disrupted in the *Prx1-Cre;Rosa*$^{5a/+}$*;Wnt5a*$^{-/-}$ and *Sox2-Cre;Rosa*$^{5a/+}$*; Wnt5a*$^{-/-}$ embryos at E11.5, a stage preceding asymmetric Vangl2 localization (*Fig. 3C*) (*Gao et al., 2011*). However, *Wnt5a* expression in the *Prx1-Cre; Rosa*$^{5a/+}$*;Wnt5a*$^{-/-}$ was lower compared to those in the *Wnt5a*$^{+/-}$ and the *Sox2-Cre;Rosa*$^{5a/+}$*;Wnt5a*$^{-/-}$ embryos (*Fig. 3C*). This was confirmed by quantitative PCR (qPCR) of *Wnt5a* expression in the limb buds (*Fig. 3D*). To increase *Wnt5a* expression driven by *Prx1-Cre*, we induced *Wnt5a* expression from both alleles of the *Rosa26* locus by generating *Prx1-Cre;Rosa*$^{5a/5a}$*;Wnt5a*$^{-/-}$ embryos, which had comparable *Wnt5a* expression as *Sox2-Cre;Rosa*$^{5a/+}$*;Wnt5a*$^{-/-}$ or *Wnt5a*$^{+/-}$ embryos (*Fig. 3C, D*). To further test whether this strategy resulted in non-graded Wnt5a expression and protein distribution, we examined both *Wnt5a* mRNA and Wnt5a protein levels in different regions of the limb buds along the P-D axis by

qPCR and Western Blotting (*Fig. 3E-G*). The distal-to-proximal gradients of Wnt5a were much diminished in the limb buds of both *Prx1-Cre;Rosa$^{5a/5a}$;Wnt5a$^{-/-}$* and *Sox2-Cre;Rosa$^{5a/+}$;Wnt5a$^{-/-}$* embryos (*Fig. 3E-G*). These results indicate that, by expressing *Wnt5a* from the *Rosa26* locus in the *Wnt5a$^{-/-}$* background, we have created a much flattened Wnt5a pattern along the P-D axis in the developing limb bud.

In situ hybridization and cartilage staining of late stage embryos showed that the flattened *Wnt5a* expression was able to partially rescue digit outgrowth in limbs of both *Prx1-Cre;Rosa$^{5a/5a}$;Wnt5a$^{-/-}$* and *Sox2-Cre;Rosa$^{5a/+}$;Wnt5a$^{-/-}$* embryos (*Fig. 4A, B*). In support of our previous findings that Wnt5a signaling promotes chondrogenesis (*Topol et al., 2003*), we found that ectopic *Wnt5a* expression throughout the limb bud led to rescued digit formation and even ectopic cartilage formation in the interdigital area of the limbs of the *Prx1-Cre;Rosa$^{5a/5a}$;Wnt5a$^{-/-}$* and *Sox2-Cre;Rosa$^{5a/+}$;Wnt5a$^{-/-}$* embryos (*arrows in Fig. 4A*). These results indicate that induced non-graded *Wnt5a* expression was already strong enough to allow normal and ectopic cartilage formation. As the rescued digits were still shortened than the wild type controls but better than the *Vangl1$^{-/-}$;Vangl2$^{-/-}$* embryos (*Fig. S1C*), in which PCP is completely abolished (*Song et al., 2010*), we reasoned that PCP may be also partially restored in these embryos. Indeed, while Vangl2 asymmetric localization was not detected at all in the absence of *Wnt5a*, it was partially restored in the distal digits of both *Prx1-Cre;Rosa$^{5a/5a}$;Wnt5a$^{-/-}$* and *Sox2-Cre; Rosa$^{5a/+}$; Wnt5a$^{-/-}$* embryos at E13.5 (*Fig. 4C*). Compared to the wild type control embryo, the number of cells with discernable Vangl2 asymmetric localization was reduced (*Fig. 4C, D*) and more cells with Vangl2 asymmetric localization deviated from the y axis in both mutant embryos (*Fig. 4E*). Consistent with partially restored Vangl2 asymmetry, the shape (and to less extent for orientation) of distal chondrocytes were also partially rescued in both mutant limbs compared to *Wnt5a* null limb (*Fig. S8A, B*). The partial rescue of PCP observed both morphologically and molecularly

suggests that PCP is still present to certain extent in the presence of non-graded *Wnt5a* expression. Other directional cue(s) may have been provided.

As *Fgf8* can regulate PCP (*Fig. 1, 2*) and its expression later in limb development is maintained by elongating digit cartilage in the overlying AER (*Fig. 1A*) (*Ganan et al., 1998, Pizette and Niswander, 1999*), we examined *Fgf8* expression in *Prx1-Cre;Rosa*$^{5a/5a}$*;Wnt5a*$^{-/-}$ and *Sox2-Cre;Rosa*$^{5a/+}$*;Wnt5a*$^{-/-}$ embryos. Indeed, *Fgf8* expression was restored at levels similar to that in wild type controls in the AER overlying the rescued digit cartilage (*Fig. S9A*). Therefore, it is possible that the collective effects of non-graded *Wnt5a* and graded Fgf signaling resulted in a PCP signaling gradient, though less steep than that in the wild type limb. In support of this, the ectopic cartilage formed in the interdigital region of the *Prx1-Cre;Rosa*$^{5a/5a}$*;Wnt5a*$^{-/-}$ embryos showed no Vangl2 asymmetric localization (*arrows in Fig. 4A* and *Fig. S9B*), likely due to lack of Wnt5a gradient and weak to none Fgf signaling in the proximal interdigital region. Taken together, our results suggest that distal digit elongation is regulated by integrated Wnt5a and Fgf signaling in PCP.

Altered Wnt5a gradient re-orients Vangl2 localization

As restored *Fgf8* expression is not sufficient to completely restore PCP in the presence of non-graded Wnt5a (*Fig. 3, 4*), graded *Wnt5a* expression may still play a major instructive role in directing digit outgrowth by regulating PCP. To directly test the instructive role of *Wnt5a* in limb mesenchyme, we have re-oriented the *Wnt5a* gradient in the developing limb bud using the *Shh-Cre* line (*Fig. 5A*). *Shh* is expressed in the posterior limb margin in the Zone of Polarizing Activity (ZPA) (*Todt and Fallon, 1987, Riddle et al., 1993*) and *Shh* expressing cell lineage gives rise to digit 5, digit 4 and part of posterior half of the digit 3 (*Harfe et al., 2004*) (*Fig. S10A*). Therefore, we were able to create a posterior to anterior Wnt5a gradient by inducing *Wnt5a* expression from the *Rosa26* locus using the *Shh-Cre* line in the *Wnt5a*$^{-/-}$ background (*Fig. 5A*). This new Wnt5a gradient was nearly perpendicular to the endogenous distal to proximal one,

particularly in digit 3 (*Fig. 5A*). In the limb of the *Shh-Cre;Rosa*$^{5a/+}$*;Wnt5a*$^{-/-}$ embryo, while digit 4 and digit 5 are immersed in the *Wnt5a* expressing cells, digit 3 should experience a steep posterior to anterior *Wnt5a* gradient (*Fig. S10A*). If the role of Wnt5a is instructive, this operation should lead to reorientation of the asymmetric Vangl2 localization and corresponding change of digit morphology.

We first confirmed by *in situ* hybridization that in the absence of endogenous *Wnt5a*, *Shh-Cre* was able to induce a gradient of *Wnt5a* expression from the *Rosa26* locus along the A-P axis of the limb bud at E11.5 (*Fig. 5B*). At E12.5, elongation of digit 4 and 5 in the *Shh-Cre;Rosa*$^{5a/+}$*;Wnt5a*$^{-/-}$ embryo was partially rescued, and digit 4 was oriented towards the posterior limb margin (*Fig. 5C*). Digit 3, which received much less Wnt5a signal, also grew out towards the posterior side, albeit to a much less extent (*Fig. 5C*). At E13.5, while digit 4 outgrowth was still tilted towards the posterior limb, outgrowth of digit 3 stopped (*Fig. S10B*). This is likely due to the low dose of Wnt5a it received, which was not sufficient to support continuous chondrogenesis. Lethality of *Shh-Cre;Rosa*$^{5a/+}$*; Wnt5a*$^{+/-}$ mouse precludes the production of *Shh-Cre;Rosa*$^{5a/5a}$*;Wnt5a*$^{-/-}$ embryos to increase the dose. Interestingly, when the endogenous *Wnt5a* expression with a P-D gradient was progressively reduced while artificial *Wnt5a* gradient was induced along the A-P axis in the *Shh-Cre;Rosa*$^{5a/+}$*;Wnt5a*$^{+/+}$, *Shh-Cre;Rosa*$^{5a/+}$*; Wnt5a*$^{+/-}$ and *Shh-Cre;Rosa*$^{5a/+}$*;Wnt5a*$^{-/-}$ mouse embryo, digit 4 bent progressively more to the posterior limb margin (*Fig. S10B*). Thus, reoriented *Wnt5a* gradient changed the orientation of digit outgrowth.

To test whether the observed reorientation of digit outgrowth is associated with altered PCP, we examined Vangl2 localization in the *Shh-Cre;Rosa*$^{5a/+}$*;Wnt5a*$^{-/-}$ limb (*Fig. 6*). Because of the radial outgrowth of the digits, only the x and y axes of digit 3 overlap with the A-P and P-D axes of the whole limb. While the number of cells with discernable Vangl2 asymmetric localization was comparable in different regions of partially rescued digit 4 and digit 5 (*Fig. 6A, E*), fewer cells displayed asymmetric Vangl2 in digit 3 likely due to the limited Wnt5a dosage

(*Fig. 6E*). In digit 3 that experienced the steepest *Wnt5a* gradient (*Fig. 6A, B*), Vangl2 asymmetric localization had been reoriented along the A-P axis (orientation angle <-45° or >45° with reference to the x axis or A-P axis) in almost all cells with detectable Vangl2 asymmetric localization (*Fig. 6B, F*). Vangl2 localization in digit 4 and 5 that were completely immersed in *Wnt5a* expressing cells was more complex. In the proximal regions of digit 4 and 5 (*Fig. 6A, C*), Vangl2 localization in a few cells was reoriented along the x axis in lieu of y axis (orientation angle -45° to +45° with reference to the x axis) (*Fig. 6C, F*). But in the distal regions of digit 4 and 5 (*Fig. 6A, D*), Vangl2 asymmetric localization was largely oriented along the y axis (*Fig. 6D, F*). Consistent with Vangl2 localization pattern, while there is no significant change of chondrocyte shape (*Fig. S11A*), a large number of cells in digit 3 (Region I) had reoriented their major axes along the y axis (*Fig. S11B*). In addition, more reorientation was also observed in proximal regions of digit 4 and 5 (Regions II and III), compared to distal regions (Regions IV and V) (*Fig. S11B*). These results demonstrate that altered Wnt5a gradient is able to reorient PCP in forming chondrocytes in digit 3 (Region I), less well in proximal regions of digit 4 and 5 (Regions II and III) and failed to do so in distal regions of digit 4 and 5 (Regions IV and V) (*Fig. 6A*). It is intriguing that, in distal regions of digit 4 and 5, Vangl2 still orient towards the distal end, suggesting another cue was provided. Indeed, *Fgf8* expression in the AER was restored in the partially rescued digit 4 and 5 of *Shh-Cre;Rosa*$^{5a/+}$*;Wnt5a*$^{-/-}$ embryos (*Fig. 7A*). Thus, signal(s) from the distal limb, likely Fgf signaling, may compete with the posterior limb-derived Wnt5a signaling to orient chondrocytes and Vangl2 localization, resulting in a more complicated limb phenotype and Vangl2 localization pattern (*Fig. 6A*).

Inhibition of Fgf signaling enhanced reorientation response to altered Wnt5a gradient

To further test whether the distal Fgf signaling and posterior-limb derived Wnt5a signaling compete in orienting chondrocytes and Vangl2 asymmetric localization in distal regions of the digit 4 and 5 in the *Shh-Cre;Rosa*$^{5a/+}$*;Wnt5a*$^{-/-}$ limb (*Fig. 6A*), we inhibited Fgf signaling by treating the E11.5 limbs with an Fgf receptor inhibitor SU5402 *(Mohammadi et al., 1997*). In *ex utero* culture, *Shh-Cre; Rosa*$^{5a/+}$*;Wnt5a*$^{-/-}$ embryos only formed one posterior digit instead of two (*Fig. 7B*). In this digit, about 20%-30% of the distal chondrocytes showed asymmetric Vangl2 (*Fig. 7C*) and most of them were oriented towards the distal limb margin (orientation angle -45° to +45° with reference to the x axis) (*Fig. 7B, D*). Remarkably, in the SU5402-treated limb of the *Shh-Cre;Rosa*$^{5a/+}$*;Wnt5a*$^{-/-}$ embryos, there was a slight reduction of cells with asymmetric Vangl2 (*Fig. 7C*). However, among the cells with asymmetric Vangl2, the percentage with reorientation by the posterior Wnt5a signaling (orientation angle <-45° or >+45° with reference to the x axis) was increased (*Fig. 7B, D*). Interestingly, comparison of Figure 7D with Figure 6F showed that inhibition of Fgf signaling indeed converted the orientation of Vangl2 localization from that in the distal digit (*IV and V in Fig. 6F*), which received strong distal Fgf signaling, to that in the proximal digit (*II and III in Fig. 6F*), which received weak Fgf signaling. These results indicate that inhibition of distal Fgf signaling indeed promoted digit 4/5 distal chondrocyte reorientation, which was hindered by *Fgf*s expressed in the overlying AER in the *Shh-Cre;Rosa*$^{5a/+}$*;Wnt5a*$^{-/-}$ embryos (*Fig. 7E*). Consistent with the Vangl2 reorientation, while there was only slight change in cell shape, cell orientation was altered significantly by SU5402 treatment (*Fig. S12A, B*). As a result, digit outgrowth was compromised but the width of the digit was increased (*Fig. 7B* and *Fig. S12D*).

Taken together, our data show that Wnt5a does play an instructive role in orienting PCP in limb morphogenesis. Because we also found that Fgf signaling could provide an additional instructive cue in the presence of Wnt5a (either graded or non-graded), Wnt5a signaling is also permissive to allow Fgf signaling to orient PCP.

Discussion

How directional information is provided and interpreted and how it is coordinated with patterning events to guide morphogenesis are fundamentally important in the development of complex multicellular organisms. Here we show that Wnt5a plays both instructive and permissive roles in regulating PCP and limb elongation. Our finding that the direction of Wnt5a gradient determines the orientation of PCP in mouse limb mesenchymal cells is consistent with previous findings that Wnt signaling gradient provides an instructive cue in controlling PCP in epithelial tissues of *Drosophila*, *Xenopus* and mouse (*Wu et al., 2013, Chu and Sokol, 2016, Minegishi et al., 2017, Humphries and Mlodzik, 2017*). Our data also show that additional instructive cue(s) such Fgf can orient PCP during limb morphogenesis in a Wnt5a-dependent manner. Wnt5a and Fgf signaling integrate together to establish PCP in the early limb chondrocytes (*Fig. 7F*). As Fgf signaling is required for early limb P-D patterning (*Lewandoski et al., 2000, Sun et al., 2002, Mariani et al., 2008*), our results further suggest that PCP may be intrinsically linked with patterning events during morphogenesis. Fgf signaling can regulate both pattern formation and PCP, whereas PCP can be regulated by multiple instructive cues.

Among all other morphogen gradients in the developing limb, only Fgf signaling has been shown to play an instructive role in P-D patterning possibly through regulating cell proliferation/apoptosis, acting as chemoattractants or stimulating random cell movements (*Niswander et al., 1993, Li and Muneoka, 1999, Sun et al., 2002, Benazeraf et al., 2010, Gros et al., 2010*). Wnt5a and Fgf8 exert

coordinated but distinct effects in mesenchymal cells in the early limb bud before chondrogenesis, with Wnt5a acting as chemoattractant but Fgf8 stimulating random cell movements (*Gros et al., 2010*). It has been shown that directional cell behaviors, such as directional mesenchymal cell movement and cartilage P-D elongation, rather than graded proliferation, drive preferential elongation of the limb along the P–D axis (*Boehm et al., 2010, Hopyan et al., 2011, Gao and Yang, 2013*). However, limb P-D elongation occurs mostly at later stages of development via cartilage P-D elongation and chondrocytes do not move. Our genetic and explant culture experiments demonstrated that loss of *Fgf4* and *Fgf8* led to PCP defects in limb chondrocytes and Fgf8 proteins were able to re-orient PCP in the presence of Wnt5a. In this regard, Wnt5a signal is required to provide a permissive condition for Fgf signaling to orient PCP. Although the exact mechanism remains to be further investigated, one possibility suggested by our data is that Fgf regulates PCP by promoting Wnt5a-induced Vangl2 phosphorylation and/or protein stability to steepen Wnt/PCP signaling gradient. When Wnt-induced PCP gradient is flattened or its direction is altered, the remaining Fgf signaling gradient established partial PCP. It is also possible that Wnt5a is only required to promote chondrogenesis, then Fgf8 orients chondrocytes through some other mechanisms. Interestingly, the Fgf-Erk1/2 pathway has been shown to regulate mitotic spindle orientation in the lung epithelium (*Tang et al., 2011*), and a possible downstream effect of PCP is to control oriented cell division in many contexts (*Saburi et al., 2008, Baena-Lopez et al., 2005, Gong et al., 2004, Ciruna et al., 2006*). It is unclear whether Fgf controls oriented cell division or cell rearrangement in chondrocytes. But it has been shown that PCP can regulate chondrocyte orientation through daughter cell spreading or pivoting-like process after oriented cell division. (*Li and Dudley, 2009, Romereim et al., 2014, Li et al., 2017*).

Our results indicated that Wnt/PCP signaling can receive inputs from other signaling pathways such as those mediated by Fgfs that regulate patterning, which forms a molecular base for coordination of different developmental events that occur at the same time of morphogenesis. Notably, in addition to its limb AER expression, *Fgf8* is also expressed in tail bud and frontonasal process where *Wnt5a* is expressed (*Heikinheimo et al., 1994, Yamaguchi et al., 1999, Dubrulle and Pourquie, 2004*). As PCP mutant mice exhibited severe directional outgrowth defects in those places (*Song et al., 2010, Gao, 2012*), the mechanism of coordinating patterning and PCP by Wnt5a and Fgf signaling may be fundamentally important in morphogenesis of other tissues and organs. In the tissue or organ bigger in size than the limb bud, signaling gradients across a longer distance is required to orient PCP in a larger group of cells. In the tail bud, both *Wnt5a* and *Fgf8* are expressed in a gradient across a larger spatial scale (*Yamaguchi et al., 1999, Dubrulle and Pourquie, 2004*). Steeper gradient may also provide more robust directional cue by making a bigger signaling difference within the same spatial scale. PCP regulation by Wnt5a signaling gradient could be enhanced in responding cells by Fgf signaling or modified by other signaling molecules. The effects of the other signaling cues become more apparent when Wnt5a signaling gradient is diminished or altered in its direction. Indeed, we uncovered the effects of Fgf signaling in PCP when Wnt5a gradient was flattened in this study. This may explain why permissive *Wnt11* can rescue zebrafish *slb* mutant (*Heisenberg et al., 2000)* and are in line with a previous report that in cultured melanoma cells, Wnt5a also acts permissively to allow directional migration in response to other positional cues such as a CXCL12 chemokine gradient (*Witze et al., 2008*). In addition, Wnt antagonists Sfrp (secreted frizzled-related protein) family members, Sfrp1, 2 and 5 can regulate PCP during early trunk formation (*Satoh et al., 2008*). A recent study also provided genetic evidence that opposing gradients of Wnt5a/b and their Sfrp inhibitors polarize node cells along the anterior-posterior body axis (*Minegishi et al., 2017*). Interestingly, *Sfrp2, Sfrp3* and *Wif1* are expressed in the limb mesenchyme (*Witte et al., 2009*). It is possible that Sfrps and Wif1 also shape the Wnt

signaling gradient during limb morphogenesis. Other Wnts may contribute to limb PCP. However, as PCP is completely lost in the *Wnt5a* null mutant limb, the activities of other Wnts in regulating PCP are much weaker. In addition, as a feedback mechanism, the Wnt5a gradient may also be shaped by Wnt-binding PCP signaling components such as Frizzleds and Ror2 whose membrane availability can be regulated by Wnts (*van Amerongen, 2012*). These highlight the complexity of Wnt-regulated PCP and future studies are required to understand how global cues are formed and accurately deciphered by responding cells.

Materials and Methods

Mouse lines and breeding. *Prx1-Cre*, *Sox2-Cre* and *Shh-Cre:EGFP* mice were purchased from the Jackson Laboratories. *Wnt5a*$^{+/-}$, *Msx2-Cre*, *Fgf4*$^{c/c}$ and *Fgf8*$^{c/c}$ mouse strains have been described previously (*Yamaguchi et al., 1999, Logan et al., 2002, Hayashi et al., 2002, Harfe et al., 2004, Sun et al., 2002, Lewandoski et al., 2000*). The inducible *Wnt5a* line (*Rosa*$^{5a/+}$) was generated by knocking the mouse *Wnt5a* cDNA into the *Rosa26* locus in ES cells. A PGK-Neo cassette flanked by loxp sites was inserted before the *Wnt5a* cDNA. The details of generation of *Rosa*$^{5a/+}$ have been described previously (*Cha et al., 2014*). The study was approved by the ethics committees of the National Human Genome Research Institute, National Institutes of Health, U.S.A., and the University of Hong Kong, China.

Antibodies and proteins. Sox9 (1:150, H-90, Santa Cruz), Vangl2 (1:100, N-13, Santa Cruz), ß-catenin (1:500, #610154, BD Transduction Lab), cleaved caspase 3 (1:100, #9661, Cell signaling) and p-Histone H3 (1:500, #9701, Cell Signaling) were used for immunofluorescent staining. Wnt5a (1:100, BAF645, R&D), Vangl2 (1:200, gift of M. Montcoquiol), GAPDH (1:10000, G8795, Sigma), alpha-tubulin (1:10000, ab7291, Abcam), Erk1/2 (1:1000, #9102, Cell Signaling) and p-Erk1/2 (1:1000, #9106, Cell Signaling) were used for Western blot. Recombinant

proteins were purchased from R&D: Wnt5a (645-WN-010), FGF-8b (423-F8-025), Shh (461-SH-025).

Immunofluorescence and Confocal Microscopy. Embryos were fixed in 4% PFA for 30 min at 4ºC and then processed for cryosections. The tissue sections were permeabilized for 5 min in 0.5% Triton X-100, blocked for 1hr in 5% BSA, 0.1% Triton X-100 and incubated with primary antibodies overnight at 4ºC. Secondary antibodies coupled to Alexa Fluor 488 or 594 (Invitrogen) were diluted 1:500 and applied to the sections for 1hr at room temperature. The longitudinal axis of the target digit was defined as the vertical y axis (an example is shown in *Fig. S13A*). Confocal images were acquired by a Zeiss LSM 510 NLO Meta system (63x oil objective). Projected Z-stack images were acquired at 0.3µm intervals for ~6µm and projected by Zeiss LSM 510 software.

Quantification of Vangl2 localization pattern.

Frist, projected Z-stack images were used to manually count the number of cells with polarized Vangl2. Cells were classified into two categories: “Asymmetry” and “No asymmetry determined”. A cell with polarized Vangl2 (any orientation direction) was counted as “Asymmetry”, but a cell with no polarized Vangl2 was counted as “No asymmetry determined”. An example is illustrated in Fig. S13B. Then the orientation angle of asymmetric Vangl2 localization was measured and quantified by CellProfiler 2.1.1 (http://cellprofiler.org/). CellProfiler automatically identifies objects in terms of the custom-designed pipeline and the preset parameters (e.g., the range of the object size, the intensity threshold). The orientation of the Vangl2 staining is determined by the angle of the identified object between its major axis and the x-axis of the image (in degrees ranging from -90° to 90°). An example is illustrated in *Fig. S13C*. In mesenchymal cells, the rich extracellular matrix allows us to determine where Vangl2 localize between neighboring cells (See *Fig. S14* for examples). Notably, within the 6 µm that was scanned, only a fraction of the digit cells showed discernable Vangl2 asymmetric localization.

Quantification of chondrocytes orientation and shape. Immunofluorescent images of chondrocytes with DAPI or Sox9 (nucleus) and β-catenin (cell membrane) staining were processed by CellProfiler 2.1.1, software application used to quantitatively measure cell phenotypes. The orientation of the cell is determined by the angle of the identified cell object between its major axis and the x-axis of the image (in degrees ranging from -90° to 90°) with the y axis defined as the longitudinal axis of a particular digit. An example is illustrated in *Fig. S15*. The shape of the cell is reflected by the ratio of length to width (LWR) of the cell. The cell length (the longest dimension of the cell) was measured as Major-Axis-Length and the cell width (the shortest dimension of the cell) was measured as Minor-Axis-Length automatically by CellProfiler. Data was analyzed using GraphPad Prism 6 (two-tailed *t* test for LWR and kolmogorov smirnov test for orientation angle distribution). The orientation schematics were plotted using Origin 9 software.

Limb culturing. The E11.5 embryonic forelimbs were dissected in pre-warmed DMEM containing 10% FBS, pen/strep and 20mM HEPES and cultured in pre-warmed 1:1 mixed DMEM (10% FBS, pen/strep) and freshly prepared Rat serum on a rotator at 37ºC with 5% CO_2 for 2 days. The culturing medium was changed every 24hr. This culturing method allows digit morphogenesis comparable to *in vivo* digit development at E12.5~E13.5, a time point when PCP has been already established. Fgf receptor inhibitor (10uM, SU5402, Sigma) was directly added into the culturing medium and changed every 24hr.

Beads implantation. Beads implantation experiments were done according to the procedures described previously (Niswander et al., 1993). Heparin acrylic beads (H5263, Sigma) were washed in PBS 4-6 times and then soaked in 2~3ul 1mg/ml FGF-8b recombinant proteins (423-F8-025, R&D) for at least 1 hr at room temperature. Control beads were soaked in PBS. The beads were inserted into the interdigital mesenchyme of the distal wild type limb when digital

condensations were just visible (~E11.5) or distal limb mesenchyme distal to digit formation in the *Wnt5a*$^{-/-}$ limb bud.

Limb mesenchymal cell culturing. The E10.5~E11.5 limb buds were isolated in calcium-magnesium-free PBS buffer containing 0.1% glucose and pen/strep. The limb buds were then digested in calcium-magnesium-free PBS buffer containing 0.01% trypsin, 0.002%EDTA, 0.1% glucose and pen/strep for 20~30 minutes at 37ºC. The mesenchymal cells were completely disassociated by pipetting up and down and then they were transferred to equal volume of culture medium (10% FBS in DMEM). The cells were filtered through the Nitex filter (20μm mesh, 03-20/14 Sefar America) to eliminate fibrous materials and tissue debris and plated. The cells were confluent 24 hours later. Confluent cells were treated with recombinant proteins (Fgf8, 250ng/ml and Wnt5a 100ng/ml or 500ng/ml) for 2-hr after 6-hr serum starvation (0.2% FBS in DMEM).

Skeletal preparation. E17.5 fetuses were eviscerated, fixed overnight in 100% ethanol, and then transferred into 100% acetone, followed by staining with Alizarin Red S (bone) and Alcian Blue (cartilage). Embryos were cleared by 1% KOH and stored and photographed in 80% glycerol.

***In situ* hybridization.** Whole-mount *in situ* hybridizations of mouse embryos using digoxigenin-labeled antisense RNA were performed as described previously (*Wilkinson and Nieto, 1993*). Riboprobes used in this study have been described previously: *Sox9* (*Bi et al., 1999*), *Fgf8 (Crossley and Martin, 1995*) and *Sprouty4* (Minowada et al., 1999). The antisense riboprobe of *Wnt5a*, which doesn't detect *Wnt5a* transcripts from the *Wnt5a* null locus, was synthesized based on a 190bp PCR product using the primers 5'-GGAATATTAAGCCCGGGAGTG-3' and 5'-AGAGAGGCTGTGCACCTATGAT-3'.

Quantitative PCR. Total RNA was extracted using the Trizol reagent (Invitrogen) and reverse transcribed using the SuperScript First-Strand Synthesis-System. RT-PCR (Invitrogen) was performed according to manufacturer's instruction. Quantitative PCR using SYBR Select Master Mix (Applied Biosystems) was performed on 7500 Fast Real-Time PCR system (Applied Biosystems). Endogenous mouse *Wnt5a* was detected using the following primers: 5'-ATTGTCCCCCAAGGCTTAAC-3' and 5'- CTTCTATAACAACCTGGGCGAAG-3'; Total mouse *Wnt5a* was detected using the following primers: 5'-CCATGTCTTCCAAGTTCTTCCTA-3'and 5'-CCAGACACTCCATGACACTTACA-3'. The mouse *Sprouty4* was detected using the following primers: 5'-GCAGCGTCCCTGTGAATCC-3' and 5'- TCTGGTCAATGGGTAAGATGGT-3'. *GAPDH* mRNA level was used as internal control.

LacZ staining. Embryos were fixed in fixative (0.5% formaldehyde, 0.1% glutaraldehyde, 2mM MgCl2, 5mM EGTA, 0.02% NP-40) for 15 minutes. Cryosectioned tissues was stained with the X-gal buffer (5mM K3Fe(CN)6, 5mM K4Fe(CN)6, 2mM MgCl2, 0.01% NaDeoxycholate, 0.02% NP-40) for 2~4 hrs at 37°C and post-fixed in 4% PFA.

Acknowledgements

We thank C. Rivas and E. Escobar for their assistance in the mouse work, M. Montcoquiol (Neurocentre Magendie, France) for the rabbit Vangl2 antibodies and S.Mackem (NCI, NIH) for sharing the *Shh-Cre:EGFP* mice.

Competing interests

The authors declare no competing or financial interests.

Author contributions

Conceptualization: B.G., Y.Y.; Methodology: B.G., R.A., H.S., M.B.L., T.P.Y., Y.Y.; Formal analysis: B.G., W.Y., M.J.A.; Investigation: B.G., R.A., W.Y., C.L., M.J.A., R.R.L.; Resources: B.G., R.A., H.S., M.J.A., M.B.L., T.P.Y., Y.Y.; Writing - original draft: B.G., Y.Y.; Writing - review & editing: B.G., M.B.L., T.P.Y., Y.Y.; Supervision: B.G., M.B.L., T.P.Y., Y.Y.; Project administration: B.G., Y.Y.; Funding acquisition: B.G., M.B.L., T.P.Y., Y.Y..

Funding

The work in the Yang laboratory was supported by the intramural research program of National Human Genome Research Institute at the National Institutes of Health and NIH/NIAMS grant R01AR070877. The work in the Gao laboratory was supported by The University of Hong Kong start-up funds and Hong Kong Research Grants Council (27115317). The work in the Yamaguchi and Lewandoski laboratories was supported by the intramural research program of National Cancer Institute, Center for Cancer Research.

References

ADLER, P. N. 2012. The frizzled/stan pathway and planar cell polarity in the Drosophila wing. *Curr Top Dev Biol,* 101**,** 1-31.

ADLER, P. N., KRASNOW, R. E. & LIU, J. 1997. Tissue polarity points from cells that have higher Frizzled levels towards cells that have lower Frizzled levels. *Curr Biol,* 7**,** 940-9.

AIGOUY, B., FARHADIFAR, R., STAPLE, D. B., SAGNER, A., ROPER, J. C., JULICHER, F. & EATON, S. 2010. Cell flow reorients the axis of planar polarity in the wing epithelium of Drosophila. *Cell,* 142**,** 773-86.

BAENA-LOPEZ, L. A., BAONZA, A. & GARCIA-BELLIDO, A. 2005. The orientation of cell divisions determines the shape of Drosophila organs. *Current biology : CB,* 15**,** 1640-4.

BENAZERAF, B., FRANCOIS, P., BAKER, R. E., DENANS, N., LITTLE, C. D. & POURQUIE, O. 2010. A random cell motility gradient downstream of FGF controls elongation of an amniote embryo. *Nature,* 466**,** 248-52.

BI, W., DENG, J. M., ZHANG, Z., BEHRINGER, R. R. & DE CROMBRUGGHE, B. 1999. Sox9 is required for cartilage formation. *Nat Genet,* 22**,** 85-9.

BOEHM, B., WESTERBERG, H., LESNICAR-PUCKO, G., RAJA, S., RAUTSCHKA, M., COTTERELL, J., SWOGER, J. & SHARPE, J. 2010. The role of spatially controlled cell proliferation in limb bud morphogenesis. *PLoS Biol,* 8**,** e1000420.

CASAL, J., STRUHL, G. & LAWRENCE, P. A. 2002. Developmental compartments and planar polarity in Drosophila. *Curr Biol,* 12**,** 1189-98.

CHA, J., BARTOS, A., PARK, C., SUN, X., LI, Y., CHA, S. W., AJIMA, R., HO, H. Y., YAMAGUCHI, T. P. & DEY, S. K. 2014. Appropriate crypt formation in the uterus for embryo homing and implantation requires Wnt5a-ROR signaling. *Cell Rep,* 8**,** 382-92.

CHU, C. W. & SOKOL, S. Y. 2016. Wnt proteins can direct planar cell polarity in vertebrate ectoderm. *Elife,* 5.

CIRUNA, B., JENNY, A., LEE, D., MLODZIK, M. & SCHIER, A. F. 2006. Planar cell polarity signalling couples cell division and morphogenesis during neurulation. *Nature,* 439**,** 220-4.

CROSSLEY, P. H. & MARTIN, G. R. 1995. The mouse Fgf8 gene encodes a family of polypeptides and is expressed in regions that direct outgrowth and patterning in the developing embryo. *Development,* 121**,** 439-51.

DABDOUB, A. & KELLEY, M. W. 2005. Planar cell polarity and a potential role for a Wnt morphogen gradient in stereociliary bundle orientation in the mammalian inner ear. *J Neurobiol,* 64**,** 446-57.

DEVENPORT, D. & FUCHS, E. 2008. Planar polarization in embryonic epidermis orchestrates global asymmetric morphogenesis of hair follicles. *Nat Cell Biol,* 10**,** 1257-68.

DUBRULLE, J. & POURQUIE, O. 2004. fgf8 mRNA decay establishes a gradient that couples axial elongation to patterning in the vertebrate embryo. *Nature,* 427**,** 419-22.

FISHER, M. E., CLELLAND, A. K., BAIN, A., BALDOCK, R. A., MURPHY, P., DOWNIE, H., TICKLE, C., DAVIDSON, D. R. & BUCKLAND, R. A. 2008. Integrating technologies for comparing 3D gene expression domains in the developing chick limb. *Dev Biol,* 317**,** 13-23.

FURTHAUER, M., REIFERS, F., BRAND, M., THISSE, B. & THISSE, C. 2001. sprouty4 acts in vivo as a feedback-induced antagonist of FGF signaling in zebrafish. *Development,* 128**,** 2175-86.

GANAN, Y., MACIAS, D., BASCO, R. D., MERINO, R. & HURLE, J. M. 1998. Morphological diversity of the avian foot is related with the pattern of msx gene expression in the developing autopod. *Developmental biology,* 196**,** 33-41.

GAO, B. 2012. Wnt regulation of planar cell polarity (PCP). *Curr Top Dev Biol,* 101**,** 263-95.

GAO, B., SONG, H., BISHOP, K., ELLIOT, G., GARRETT, L., ENGLISH, M. A., ANDRE, P., ROBINSON, J., SOOD, R., MINAMI, Y., ECONOMIDES, A. N. & YANG, Y. 2011. Wnt signaling gradients establish planar cell polarity by inducing Vangl2 phosphorylation through Ror2. *Dev Cell,* 20**,** 163-76.

GAO, B. & YANG, Y. 2013. Planar cell polarity in vertebrate limb morphogenesis. *Curr Opin Genet Dev,* 23**,** 438-44.

GONG, Y., MO, C. & FRASER, S. E. 2004. Planar cell polarity signalling controls cell division orientation during zebrafish gastrulation. *Nature,* 430**,** 689-93.

GOODRICH, L. V. & STRUTT, D. 2011. Principles of planar polarity in animal development. *Development,* 138**,** 1877-92.

GRAY, R. S., ROSZKO, I. & SOLNICA-KREZEL, L. 2011. Planar cell polarity: coordinating morphogenetic cell behaviors with embryonic polarity. *Dev Cell,* 21**,** 120-33.

GROS, J., HU, J. K., VINEGONI, C., FERUGLIO, P. F., WEISSLEDER, R. & TABIN, C. J. 2010. WNT5A/JNK and FGF/MAPK pathways regulate the cellular events shaping the vertebrate limb bud. *Curr Biol,* 20**,** 1993-2002.

GROS, J., SERRALBO, O. & MARCELLE, C. 2009. WNT11 acts as a directional cue to organize the elongation of early muscle fibres. *Nature,* 457**,** 589-93.

HARFE, B. D., SCHERZ, P. J., NISSIM, S., TIAN, H., MCMAHON, A. P. & TABIN, C. J. 2004. Evidence for an expansion-based temporal Shh gradient in specifying vertebrate digit identities. *Cell,* 118**,** 517-28.

HASHIMOTO, M., SHINOHARA, K., WANG, J., IKEUCHI, S., YOSHIBA, S., MENO, C., NONAKA, S., TAKADA, S., HATTA, K., WYNSHAW-BORIS, A. & HAMADA, H. 2010. Planar polarization of node cells determines the rotational axis of node cilia. *Nature cell biology,* 12**,** 170-6.

HAYASHI, S., LEWIS, P., PEVNY, L. & MCMAHON, A. P. 2002. Efficient gene modulation in mouse epiblast using a Sox2Cre transgenic mouse strain. *Mech Dev,* 119 Suppl 1**,** S97-S101.

HEIKINHEIMO, M., LAWSHE, A., SHACKLEFORD, G. M., WILSON, D. B. & MACARTHUR, C. A. 1994. Fgf-8 expression in the post-gastrulation mouse suggests roles in the development of the face, limbs and central nervous system. *Mech Dev,* 48**,** 129-38.

HEISENBERG, C. P., TADA, M., RAUCH, G. J., SAUDE, L., CONCHA, M. L., GEISLER, R., STEMPLE, D. L., SMITH, J. C. & WILSON, S. W. 2000. Silberblick/Wnt11 mediates convergent extension movements during zebrafish gastrulation. *Nature,* 405**,** 76-81.

HERNANDEZ-MARTINEZ, R., CASTRO-OBREGON, S. & COVARRUBIAS, L. 2009. Progressive interdigital cell death: regulation by the antagonistic interaction between fibroblast growth factor 8 and retinoic acid. *Development,* 136**,** 3669-78.

HOPYAN, S., SHARPE, J. & YANG, Y. 2011. Budding behaviors: Growth of the limb as a model of morphogenesis. *Dev Dyn,* 240**,** 1054-62.

HUMPHRIES, A. C. & MLODZIK, M. 2017. From instruction to output: Wnt/PCP signaling in development and cancer. *Curr Opin Cell Biol,* 51**,** 110-116.

KELLY, L. K., WU, J., YANFENG, W. A. & MLODZIK, M. 2016. Frizzled-Induced Van Gogh Phosphorylation by CK1epsilon Promotes Asymmetric Localization of Core PCP Factors in Drosophila. *Cell Rep,* 16**,** 344-56.

KILIAN, B., MANSUKOSKI, H., BARBOSA, F. C., ULRICH, F., TADA, M. & HEISENBERG, C. P. 2003. The role of Ppt/Wnt5 in regulating cell shape and movement during zebrafish gastrulation. *Mech Dev,* 120**,** 467-76.

LAWRENCE, P. A., CASAL, J. & STRUHL, G. 2004. Cell interactions and planar polarity in the abdominal epidermis of Drosophila. *Development,* 131**,** 4651-64.

LAWRENCE, P. A., SANSON, B. & VINCENT, J. P. 1996. Compartments, wingless and engrailed: patterning the ventral epidermis of Drosophila embryos. *Development,* 122**,** 4095-103.

LAWRENCE, P. A., STRUHL, G. & CASAL, J. 2007. Planar cell polarity: one or two pathways? *Nat Rev Genet,* 8**,** 555-63.

LEWANDOSKI, M., SUN, X. & MARTIN, G. R. 2000. Fgf8 signalling from the AER is essential for normal limb development. *Nat Genet,* 26**,** 460-3.

LI, S. & MUNEOKA, K. 1999. Cell migration and chick limb development: chemotactic action of FGF-4 and the AER. *Dev Biol,* 211**,** 335-47.

LI, Y. & DUDLEY, A. T. 2009. Noncanonical frizzled signaling regulates cell polarity of growth plate chondrocytes. *Development,* 136**,** 1083-92.

LI, Y., LI, A., JUNGE, J. & BRONNER, M. 2017. Planar cell polarity signaling coordinates oriented cell division and cell rearrangement in clonally expanding growth plate cartilage. *Elife,* 6.

LOGAN, M., MARTIN, J. F., NAGY, A., LOBE, C., OLSON, E. N. & TABIN, C. J. 2002. Expression of Cre Recombinase in the developing mouse limb bud driven by a Prxl enhancer. *Genesis,* 33**,** 77-80.

MARIANI, F. V., AHN, C. P. & MARTIN, G. R. 2008. Genetic evidence that FGFs have an instructive role in limb proximal-distal patterning. *Nature,* 453**,** 401-5.

MATIS, M. & AXELROD, J. D. 2013. Regulation of PCP by the Fat signaling pathway. *Genes & development,* 27**,** 2207-20.

MINEGISHI, K., HASHIMOTO, M., AJIMA, R., TAKAOKA, K., SHINOHARA, K., IKAWA, Y., NISHIMURA, H., MCMAHON, A. P., WILLERT, K., OKADA, Y., SASAKI, H., SHI, D., FUJIMORI, T., OHTSUKA, T., IGARASHI, Y., YAMAGUCHI, T. P., SHIMONO, A., SHIRATORI, H. & HAMADA, H. 2017. A Wnt5 Activity Asymmetry and Intercellular Signaling via PCP Proteins Polarize Node Cells for Left-Right Symmetry Breaking. *Dev Cell,* 40**,** 439-452 e4.

MINOWADA, G., JARVIS, L. A., CHI, C. L., NEUBUSER, A., SUN, X., HACOHEN, N., KRASNOW, M. A. & MARTIN, G. R. 1999. Vertebrate Sprouty genes are induced by FGF signaling and can cause chondrodysplasia when overexpressed. *Development,* 126**,** 4465-75.

MOFTAH, M. Z., DOWNIE, S. A., BRONSTEIN, N. B., MEZENTSEVA, N., PU, J., MAHER, P. A. & NEWMAN, S. A. 2002. Ectodermal FGFs induce perinodular

inhibition of limb chondrogenesis in vitro and in vivo via FGF receptor 2. *Developmental biology,* 249**,** 270-82.

MOHAMMADI, M., MCMAHON, G., SUN, L., TANG, C., HIRTH, P., YEH, B. K., HUBBARD, S. R. & SCHLESSINGER, J. 1997. Structures of the tyrosine kinase domain of fibroblast growth factor receptor in complex with inhibitors. *Science,* 276**,** 955-60.

MONTCOUQUIOL, M., RACHEL, R. A., LANFORD, P. J., COPELAND, N. G., JENKINS, N. A. & KELLEY, M. W. 2003. Identification of Vangl2 and Scrb1 as planar polarity genes in mammals. *Nature,* 423**,** 173-7.

MONTERO, J. A., GANAN, Y., MACIAS, D., RODRIGUEZ-LEON, J., SANZ-EZQUERRO, J. J., MERINO, R., CHIMAL-MONROY, J., NIETO, M. A. & HURLE, J. M. 2001. Role of FGFs in the control of programmed cell death during limb development. *Development,* 128**,** 2075-84.

NISWANDER, L., TICKLE, C., VOGEL, A., BOOTH, I. & MARTIN, G. R. 1993. FGF-4 replaces the apical ectodermal ridge and directs outgrowth and patterning of the limb. *Cell,* 75**,** 579-87.

OSSIPOVA, O., KIM, K. & SOKOL, S. Y. 2015. Planar polarization of Vangl2 in the vertebrate neural plate is controlled by Wnt and Myosin II signaling. *Biol Open,* 4**,** 722-30.

PAJNI-UNDERWOOD, S., WILSON, C. P., ELDER, C., MISHINA, Y. & LEWANDOSKI, M. 2007. BMP signals control limb bud interdigital programmed cell death by regulating FGF signaling. *Development,* 134**,** 2359-68.

PARR, B. A., SHEA, M. J., VASSILEVA, G. & MCMAHON, A. P. 1993. Mouse Wnt genes exhibit discrete domains of expression in the early embryonic CNS and limb buds. *Development,* 119**,** 247-61.

PIZETTE, S. & NISWANDER, L. 1999. BMPs negatively regulate structure and function of the limb apical ectodermal ridge. *Development,* 126**,** 883-94.

QIAN, D., JONES, C., RZADZINSKA, A., MARK, S., ZHANG, X., STEEL, K. P., DAI, X. & CHEN, P. 2007. Wnt5a functions in planar cell polarity regulation in mice. *Dev Biol,* 306**,** 121-33.

RAUCH, G. J., HAMMERSCHMIDT, M., BLADER, P., SCHAUERTE, H. E., STRAHLE, U., INGHAM, P. W., MCMAHON, A. P. & HAFFTER, P. 1997. Wnt5 is required for tail formation in the zebrafish embryo. *Cold Spring Harb Symp Quant Biol,* 62**,** 227-34.

RIDDLE, R. D., JOHNSON, R. L., LAUFER, E. & TABIN, C. 1993. Sonic hedgehog mediates the polarizing activity of the ZPA. *Cell,* 75**,** 1401-16.

ROMEREIM, S. M., CONOAN, N. H., CHEN, B. & DUDLEY, A. T. 2014. A dynamic cell adhesion surface regulates tissue architecture in growth plate cartilage. *Development,* 141**,** 2085-95.

SABURI, S., HESTER, I., FISCHER, E., PONTOGLIO, M., EREMINA, V., GESSLER, M., QUAGGIN, S. E., HARRISON, R., MOUNT, R. & MCNEILL, H. 2008. Loss of Fat4 disrupts PCP signaling and oriented cell division and leads to cystic kidney disease. *Nature genetics,* 40**,** 1010-5.

SATOH, W., MATSUYAMA, M., TAKEMURA, H., AIZAWA, S. & SHIMONO, A. 2008. Sfrp1, Sfrp2, and Sfrp5 regulate the Wnt/beta-catenin and the planar cell polarity pathways during early trunk formation in mouse. *Genesis,* 46**,** 92-103.

SIMONS, M. & MLODZIK, M. 2008. Planar cell polarity signaling: from fly development to human disease. *Annu Rev Genet,* 42**,** 517-40.

SINGH, J. & MLODZIK, M. 2012. Planar cell polarity signaling: coordination of cellular orientation across tissues. *Wiley Interdiscip Rev Dev Biol,* 1**,** 479-99.

SONG, H., HU, J., CHEN, W., ELLIOTT, G., ANDRE, P., GAO, B. & YANG, Y. 2010. Planar cell polarity breaks bilateral symmetry by controlling ciliary positioning. *Nature,* 466**,** 378-82.

SORIANO, P. 1999. Generalized lacZ expression with the ROSA26 Cre reporter strain. *Nature genetics,* 21**,** 70-1.

SUN, X., MARIANI, F. V. & MARTIN, G. R. 2002. Functions of FGF signalling from the apical ectodermal ridge in limb development. *Nature,* 418**,** 501-8.

TANG, N., MARSHALL, W. F., MCMAHON, M., METZGER, R. J. & MARTIN, G. R. 2011. Control of mitotic spindle angle by the RAS-regulated ERK1/2 pathway determines lung tube shape. *Science,* 333**,** 342-5.

TODT, W. L. & FALLON, J. F. 1987. Posterior apical ectodermal ridge removal in the chick wing bud triggers a series of events resulting in defective anterior pattern formation. *Development,* 101**,** 501-15.

TOMLINSON, A., STRAPPS, W. R. & HEEMSKERK, J. 1997. Linking Frizzled and Wnt signaling in Drosophila development. *Development,* 124**,** 4515-21.

TOPOL, L., JIANG, X., CHOI, H., GARRETT-BEAL, L., CAROLAN, P. J. & YANG, Y. 2003. Wnt-5a inhibits the canonical Wnt pathway by promoting GSK-3-independent beta-catenin degradation. *J Cell Biol,* 162**,** 899-908.

VAN AMERONGEN, R. 2012. Alternative Wnt pathways and receptors. *Cold Spring Harbor perspectives in biology,* 4.

VLADAR, E. K., ANTIC, D. & AXELROD, J. D. 2009. Planar cell polarity signaling: the developing cell's compass. *Cold Spring Harb Perspect Biol,* 1**,** a002964.

WALLINGFORD, J. B. 2012. Planar cell polarity and the developmental control of cell behavior in vertebrate embryos. *Annu Rev Cell Dev Biol,* 28**,** 627-53.

WANG, B., SINHA, T., JIAO, K., SERRA, R. & WANG, J. 2011. Disruption of PCP signaling causes limb morphogenesis and skeletal defects and may underlie Robinow syndrome and brachydactyly type B. *Hum Mol Genet,* 20**,** 271-85.

WANG, Y. & NATHANS, J. 2007. Tissue/planar cell polarity in vertebrates: new insights and new questions. *Development,* 134**,** 647-58.

WILKINSON, D. G. & NIETO, M. A. 1993. Detection of messenger RNA by in situ hybridization to tissue sections and whole mounts. *Methods in enzymology,* 225**,** 361-73.

WITTE, F., DOKAS, J., NEUENDORF, F., MUNDLOS, S. & STRICKER, S. 2009. Comprehensive expression analysis of all Wnt genes and their major secreted antagonists during mouse limb development and cartilage differentiation. *Gene Expr Patterns,* 9**,** 215-23.

WITZE, E. S., LITMAN, E. S., ARGAST, G. M., MOON, R. T. & AHN, N. G. 2008. Wnt5a control of cell polarity and directional movement by polarized redistribution of adhesion receptors. *Science,* 320**,** 365-9.

WU, J. & MLODZIK, M. 2008. The frizzled extracellular domain is a ligand for Van Gogh/Stbm during nonautonomous planar cell polarity signaling. *Dev Cell,* 15**,** 462-9.

WU, J. & MLODZIK, M. 2009. A quest for the mechanism regulating global planar cell polarity of tissues. *Trends Cell Biol,* 19**,** 295-305.

WU, J., ROMAN, A. C., CARVAJAL-GONZALEZ, J. M. & MLODZIK, M. 2013. Wg and Wnt4 provide long-range directional input to planar cell polarity orientation in Drosophila. *Nat Cell Biol,* 15**,** 1045-55.

YAMAGUCHI, T. P., BRADLEY, A., MCMAHON, A. P. & JONES, S. 1999. A Wnt5a pathway underlies outgrowth of multiple structures in the vertebrate embryo. *Development,* 126**,** 1211-23.

YANG, T., BASSUK, A. G. & FRITZSCH, B. 2013. Prickle1 stunts limb growth through alteration of cell polarity and gene expression. *Dev Dyn,* 242**,** 1293-306.

YANG, W., GARRETT, L., FENG, D., ELLIOTT, G., LIU, X., WANG, N., WONG, Y. M., CHOI, N. T., YANG, Y. & GAO, B. 2017. Wnt-induced Vangl2

phosphorylation is dose-dependently required for planar cell polarity in mammalian development. *Cell Res,* 27**,** 1466-1484.

YANG, Y. & MLODZIK, M. 2015. Wnt-Frizzled/Planar Cell Polarity Signaling: Cellular Orientation by Facing the Wind (Wnt). *Annu Rev Cell Dev Biol,* 31**,** 623-46.

YU, K. & ORNITZ, D. M. 2008. FGF signaling regulates mesenchymal differentiation and skeletal patterning along the limb bud proximodistal axis. *Development,* 135**,** 483-91.

ZELLER, R., LOPEZ-RIOS, J. & ZUNIGA, A. 2009. Vertebrate limb bud development: moving towards integrative analysis of organogenesis. *Nat Rev Genet,* 10**,** 845-58.

ZHU, X., ZHU, H., ZHANG, L., HUANG, S., CAO, J., MA, G., FENG, G., HE, L., YANG, Y. & GUO, X. 2012. Wls-mediated Wnts differentially regulate distal limb patterning and tissue morphogenesis. *Dev Biol,* 365**,** 328-38.

Figures

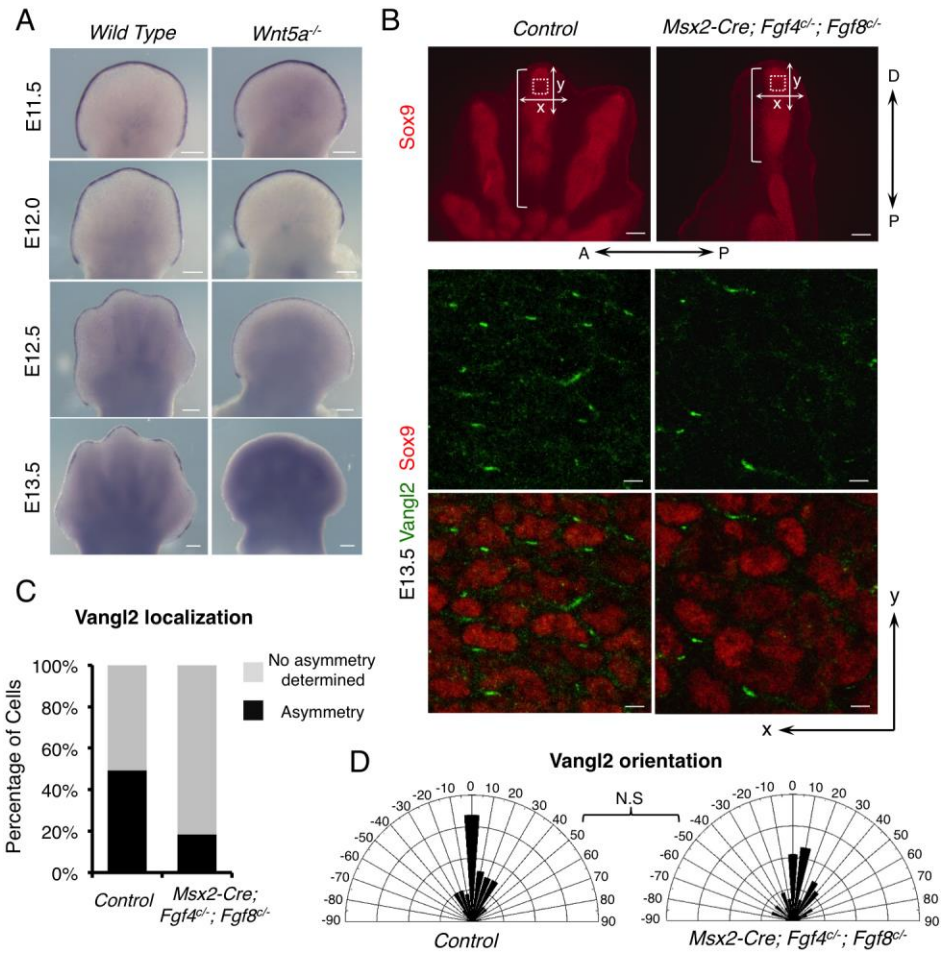

Figure 1. *Fgfs* from the AER are required for full PCP in limb development

(A) Whole mount *in situ* hybridization of *Fgf8* in *wild type* and *Wnt5a*$^{-/-}$ embryonic forelimbs. (B) Compromised Vangl2 asymmetrical localization in distal digits of the E13.5 *Msx2-Cre; Fgf4*$^{c/-}$*; Fgf8*$^{c/-}$ forelimbs. The boxed regions were subjected to confocal scanning. Enlarged images of part of the scanned regions are shown in the middle and lower panel. Vangl2 (green) and Sox9 (red) protein are shown by fluorescent Immunostaining. The brackets indicate the length of digits. P-D: proximal-distal. A-P: anterior-posterior. x and y axes of the image are defined as shown in the upper panel. (C) The percentage of cells with discernable Vangl2

asymmetric localization in control and mutant. (D) Schematic diagrams summarizing the quantification of orientation angles of Vangl2. x axis, angle of orientation (-90° to 90°); y axis, percentage of cells at angle x. kolmogorov smirnov test, N.S, no significance. (C) and (D) number of samples and number of cells analyzed for each genotype: control, N=3, n=325; *Msx2-Cre; Fgf4*$^{c/-}$*; Fgf8*$^{c/-}$, N=5, n=450. Scale bars = 200 μm in (A) and upper panel of (B) or 10 μm in middle and low panels of (B).

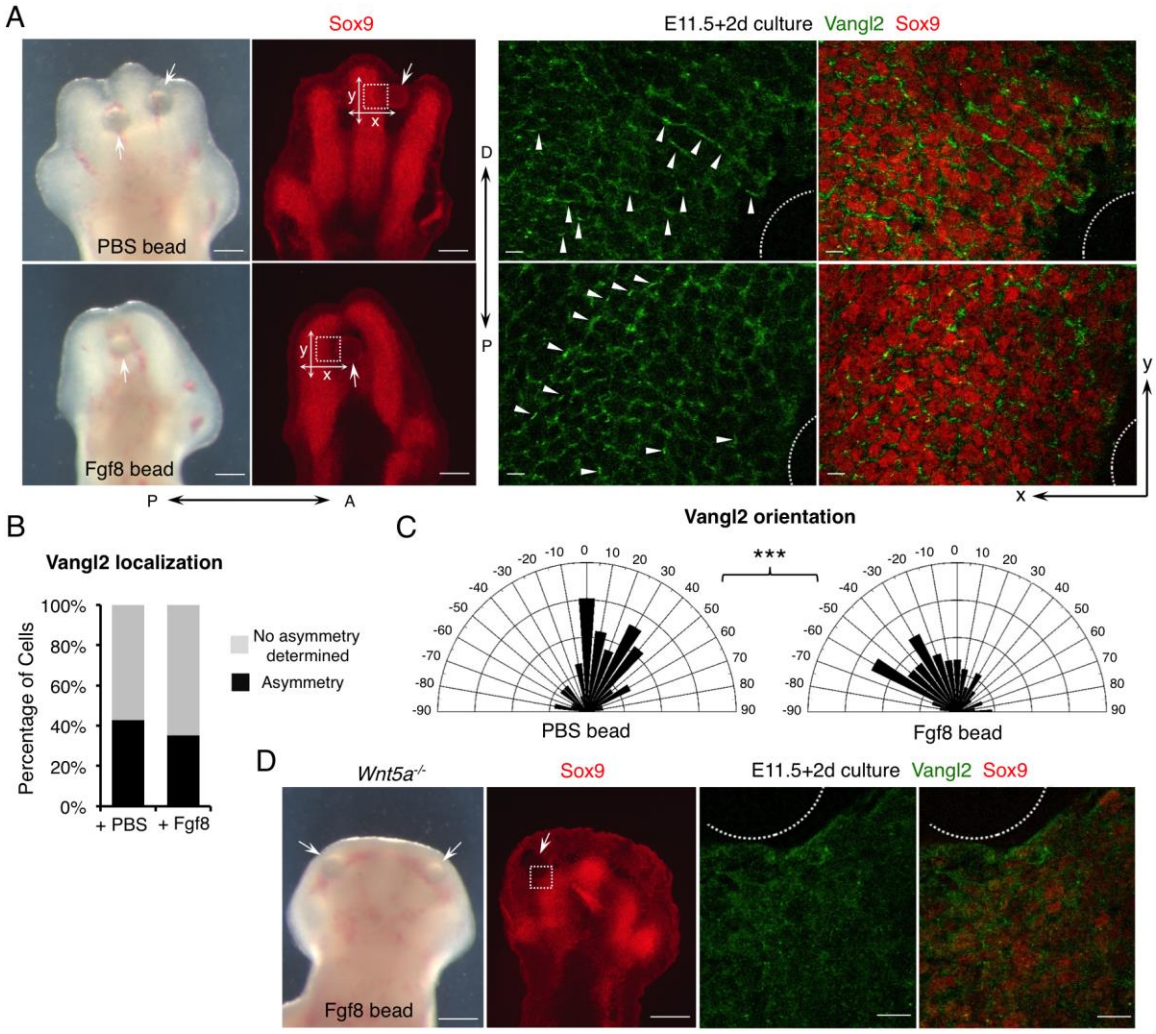

Figure 2. Fgf signaling is sufficient to regulate PCP in a Wnt5a-dependent manner (A) Representative morphological and immunofluorescent images of cultured distal limbs. Beads soaked in PBS or Fgf8 recombinant protein were inserted into the E11.5 mouse embryonic forelimbs that were then cultured for 2 days. The boxed regions lateral to the beads (arrows) were scanned by confocal microscope and representative images are shown in middle (Vangl2, green) and right panels (Vangl2/Sox9, green/red). The beads are outlined. Arrowheads point to some of asymmetrically localized Vangl2. P-D: proximal-distal; P-A: posterior-anterior. x and y axes of the image are defined as shown in the left panel. (B) The percentage of cells with discernable Vangl2 asymmetric localization in digits

implanted with PBS or Fgf8-soaked beads. (C) Schematic diagrams summarizing the quantification of orientation angles of Vangl2. x axis, angle of orientation (-90° to 90°); y axis, percentage of cells at angle x. kolmogorov smirnov test, ***p value=0.0008. (B) and (C) PBS beads-implanted limbs N=4, analyzed cells n=711; Fgf8 beads-implanted limbs N=5, analyzed cells n=678. (D) Loss of Vangl2 asymmetric localization in *Wnt5a*$^{-/-}$ limbs cannot be rescued by Fgf8-soaked beads after 2-day culture. Boxed region close to the bead (arrow) is shown in middle (Vangl2, green) and right panels (Vangl2/Sox9, green/red) with higher magnification. The bead is outlined. No Vangl2 asymmetric localization was observed. Cultured *Wnt5a*$^{-/-}$ limbs: N=4. Scale bars = 200 μm in left panels of (A) and (D) or 20 μm in right panels of (A) and (D).

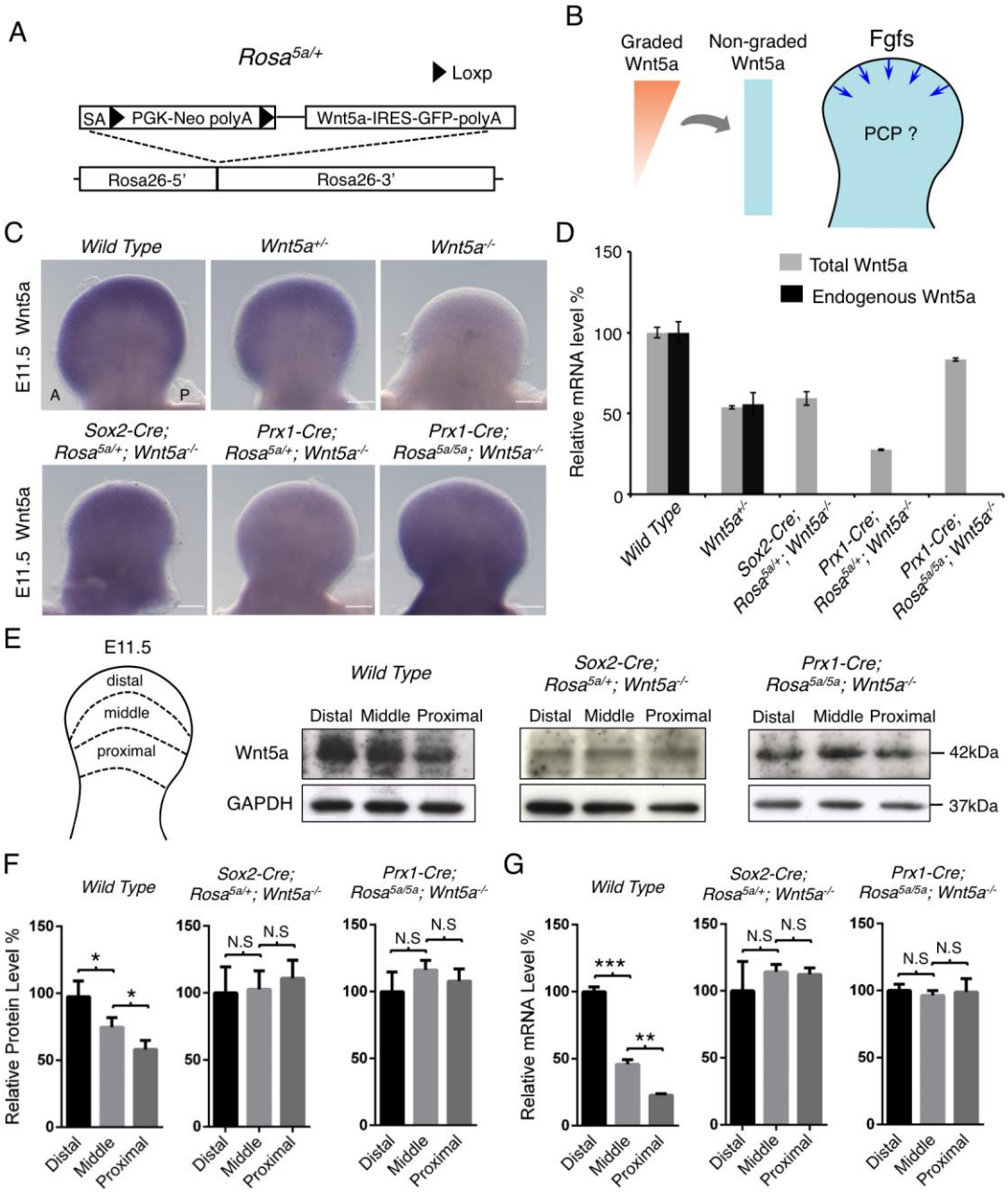

Figure 3. Generation of non-graded *Wnt5a* expression (A) Generation of an inducible *Wnt5a* mouse strain (*Rosa*$^{5a/+}$). Mouse *Wnt5a* cDNA following a PGK-Neo cassette flanked by loxp sequences was knocked into the *Rosa26* locus. IRES-GFP sequence was cloned downstream of *Wnt5a* cDNA. SA, splice acceptor sequence. (B) Schematics of strategy. The blue arrows represent Fgf

signaling from distal limb AER. (C) *Wnt5a* whole mount *in situ* hybridization in E11.5 mouse forelimb buds. P, posterior; A, anterior. Scale bar = 200 μm. (D) Levels of total or endogenous *Wnt5a* mRNA from E11.5 forelimb buds were quantified by qPCR. *Wnt5a* mRNA levels were normalized to *GAPDH* expression. Error bars are ± SD, n = 3 repetitions. (E) The E11.5 forelimb buds were dissected into 3 parts, and each part was subjected to Western blot analysis and qPCR. (F) and (G) Quantification of Wnt5a protein and mRNA levels of three parts, which were normalized to GAPDH protein and mRNA levels, respectively. Two-tailed *t* test, *p value<0.05, **p value<0.01, ***p value<0.001. N.S, no significance. Error bars are ± SD, n = 2 repetitions for WB, n=3 repetitions for qPCR.

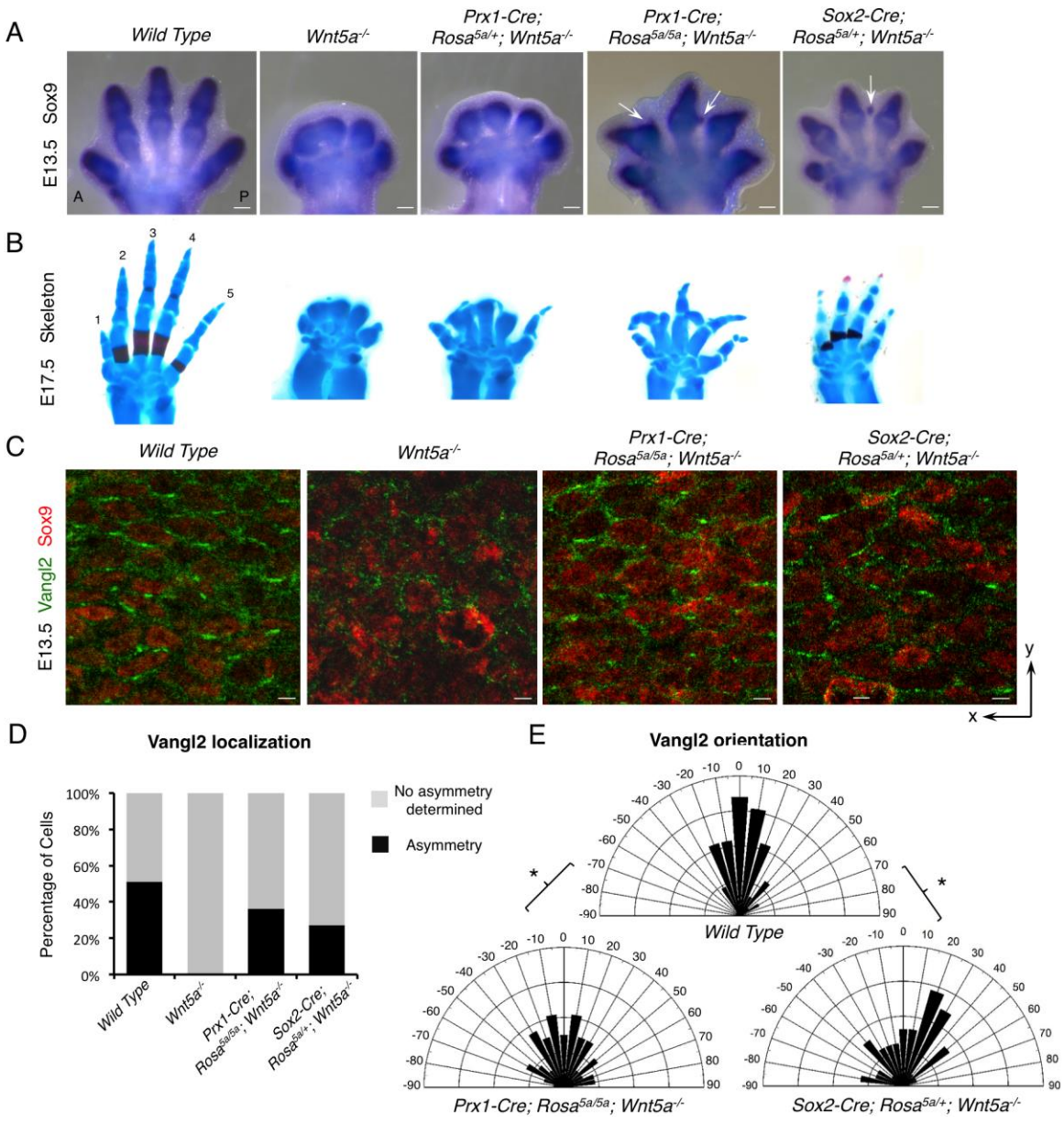

Figure 4. Non-graded *Wnt5a* expression partially rescued the PCP defects of the *Wnt5a*$^{-/-}$ embryo (A) *Sox9* whole mount *in situ* hybridization in E13.5 mouse forelimbs. Arrows point to the ectopic cartilage. (B) Alizarin red and Alcian blue staining of forelimbs from embryos with indicated genotypes at E17.5. Digit 1-5 are labeled. (C) Representative images of fluorescent Immunostaining of Vangl2 (green) and Sox9 (red). x and y axes of the image are defined as shown in Figure S13A. (D) The percentage of cells with discernable Vangl2 asymmetric

localization in each genotype. (E) Schematic diagrams summarizing the quantification of orientation angles of Vangl2 in each genotype. x axis, angle of orientation (-90° to 90°); y axis, percentage of cells at angle x. kolmogorov smirnov test, *p values=0.0466 and 0.0285. (D) and (E) number of samples and number of cells analyzed for each genotype: wild type, N=2, n=230; *Wnt5a*$^{-/-}$, N=2, n=188; *Prx1-Cre; Rosa*$^{5a/5a}$*; Wnt5a*$^{-/-}$, N=3, n=271; *Sox2-Cre; Rosa*$^{5a/+}$*; Wnt5a*$^{-/-}$, N=5, n=450. Scale bars = 200 μm in (A) or 10 μm in (C).

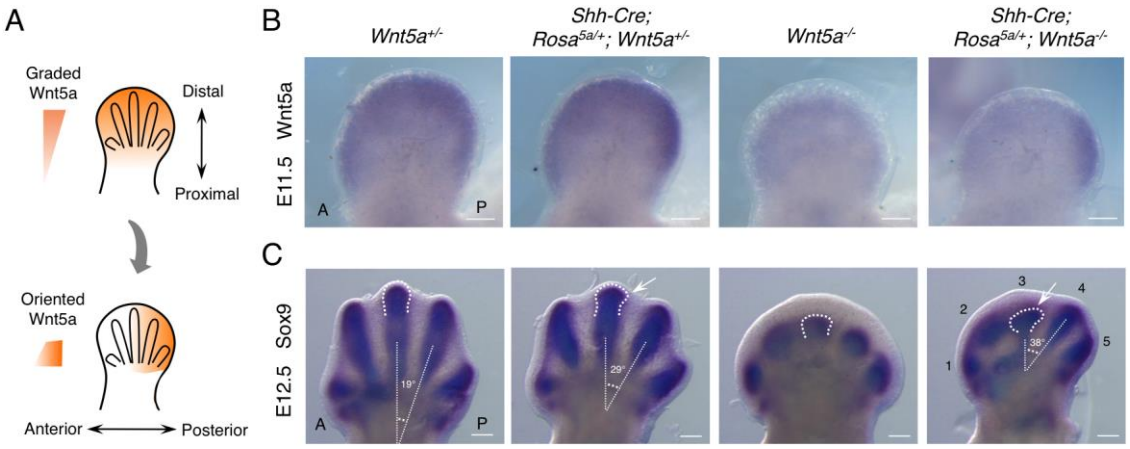

Figure 5. Reoriented *Wnt5a* expression gradient changed digit morphogenesis (A) Illustration of altering *Wnt5a* expression gradient from distal-proximal axis to posterior-anterior axis. (B) *Wnt5a* whole mount *in situ* hybridization in mouse E11.5 forelimb buds. (C) *Sox9* whole mount *in situ* hybridization in mouse E12.5 forelimb buds. Each digit is numbered and the third digit is outlined. The angles between digit 3 and digit 4 were measured by using their longitudinal axes. The arrows point to the posteriorly tilted digit 3. A: anterior; P: posterior. Digit 1-5 are labeled. Scale bar = 200 μm.

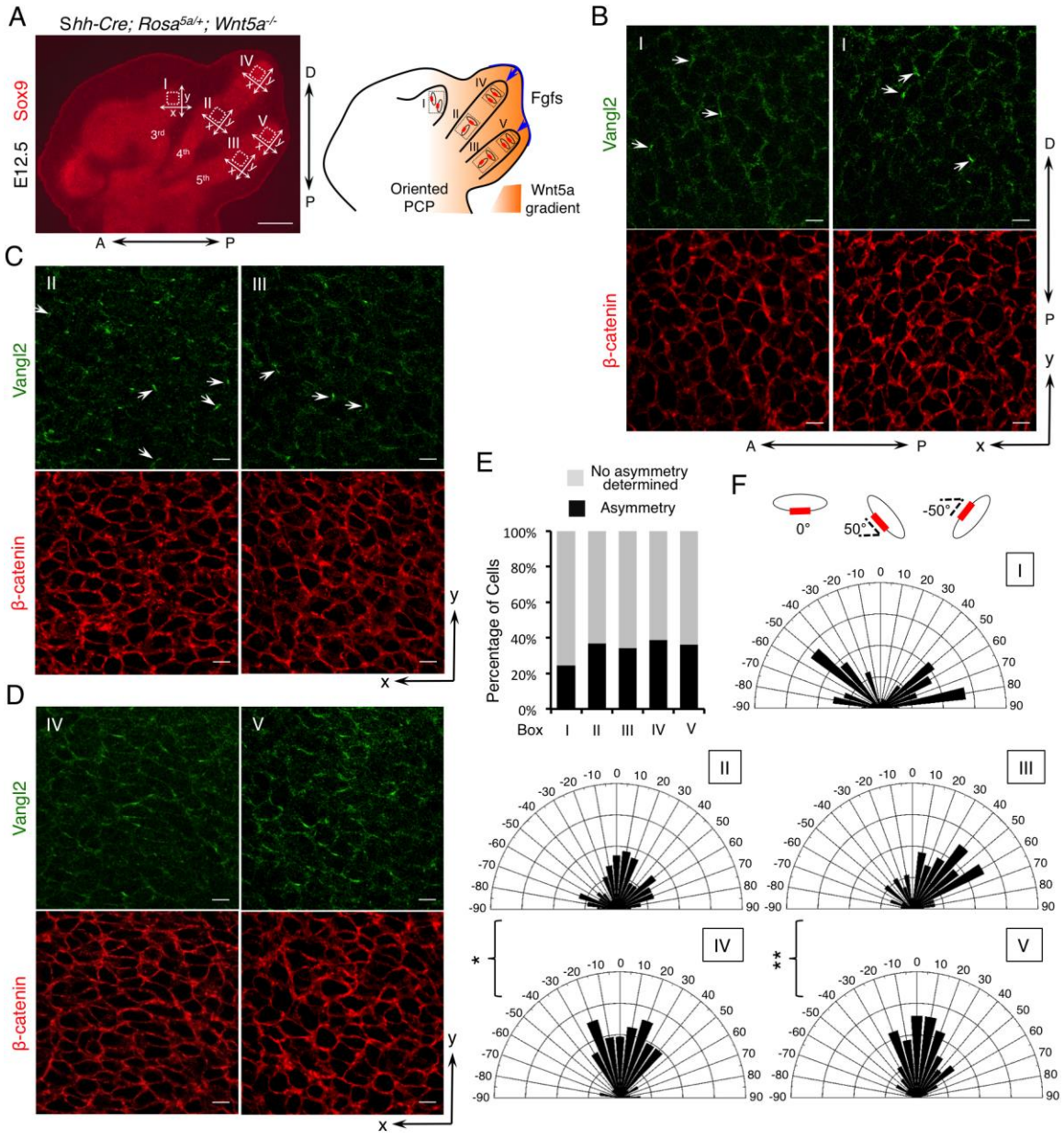

Figure 6. Vangl2 asymmetric localization is partially re-oriented by the altered *Wnt5a* gradient. (A) The forelimb digits in the E12.5 *Shh-Cre;Rosa*$^{5a/+}$*; Wnt5a*$^{-/-}$ embryos are shown by Sox9 immunofluorescent staining. The boxed regions I-V are enlarged with Vangl2 (green) and β-catenin (red) double immunofluorescent staining as shown in (B-D). A-P: anterior-posterior. P-D: proximal-distal. x and y axes of the boxed regions are defined as shown in the left panel. Right panel: schematic summary of the results. The red dots represent

Vangl2 asymmetric localization and the blue arrows represent Fgf signaling cues. (B) Representative 3rd digit (box I). (C) Representative proximal regions of the 4th (box II) and 5th digit (box III). (D) Representative distal regions of the 4th (box IV) and 5th digit (box V). Arrows point to cells with asymmetrical Vangl2 localization along the x axis. (E) The percentage of cells with discernable Vangl2 asymmetric localization shown in (B-D). (F) Schematic diagrams summarizing the quantification of orientation angles of Vangl2 in each boxed area of I-V. x axis, angle of orientation (-90° to 90°); y axis, percentage of cells at angle x. kolmogorov smirnov test, **p value=0.0128, *p value=0.0414. (E) and (F), number of samples and number of cells analyzed for each area: N=4, n=232 for area I; N=4, n=294 for area II; N=3, n=196 for area III; N=4, n=327 for area IV; N=2, n=130 for area V. Scale bars = 200 μm in (A) or 20 μm in (B)-(D).

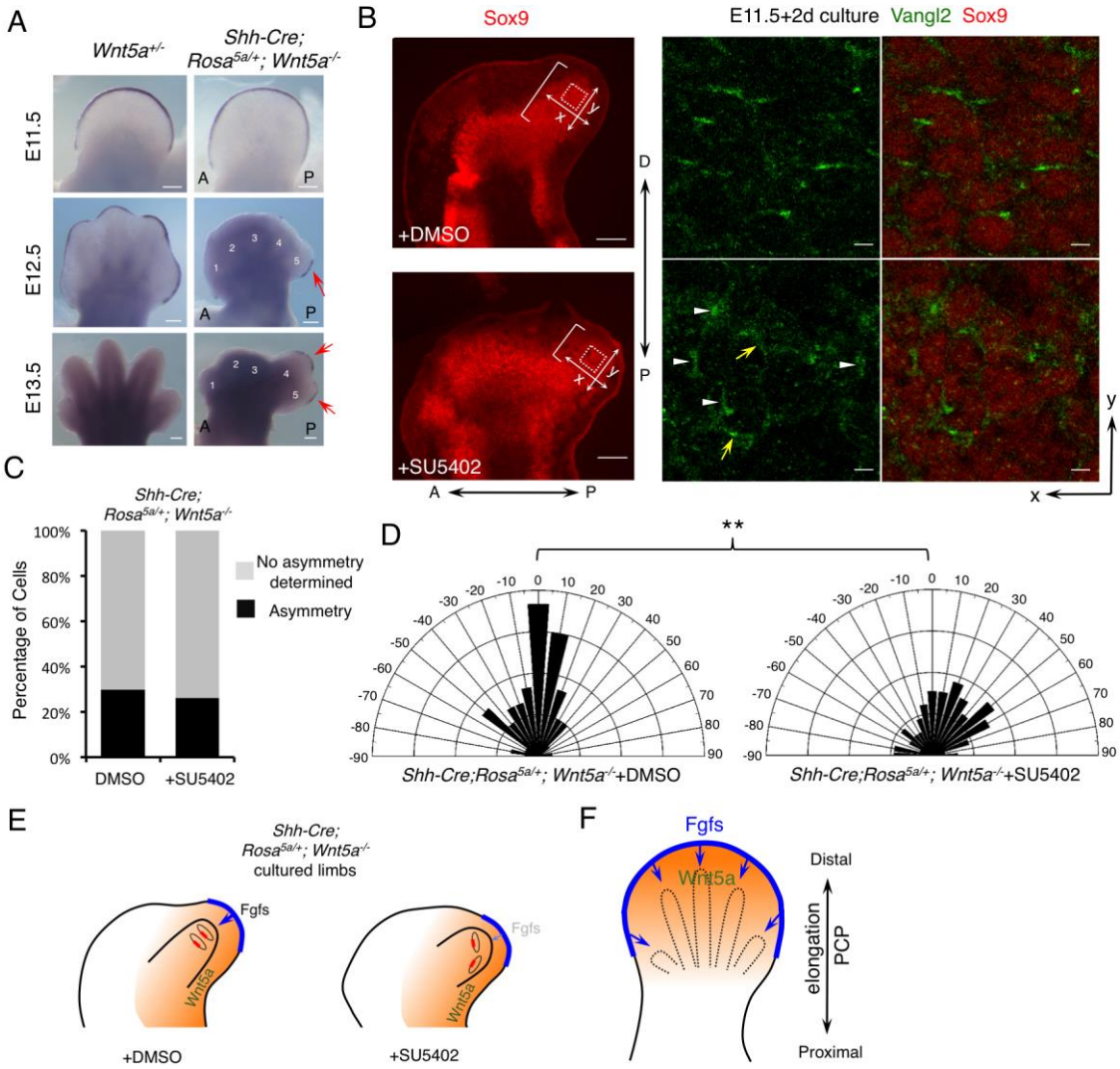

Figure 7.Inhibition of distal Fgf signaling renders cells more responsive to oriented Wnt5a signaling. (A) Whole mount *in situ* hybridization of *Fgf8* in forelimbs of the embryos with the indicated genotypes. *Fgf8* expression was restored (red arrows) in the AER overlying the posterior digits of the *Shh-Cre; Rosa*$^{5a/+}$*;Wnt5a*$^{-/-}$ embryos. A: anterior; P: posterior. Digit 1-5 is labeled in the mutant. (B) Treatment with Fgfr inhibitor (SU5402) changed the direction of Vangl2 asymmetric localization in cultured *Shh-Cre;Rosa*$^{5a/+}$*;Wnt5a*$^{-/-}$ embryonic forelimbs (E11.5 + 2-day culture). The brackets indicate the length of digit outgrowth. Part of the boxed regions (dotted squares) was shown in middle (Vangl2, green) and right panels (Vangl2/Sox9, green/red) in higher

magnification. White arrowheads point to 90 degree oriented Vangl2. Yellow arrows point to Vangl2 with other orientations. P-D: proximal-distal, A-P: anterior-posterior. x and y axes of the boxed regions are defined as shown in the left panel. (C) The percentage of cells with discernable Vangl2 asymmetric localization in distal chondrocytes of *Shh-Cre;Rosa*$^{5a/+}$*;Wnt5a*$^{-/-}$ limb with DMSO or SU5402 treatment. (D) Schematic diagrams summarizing the quantification of orientation angles of Vangl2 in each group. x axis, angle of orientation (-90° to 90°); y axis, percentage of cells at angle x. kolmogorov smirnov test, **p value=0.0027. (C) and (D) DMSO treated limbs N=6, counted cells n=414; SU5402 treated limbs N=6, counted cells n=406. (E) Schematic summary of the results shown in (B)-(D). The red dots represent Vangl2 asymmetric localization and the blue arrows represent Fgf signaling. The orange backgrounds represent Wnt5a signaling. The light blue arrow in the right panel indicates weaker Fgf signaling. (F) Schematic diagram of the proposed model: PCP establishment is coordinately regulated by both Wnt5a and Fgfs signaling. Orange: graded *Wnt5a* expression; Blue: Fgf signaling from the AER. Scale bars = 200 μm in (A) and left panel of (B) or 10 μm in right panel of (B).

Figure S1

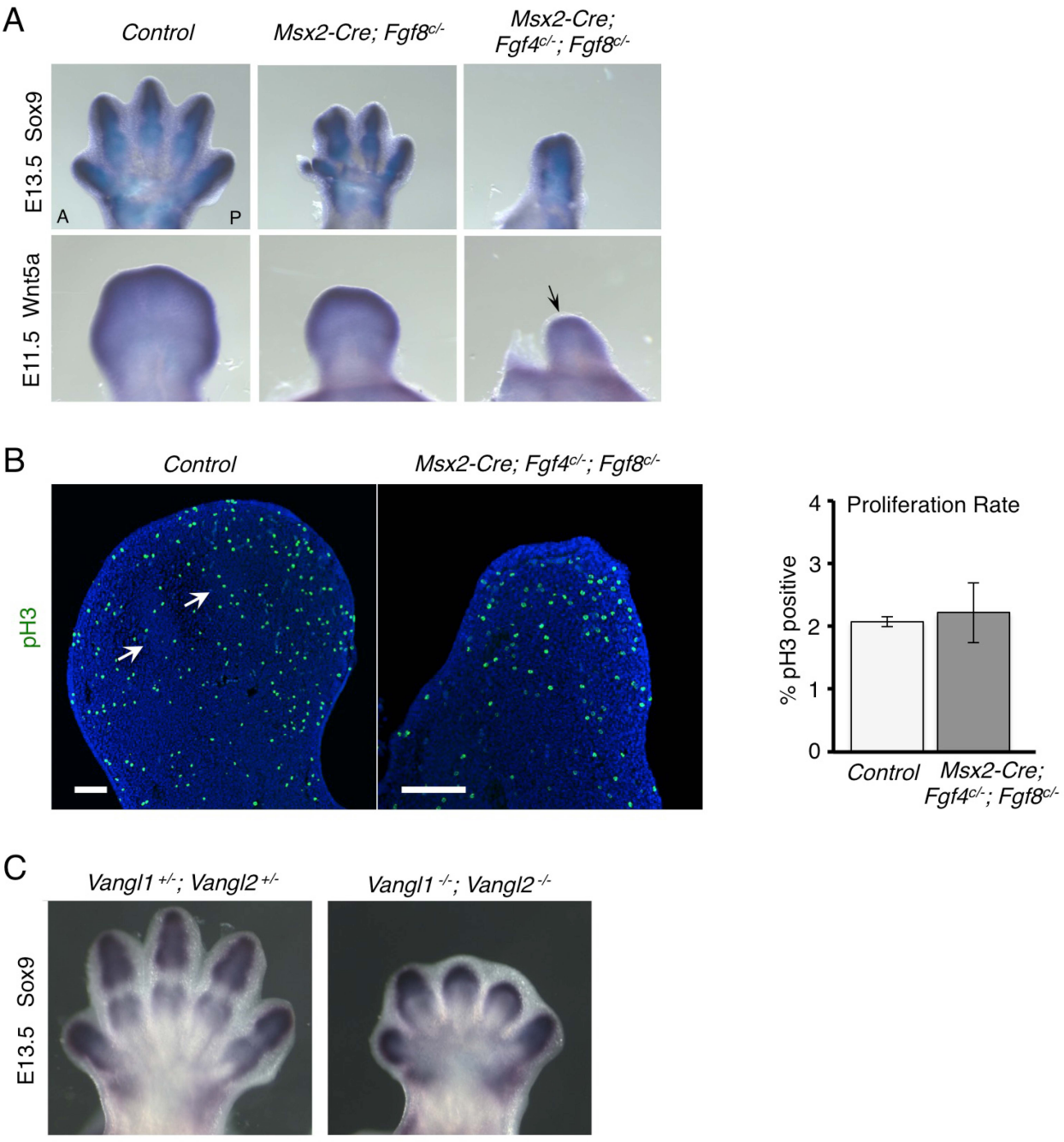

Analysis of *Fgf* and *Vangl* mutants. (A) Whole mount *in situ* hybridization of *Sox9* (upper panel) and *Wnt5a* (lower panel) on control and *Fgf* mutant embryonic forelimbs. Arrow points to the *Wnt5a* expression region of the *Msx2-Cre; Fgf4*$^{c/-}$*; Fgf8*$^{c/-}$ forelimb. (B) Immunodetection of phospho-histone H3 (Ser 10) in control and *Msx2-Cre; Fgf4*$^{c/-}$*; Fgf8*$^{c/-}$ distal forelimbs at E11.5 (44 som). Arrows point to forming digital rays. No statistically significant difference was found (two-tailed *t* test). (C) *Sox9* whole mount *in situ* hybridization in the mouse E13.5 forelimbs of control and *Vangl1/2* double mutant.

Figure S2

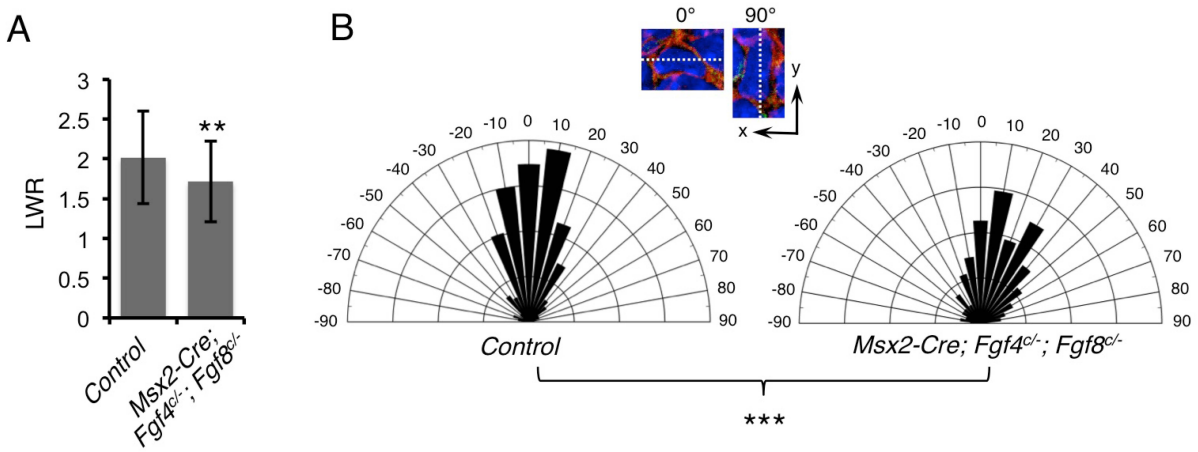

Analysis of Fgf4/8 mutant cell shape and orientation. (A) Statistical analysis of length-to-width ratio (LWR) of distal limb chondrocytes in E13.5 control and *Fgf4/8* double mutant shown in Figure 1B. Two-tailed *t* test, **p value=0.0012. Error bars are ±SD. Analyzed cells: control, n=46; *Msx2-Cre; Fgf4$^{c/-}$; Fgf8$^{c/-}$*, n=129. (B) Schematic diagrams summarizing the quantification of distal cells orientation in E13.5 control and *Fgf4/8* double mutant. The inset shows examples of cell orientation: 0°refers to the cell that orients horizontally, but 90°refers to the cell that orient vertically. The inset x and y axes were defined as shown in Figure 1B. Schematics x axis, angle of orientation; Schematics y axis, percentage of cells at angle x. kolmogorov smirnov test, ***p value=0.0004. Analyzed cells: control, n=167; *Msx2-Cre; Fgf4$^{c/-}$; Fgf8$^{c/-}$*, n=177.

Figure S3

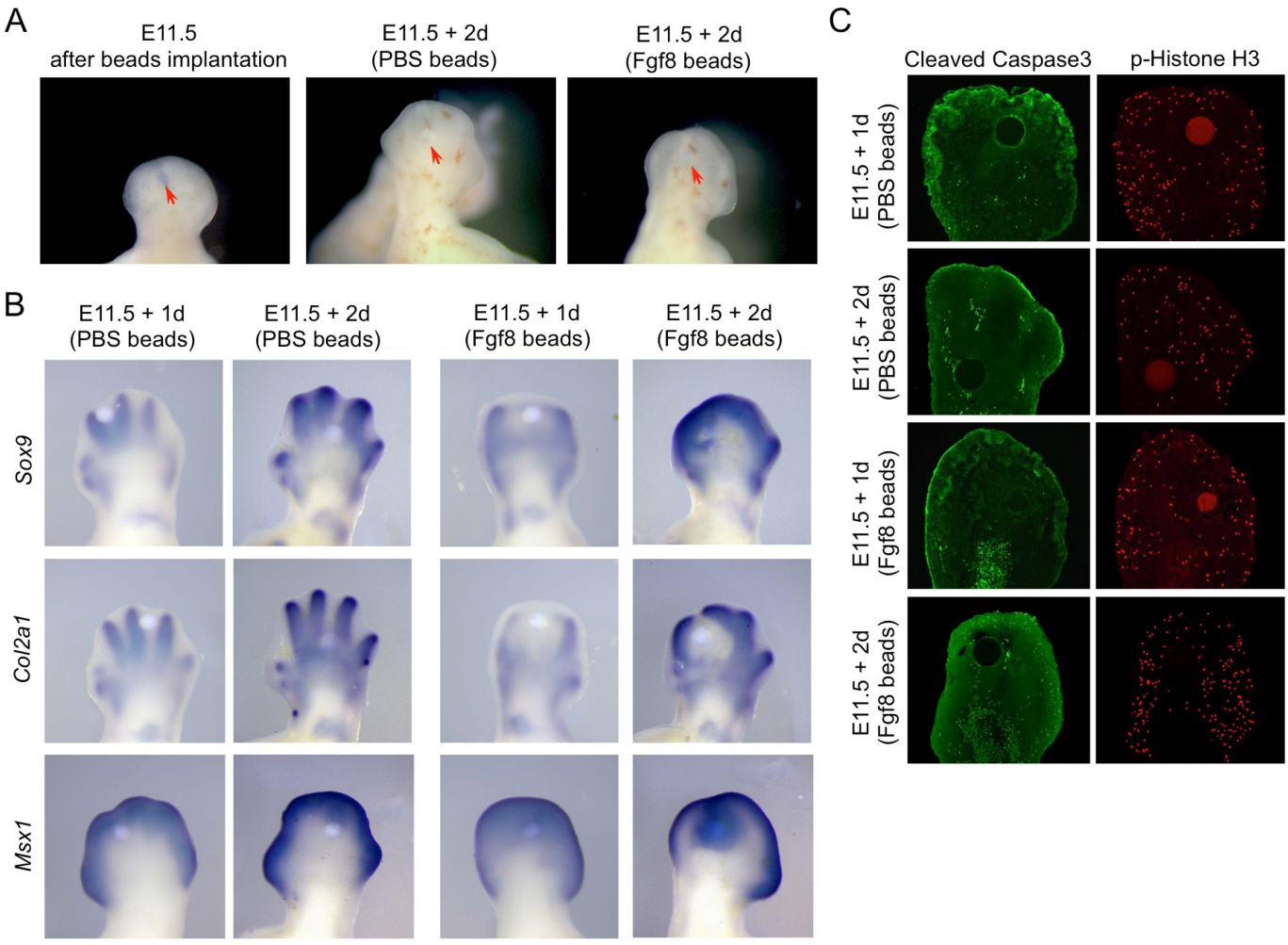

Limb culture with PBS or Fgf8 beads. (A) Appearance of mouse forelimbs before and after *ex vivo* culturing. PBS or Fgf8 beads (red arrows) were implanted between mesenchymal condensations at E11.5. (B) Normal gene expression shown by whole mount *in situ* hybridization of *Sox9*, *Col2a1*, *Msx1* of limb buds cultured for 1 or 2 days. Fgf8 beads inhibited chondrogenesis, caused digit bending and induced *Msx1* expression after 2-day culturing. (C) Immunofluorescent staining of cultured limbs showing similar pattern of apoptotic (green, cleaved caspase3) and proliferating cells (red, phospho Histone H3) with PBS or Fgf8 beads. Fgf8 beads did not cause altered proliferation or cell death.

Figure S4

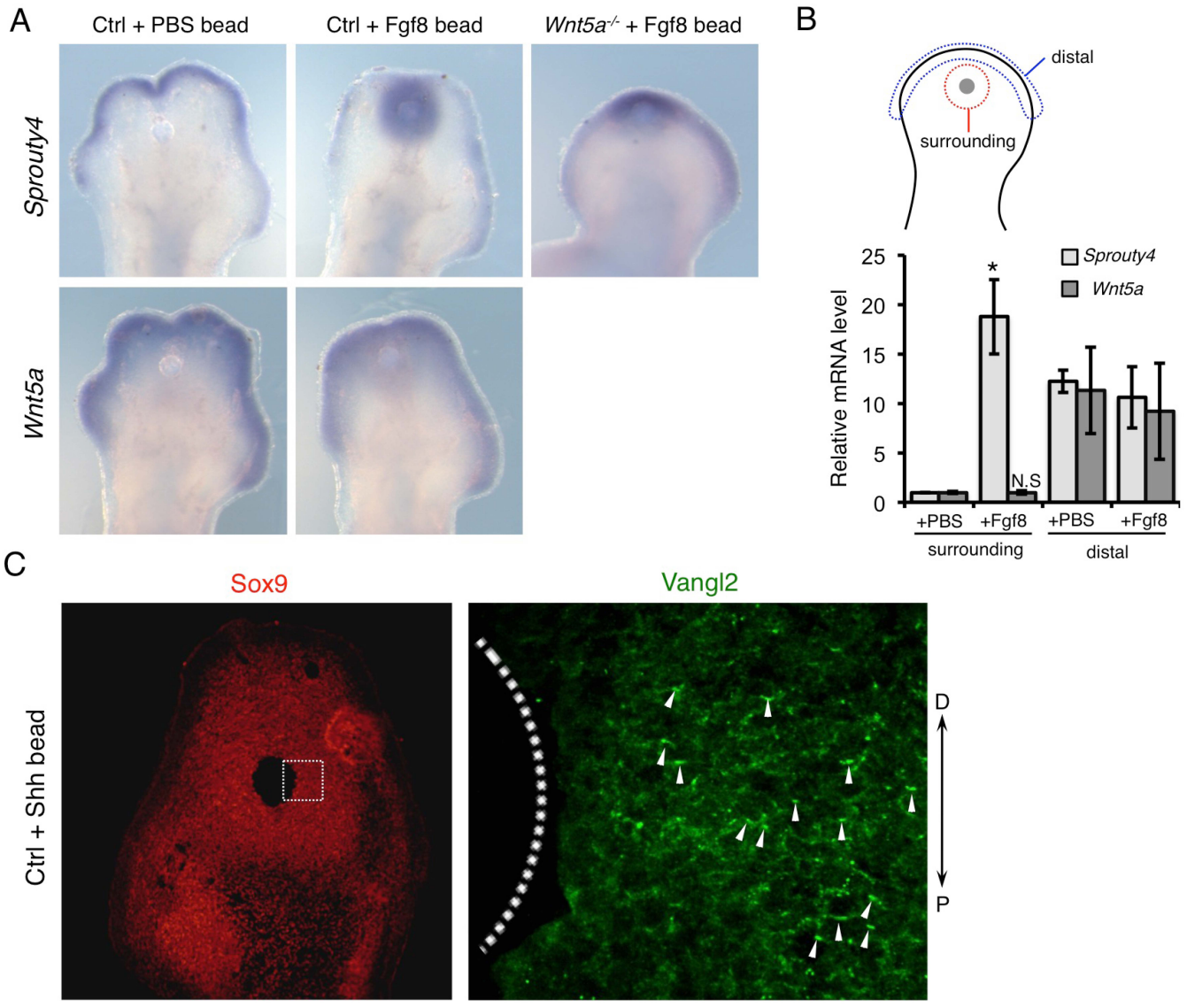

Analysis of cultured limbs (A) *Sprouty4* and *Wnt5a* whole mount *in situ* hybridization of cultured forelimbs implanted with PBS or Fgf8-soaked beads. (B) mRNA levels of *Sprouty4* and *Wnt5a* in tissues distal to (within the blue line) or surrounding (within the red circle) PBS or Fgf8 beads (grey dot) were analyzed by quantitative PCR (N=3). mRNA levels were normalized to *GAPDH* expression. Error bars are ± SD. Two-tailed *t* test, *p value =0.0146. N.S, no significance. (C) Sox9 (red) fluorescent immunostaining on cultured wild type limbs which were implanted with Shh-soaked beads and cultured for two days. The boxed region lateral to the bead was scanned by confocal microscope and representative images are shown in the right panel (Vangl2, green). The bead is outlined. Arrowheads point to some of asymmetrically localized Vangl2.

Figure S5

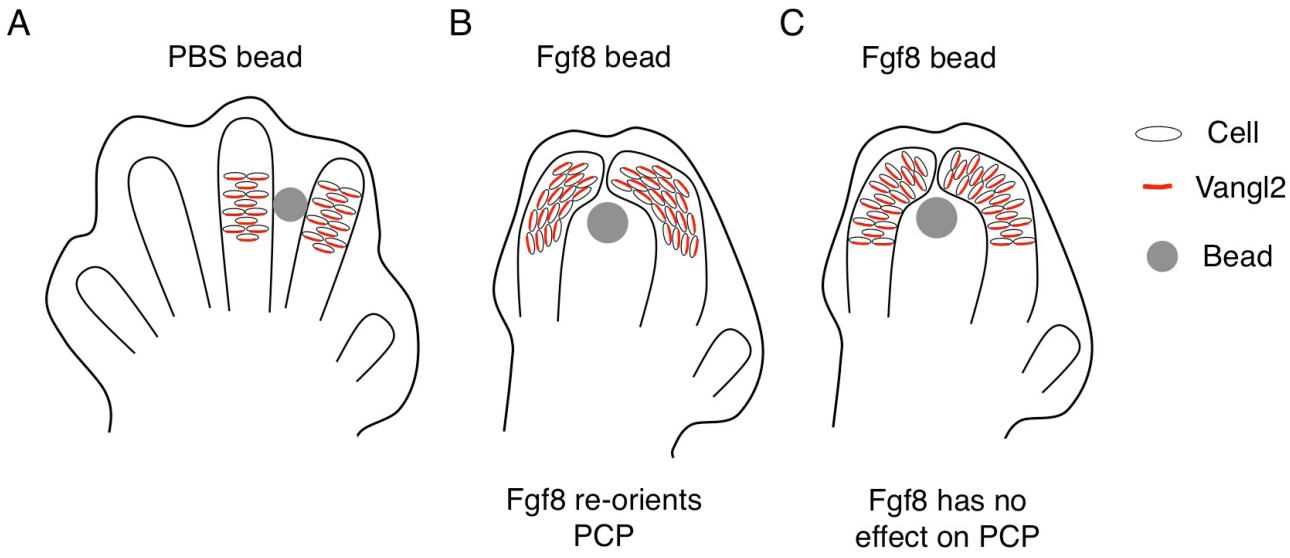

Schematics of beads experiment. (A) PBS bead does not change digit morphogenesis or PCP. Asymmetric localization of Vangl2 is shown along the axis of the digit outgrowth (proximal-distal axis). (B) and (C) Fgf8 bead implantation causes digit bending. Because our observed reorientation of asymmetric Vangl2 (B) is different from the expected Vangl2 localization pattern if Fgf8 has no effect on PCP (C), the digit bending is likely due to the combined effects of Fgf8 on both chondrogenesis and PCP.

Figure S6

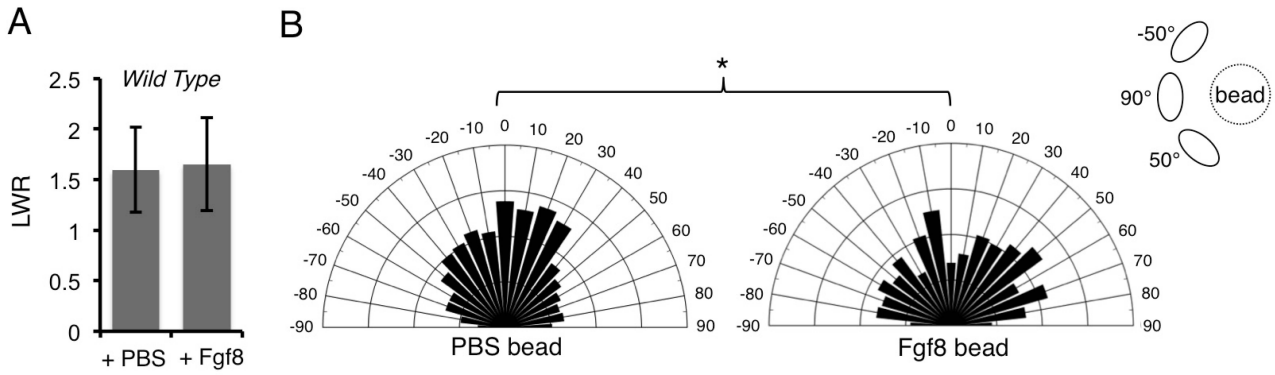

Analysis of Fgf8-regulated cell shape and orientation. (A) Statistical analysis of length-to-width ratio (LWR) of limb chondrocytes implanted with PBS or Fgf8 beads shown in Figure 2A . No significance between PBS and Fgf8 soaked beads (two-tailed *t* test). Error bars are ±SD. Analyzed cells: PBS beads, n=316; Fgf8 beads, n=274. (B) Schematic diagrams summarizing the quantification of cells orientation with implanted PBS or Fgf8 beads. x axis, angle of orientation; y axis, percentage of cells at angle x. kolmogorov smirnov test, *p value=0.0183. The inset show examples of cells surrounding the beads with different angles. Analyzed cells: PBS beads, n=615; Fgf8 beads, n=485.

Figure S7

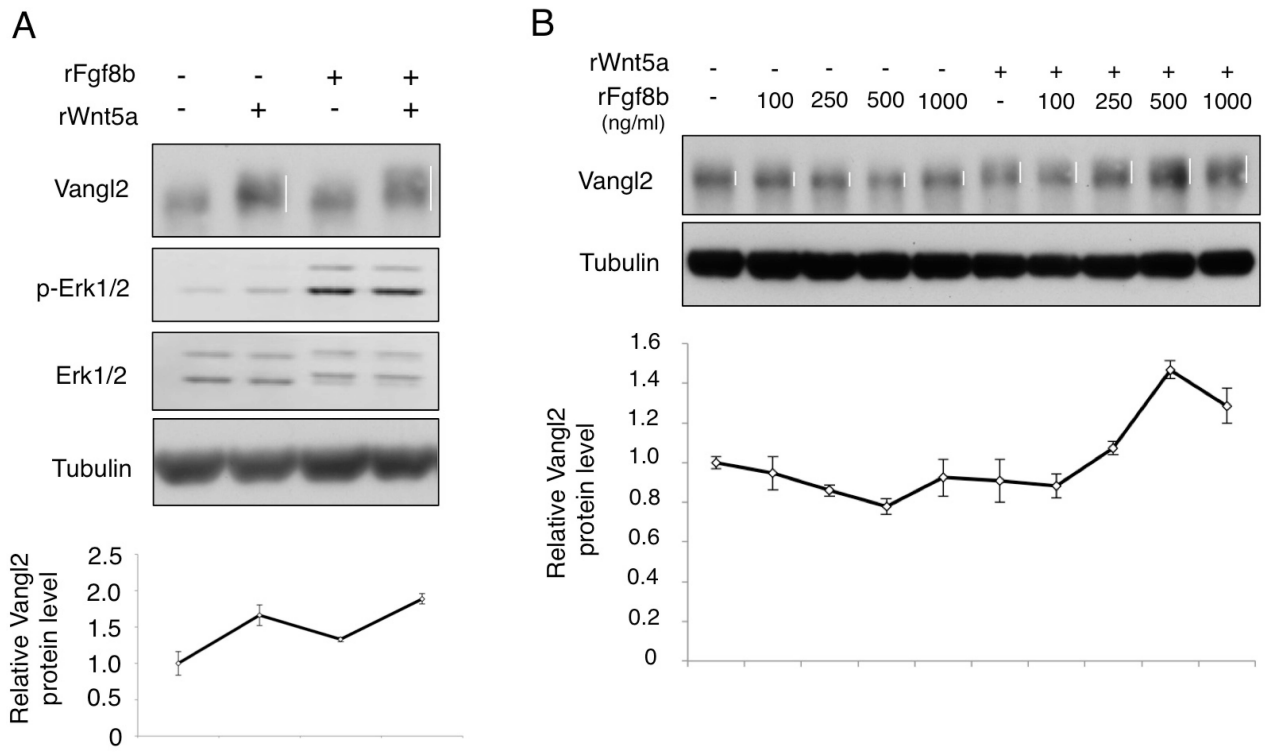

Fgf regulation of Vangl2. Vangl2 phosphorylation and protein level were analyzed in the cultured mesenchymal cells isolated from the E10.5~E11.5 mouse limb buds. Fgf8b recombinant proteins (250ng/ml) appeared to enhance Vangl2 phosphorylation induced by Wnt5a recombinant proteins (500ng/ml) (A) and in a dose-dependent manner (100ng/ml recombinant Wnt5a) (B). The white bars demarcate phosphorylation shift. The relative total Vangl2 protein level was quantified and shown in the lower panel. Fgf8b also enhanced the Vangl2 protein level in the presence of Wnt5a.

Figure S8

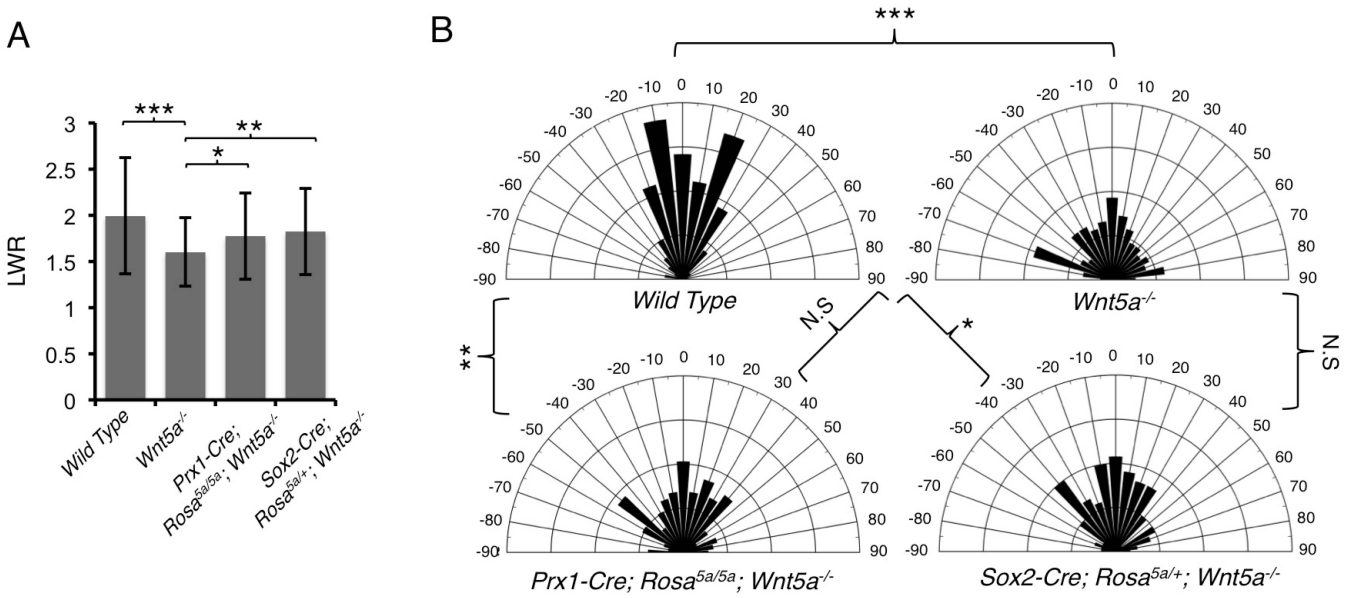

Analysis of cell shape and orientation with non-graded Wnt5a. (A) Statistical analysis of length-to-width ratio (LWR) of distal limb chondrocytes in E13.5 embryos in indicated genotypes. Significances between different genotypes are indicated (two-tailed *t* test, ***p<0.0001; **p=0.00066; *p=0.00576). Error bars are ±SD. Analyzed cells: wild type, n=165; *Wnt5a*$^{-/-}$, n=122; *Prx1-Cre; Rosa*$^{5a/5a}$*; Wnt5a*$^{-/-}$, n=84; *Sox2-Cre; Rosa*$^{5a/+}$*; Wnt5a*$^{-/-}$, n=75. (B) Schematic diagrams summarizing the quantification of cells orientation in each genotype. x axis, angle of orientation; y axis, percentage of cells at angle x. kolmogorov smirnov test, ***p value=0.0025; **p value=0.0144, *p value=0.0422. N.S, no significance (p value>0.05). Analyzed cells: wild type, n=99; *Wnt5a*$^{-/-}$, n=151; *Prx1-Cre; Rosa*$^{5a/5a}$*; Wnt5a*$^{-/-}$, n=175; *Sox2-Cre; Rosa*$^{5a/+}$*; Wnt5a*$^{-/-}$, n=121.

Figure S9

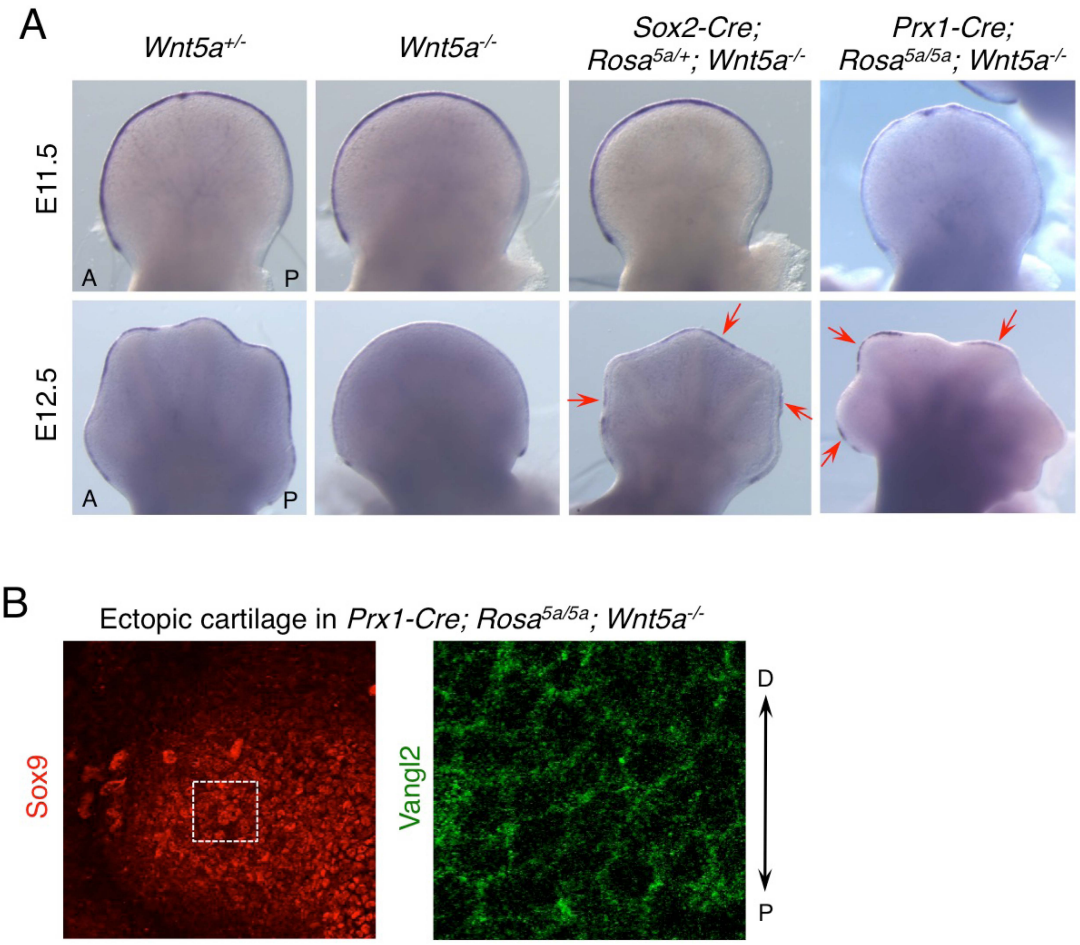

Analysis of mouse models with non-graded *Wnt5a* expression. (A) *Fgf8* expression in *Sox2-Cre;Rosa*$^{5a/+}$*;Wnt5a*$^{-/-}$ and *Prx1-Cre;Rosa*$^{5a/5a}$*;Wnt5a*$^{-/-}$ forelimbs (red arrows). A: anterior; P: posterior. (B) Representative images of fluorescent Immunostaining of Vangl2 (green) and Sox9 (red) in the Wnt5a-induced ectopic cartilage of *Prx1-Cre; Rosa*$^{5a/5a}$*; Wnt5a*$^{-/-}$ limbs. No Vangl2 asymmetric localization was observed. P: proximal; D: distal..

Figure S10

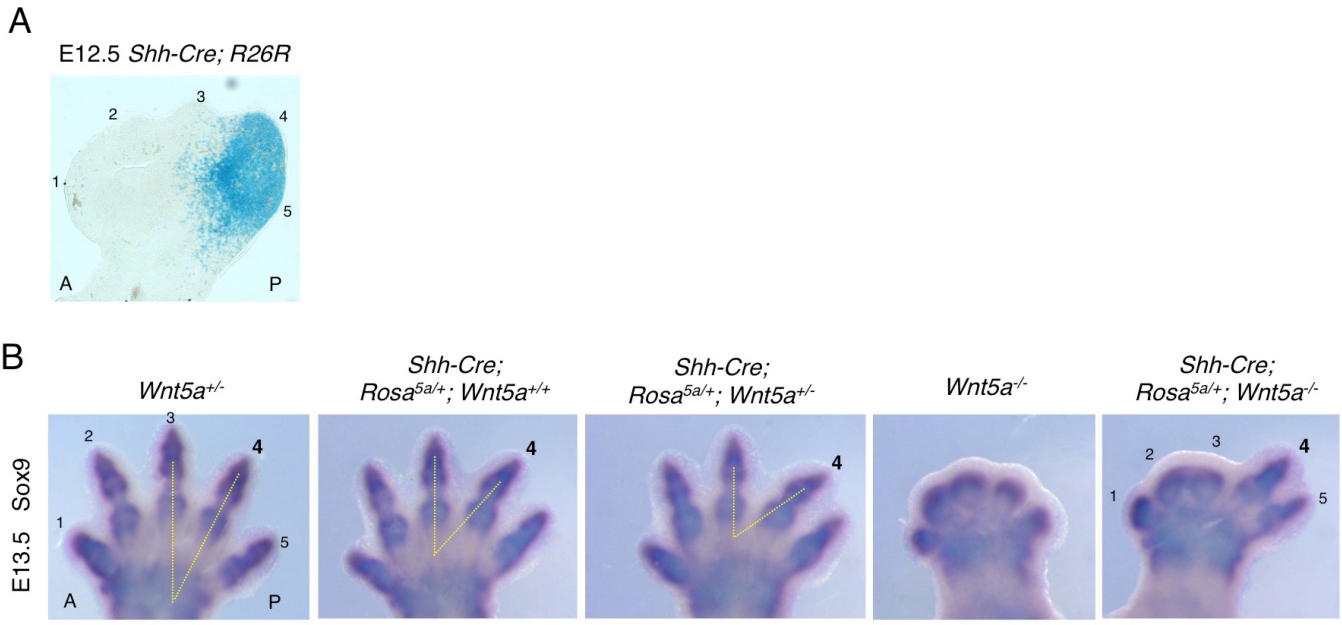

Reoriented *Wnt5a* expression gradient altered digit morphogenesis. (A) The cells derived from *Shh*-expressing cells are shown by X-gal staining of the E12.5 forelimb of the *Shh-Cre; R26R* embryo. Note that digit 3 is partially contributed by X-gal positive cells. (B) *Sox9* whole mount *in situ* hybridization in the mouse E13.5 forelimbs. The angles between longitudinal axes of digit 3 and bending distal part of the digit 4 (yellow dotted lines) were used to indicate the growth direction of digit 4. The increased angles suggest posteriorly biased growth deviation of digit 4 in *Shh Cre; Rosa*$^{5a/+}$*; Wnt5a*$^{+/+}$ and *Shh-Cre; Rosa*$^{5a/+}$*; Wnt5a*$^{+/-}$ compared to that in *Wnt5a*$^{+/-}$ control. Each digit is numbered. A: anterior; P: posterior.

Figure S11

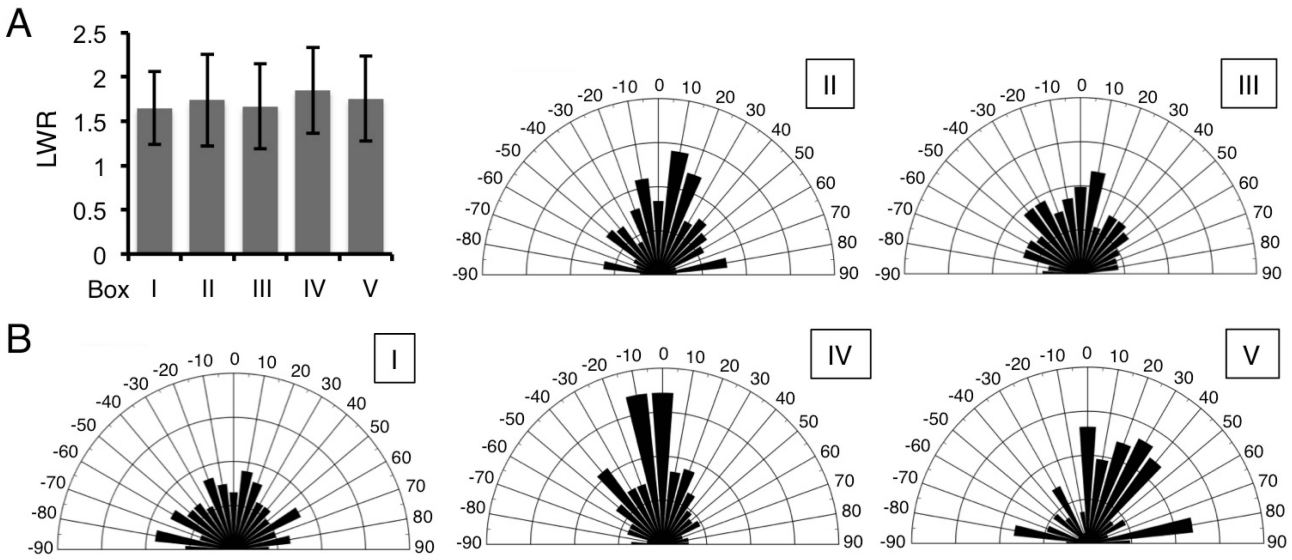

Analysis of cell shape and orientation with reoriented Wnt5a. (A) Length-to-width ratio (LWR) of chondrocytes of E12.5 *Shh-Cre;Rosa*$^{5a/+}$*;Wnt5a*$^{-/-}$ embryos shown in Figure 6A (boxed areas I-V). Error bars are ±SD. Analyzed cells: n=120 for area I; n=191 for area II; n=101 for area III; n=126 for area IV; n=50 for area V. (B) Schematic diagrams summarizing the quantification of cells orientation in each boxed area. x axis, angle of orientation; y axis, percentage of cells at angle x. Analyzed cells: n=251 for area I; n=239 for area II; n=203 for area III; n=211 for area IV; n=104 for area V.

Figure S12

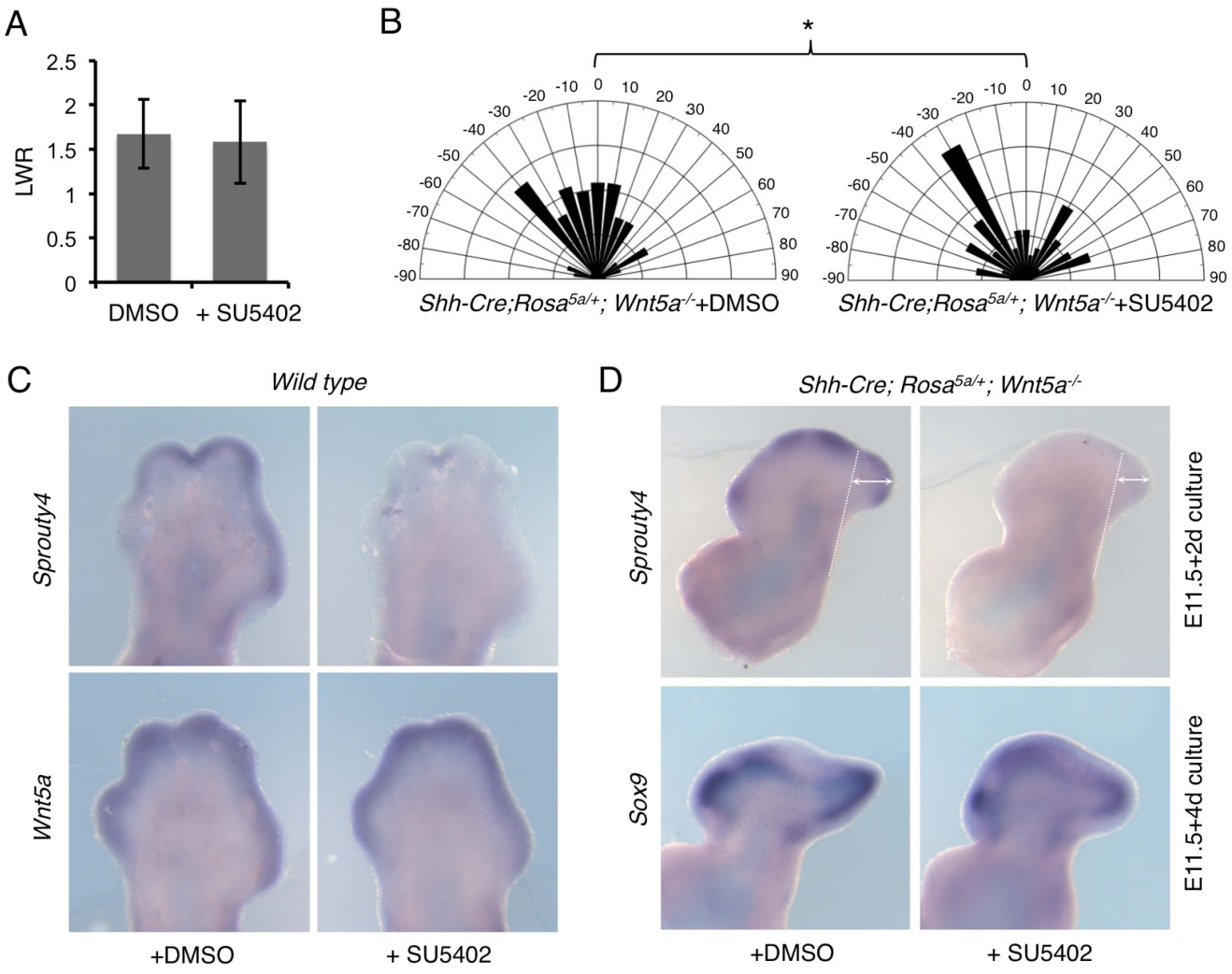

Inhibition of Fgf signaling in cultured limbs. (A) Statistical analysis of length-to-width ratio (LWR) of distal cells in the *Shh-Cre;Rosa*$^{5a/+}$*;Wnt5a*$^{-/-}$ cultured forelimbs with DMSO or SU5402 treatment. Error bars are ±SD. Analyzed cells: DMSO, n=134; SU5402, n=120. (B) Schematic diagrams summarizing the quantification of distal cells orientation in each group. x axis, angle of orientation; y axis, percentage of cells at angle x. kolmogorov smirnov test, *p value=0.0354. Analyzed cells: DMSO, n=111; SU5402, n=106. (C, D) *Sprouty 4, Wnt5a or Sox9* whole mount *in situ* hybridization in cultured limbs. SU5402 inhibited Fgf signaling, but not *Wnt5a* expression. (C) Wild type limb; (D) *Shh-Cre;Rosa*$^{5a/+}$*;Wnt5a*$^{-/-}$ limb. Double-headed arrows indicate the length of digit outgrowth, which was compromised in the *Shh-Cre;Rosa*$^{5a/+}$*;Wnt5a*$^{-/-}$ cultured forelimbs with SU5402 treatment. Dotted lines indicate the baseline of measurement. The difference is more obvious shown by *Sox9* whole mount *in situ* hybridization when the limbs were cultured for 4 days.

Figure S13

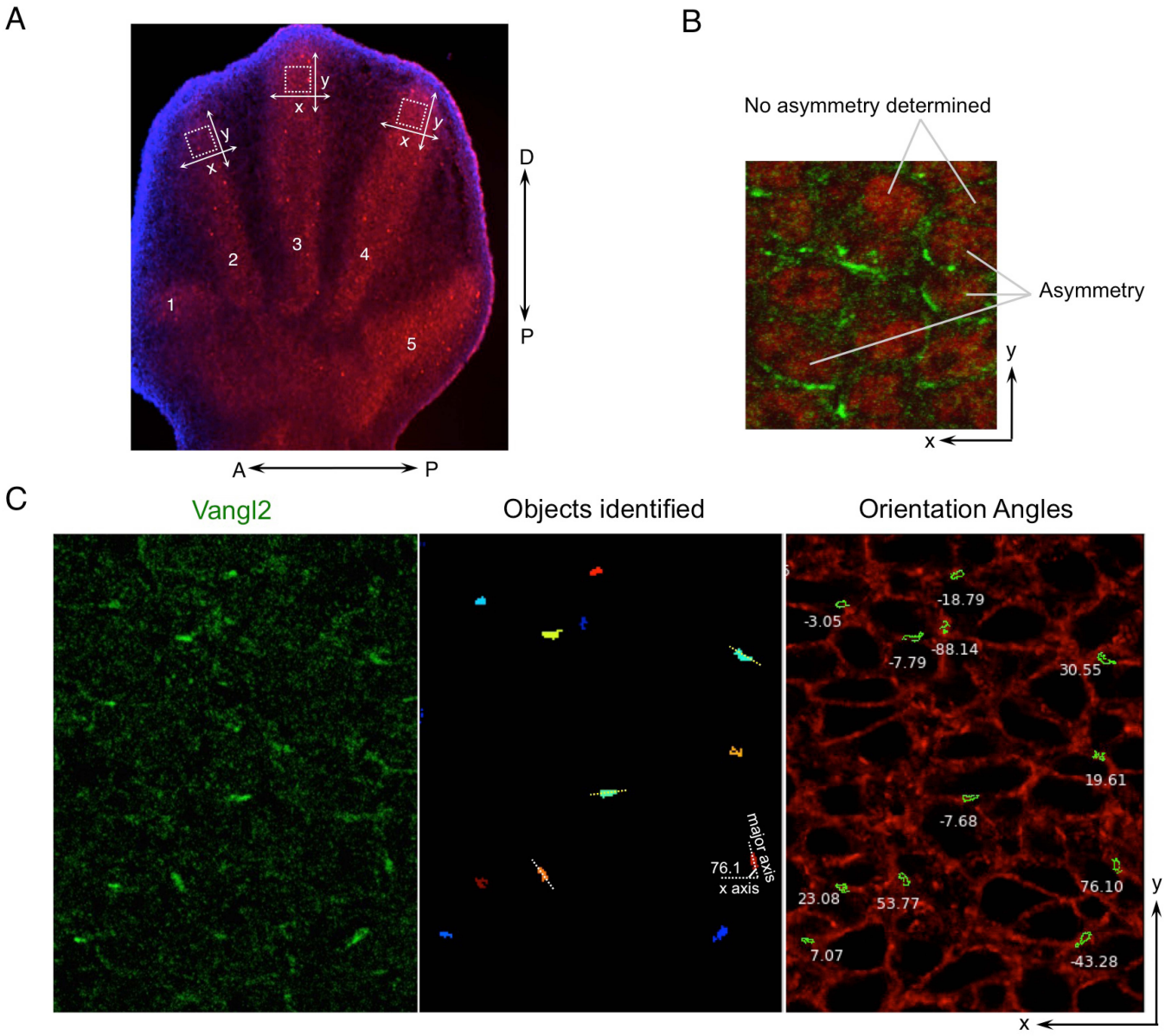

Quantification of Vangl2 orientation. (A) Schematics of vector placement to measure the Vangl2 and cell orientation. The longitudinal axes of the target digits were defined as the y axis. A-P and P-D are anterior-posterior and proximal-distal axis of the whole limb, respectively. The boxed areas were scanned. Digits 1-5 are labeled. (B) Examples of cells with “Asymmetry” or “No asymmetry determined”. “Asymmetry” means a cell has Vangl2 polarized to any direction. “No asymmetry determined” means a cell has no polarized Vangl2. (C) A confocal scanning picture of Vangl2 staining was analyzed by CellProfiler to identify the objects. The orientation was determined by the angle between the x axis and the major axis of the identified object (indicated by dotted lines in the middle picture). The angle was automatically measured by CellProfiler. The angle of each identified object was labeled, and the red signal was co-stained β-catenin to indicate the cell membrane.

Figure S14

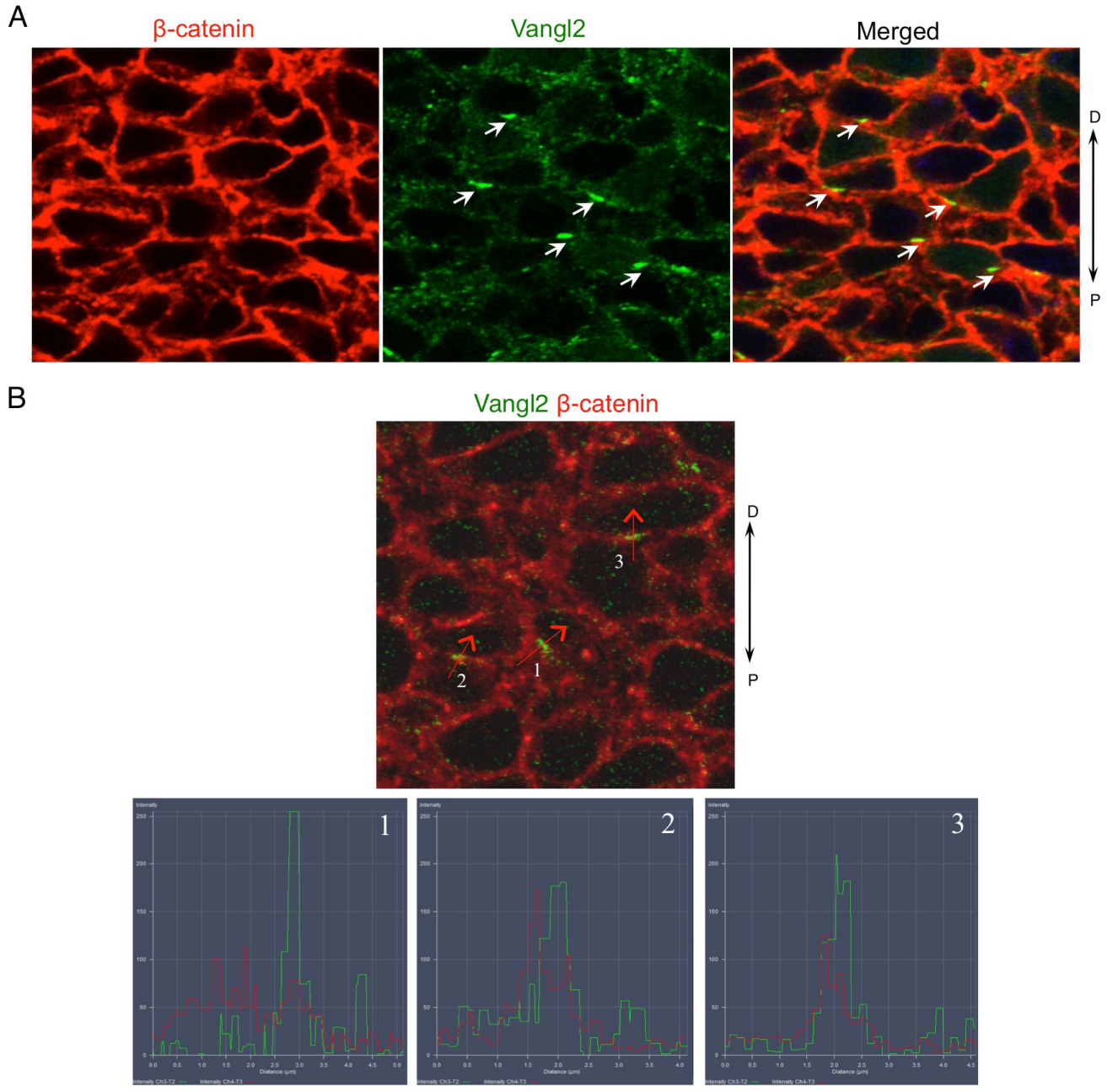

Localization of Vangl2. (A) In the distal limb, the localization of Vangl2 proteins on the membrane (arrows, green) of the cell of interest or its neighbor can be distinguished by its co-localization with β–catenin (red), which marked the cell membrane. (B) Line scan in the indicated proximal to distal direction (red arrows, #1-3) using ZEN 2012. The Vangl2 signal (green) is located to the distal side of the cell boundary shown by β–catenin signals (red), indicating that Vangl2 belongs to the distal cells and located to the proximal side of that distal cell. D-P, distal-proximal axis.

Figure S15

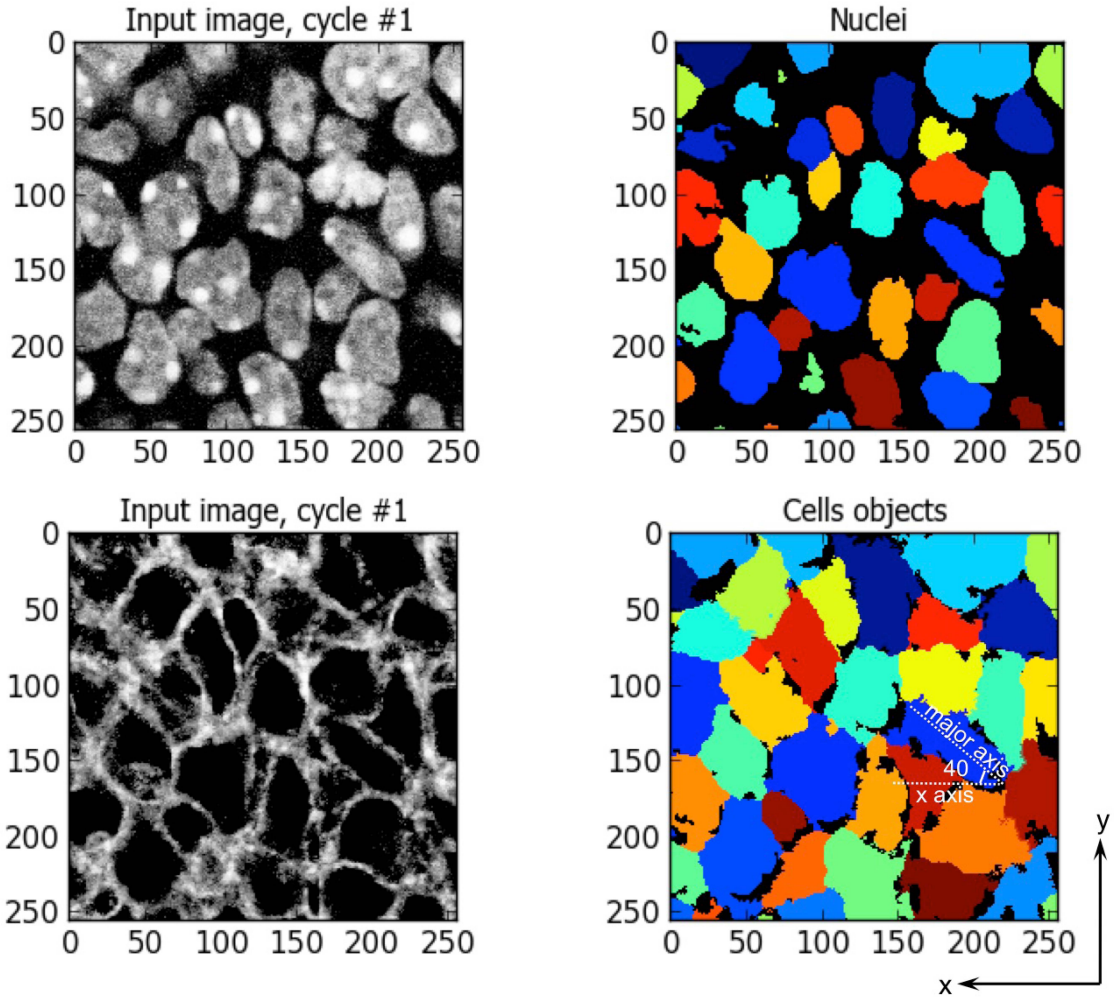

Measurement of cell shape and orientation. Illustration of cell morphology recognized by CellProfiler software. The nucleus of the cell (DAPI or Sox9 staining) was first recognized and imposed to the cell membrane (β-catenin staining) for generation of cell object, which will be subjected to cell shape and orientation analysis by CellProfiler. The orientation is determined by the angle between the x axis and the major axis (indicated by dotted line) of the identified object.

Figure S1

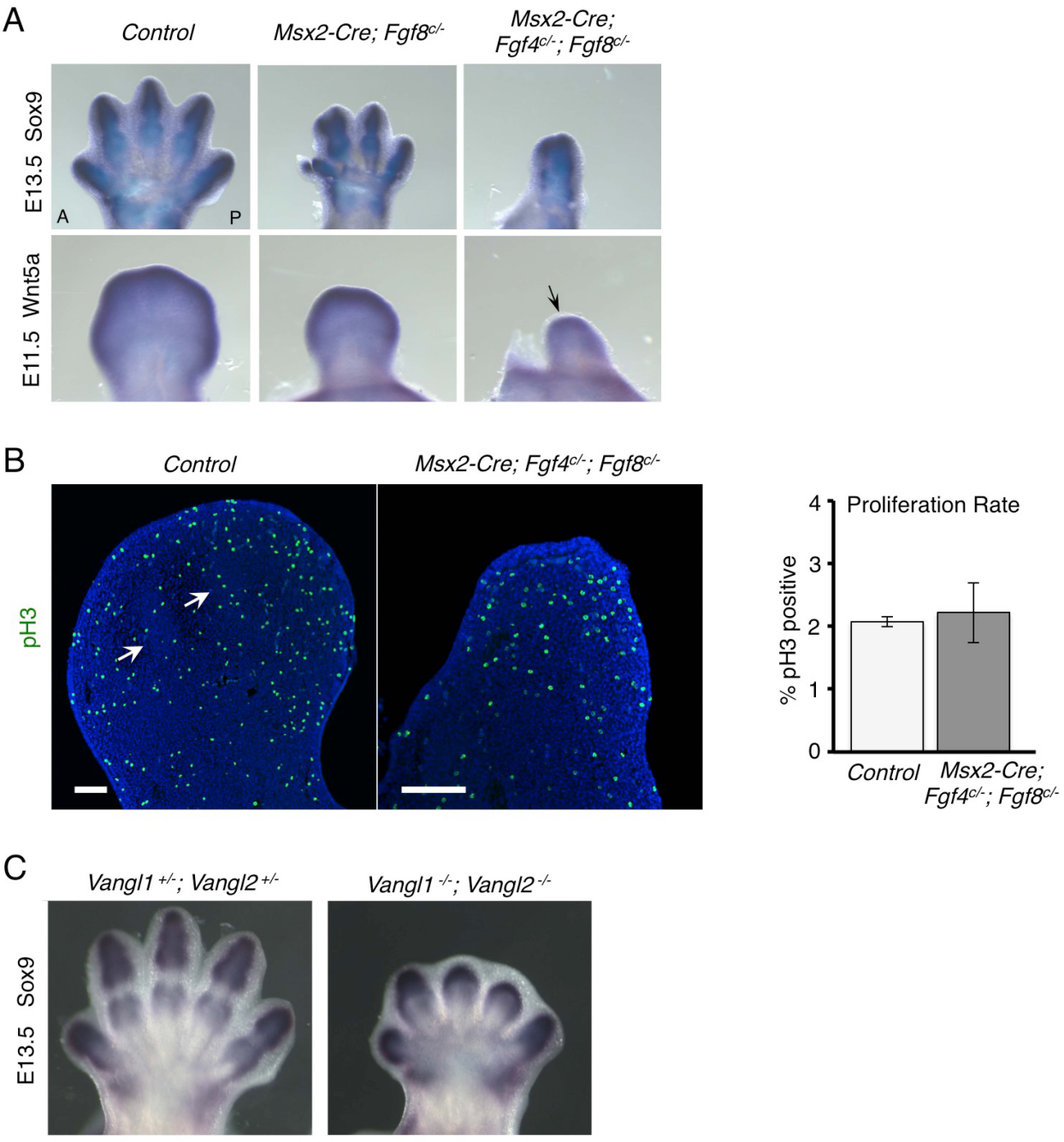

Analysis of *Fgf* and *Vangl* mutants. (A) Whole mount *in situ* hybridization of *Sox9* (upper panel) and *Wnt5a* (lower panel) on control and *Fgf* mutant embryonic forelimbs. Arrow points to the *Wnt5a* expression region of the *Msx2-Cre; Fgf4*$^{c/-}$*; Fgf8*$^{c/-}$ forelimb. (B) Immunodetection of phospho-histone H3 (Ser 10) in control and *Msx2-Cre; Fgf4*$^{c/-}$*; Fgf8*$^{c/-}$ distal forelimbs at E11.5 (44 som). Arrows point to forming digital rays. No statistically significant difference was found (two-tailed *t* test). (C) *Sox9* whole mount *in situ* hybridization in the mouse E13.5 forelimbs of control and *Vangl1/2* double mutant.

Figure S2

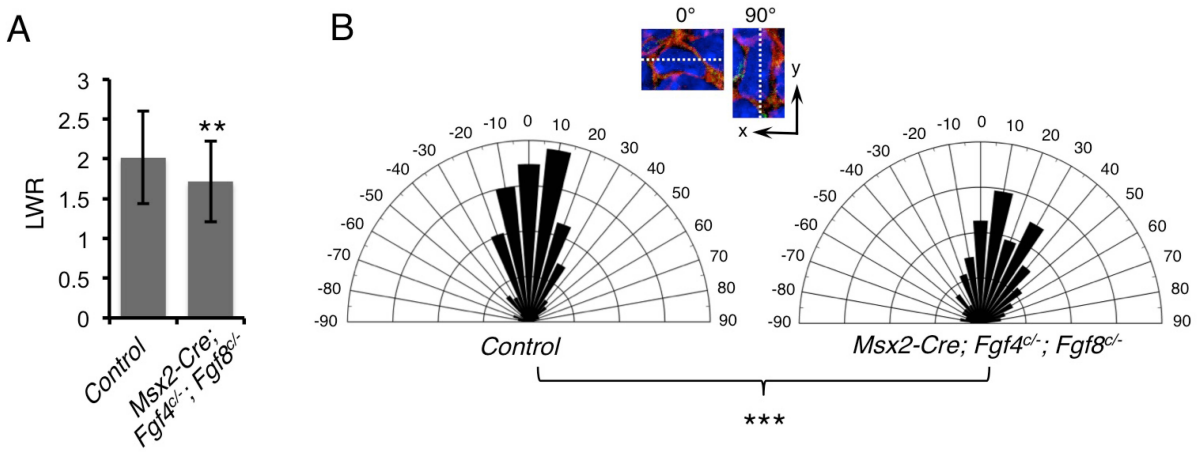

Analysis of Fgf4/8 mutant cell shape and orientation. (A) Statistical analysis of length-to-width ratio (LWR) of distal limb chondrocytes in E13.5 control and *Fgf4/8* double mutant shown in Figure 1B. Two-tailed *t* test, **p value=0.0012. Error bars are ±SD. Analyzed cells: control, n=46; *Msx2-Cre; Fgf4$^{c/-}$; Fgf8$^{c/-}$*, n=129. (B) Schematic diagrams summarizing the quantification of distal cells orientation in E13.5 control and *Fgf4/8* double mutant. The inset shows examples of cell orientation: 0°refers to the cell that orients horizontally, but 90°refers to the cell that orient vertically. The inset x and y axes were defined as shown in Figure 1B. Schematics x axis, angle of orientation; Schematics y axis, percentage of cells at angle x. kolmogorov smirnov test, ***p value=0.0004. Analyzed cells: control, n=167; *Msx2-Cre; Fgf4$^{c/-}$; Fgf8$^{c/-}$*, n=177.

Figure S3

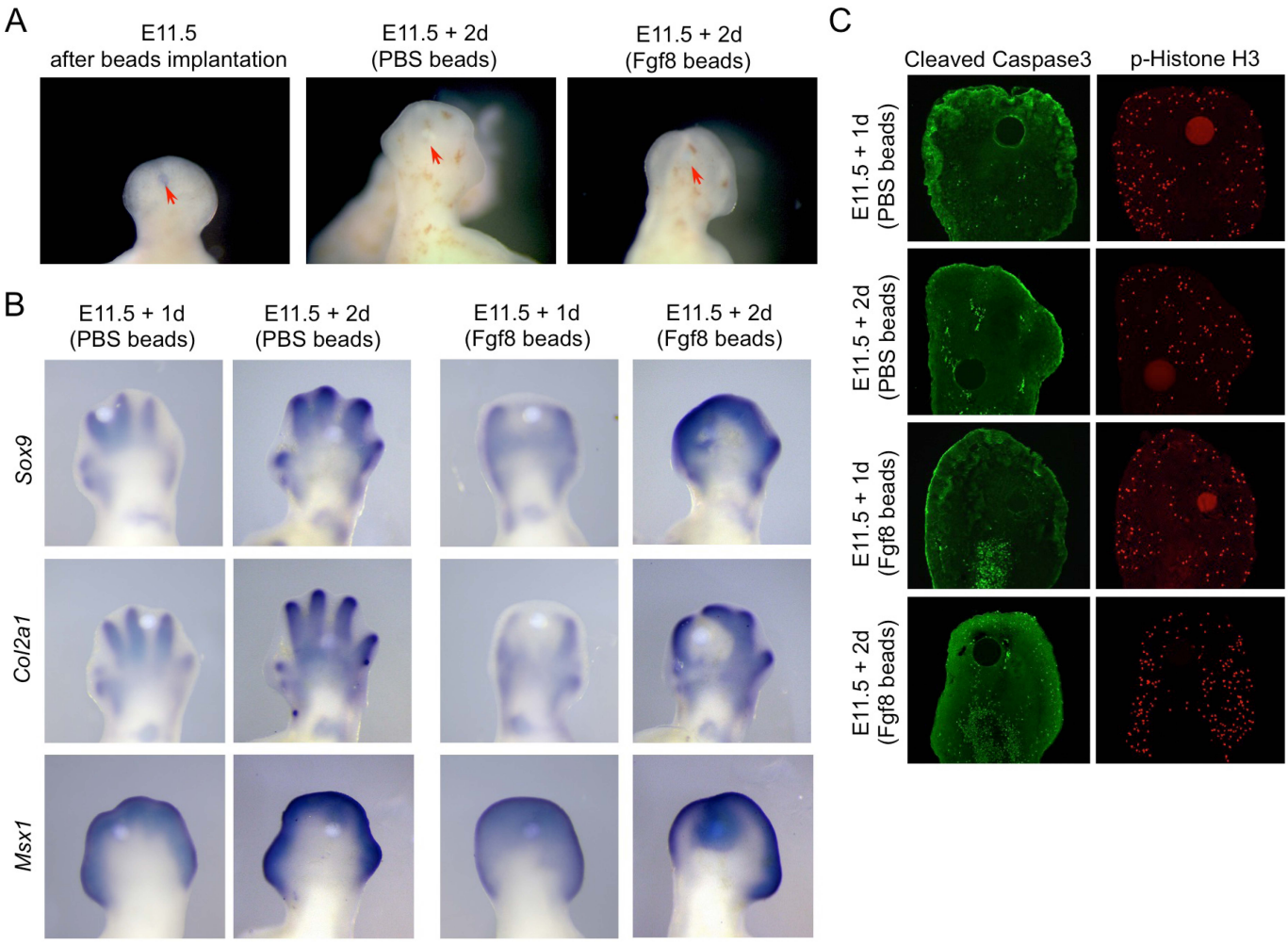

Limb culture with PBS or Fgf8 beads. (A) Appearance of mouse forelimbs before and after *ex vivo* culturing. PBS or Fgf8 beads (red arrows) were implanted between mesenchymal condensations at E11.5. (B) Normal gene expression shown by whole mount *in situ* hybridization of *Sox9*, *Col2a1*, *Msx1* of limb buds cultured for 1 or 2 days. Fgf8 beads inhibited chondrogenesis, caused digit bending and induced *Msx1* expression after 2-day culturing. (C) Immunofluorescent staining of cultured limbs showing similar pattern of apoptotic (green, cleaved caspase3) and proliferating cells (red, phospho Histone H3) with PBS or Fgf8 beads. Fgf8 beads did not cause altered proliferation or cell death.

Figure S4

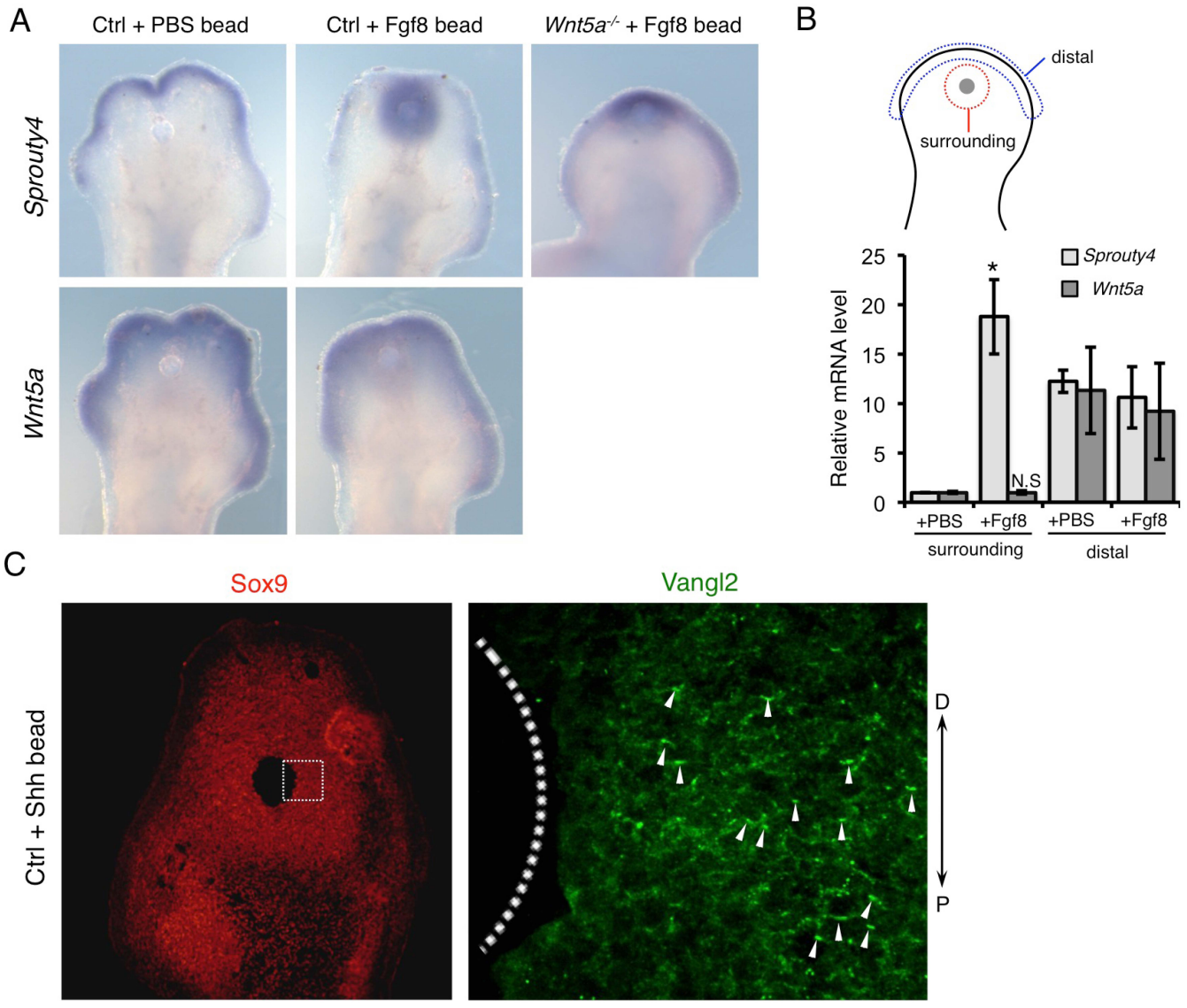

Analysis of cultured limbs (A) *Sprouty4* and *Wnt5a* whole mount *in situ* hybridization of cultured forelimbs implanted with PBS or Fgf8-soaked beads. (B) mRNA levels of *Sprouty4* and *Wnt5a* in tissues distal to (within the blue line) or surrounding (within the red circle) PBS or Fgf8 beads (grey dot) were analyzed by quantitative PCR (N=3). mRNA levels were normalized to *GAPDH* expression. Error bars are ± SD. Two-tailed *t* test, *p value =0.0146. N.S, no significance. (C) Sox9 (red) fluorescent immunostaining on cultured wild type limbs which were implanted with Shh-soaked beads and cultured for two days. The boxed region lateral to the bead was scanned by confocal microscope and representative images are shown in the right panel (Vangl2, green). The bead is outlined. Arrowheads point to some of asymmetrically localized Vangl2.

Figure S5

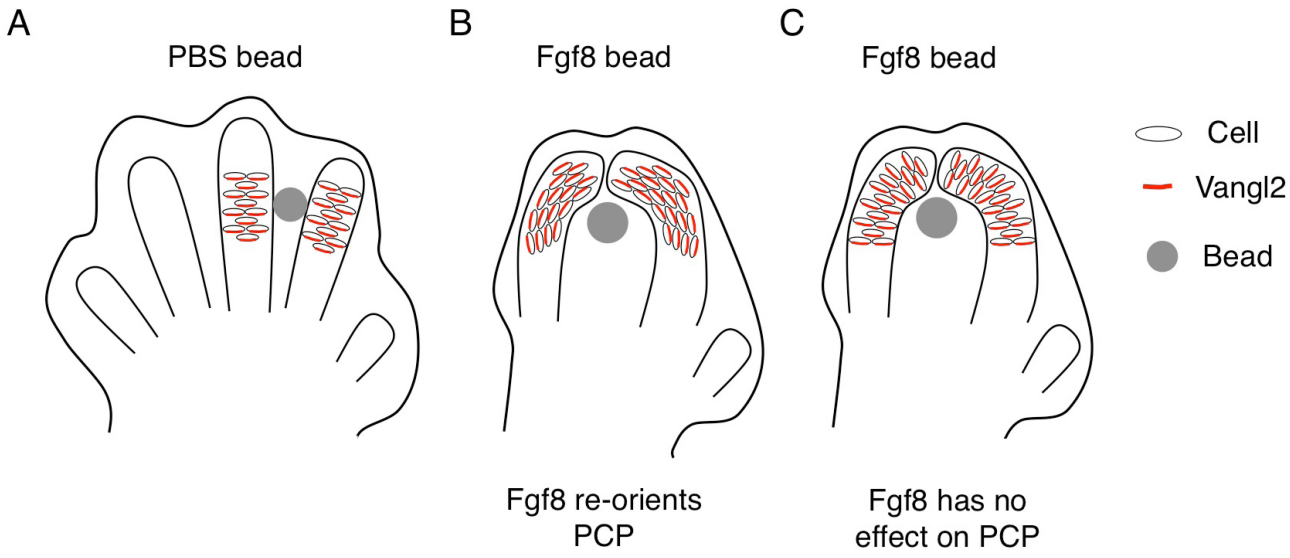

Schematics of beads experiment. (A) PBS bead does not change digit morphogenesis or PCP. Asymmetric localization of Vangl2 is shown along the axis of the digit outgrowth (proximal-distal axis). (B) and (C) Fgf8 bead implantation causes digit bending. Because our observed reorientation of asymmetric Vangl2 (B) is different from the expected Vangl2 localization pattern if Fgf8 has no effect on PCP (C), the digit bending is likely due to the combined effects of Fgf8 on both chondrogenesis and PCP.

Figure S6

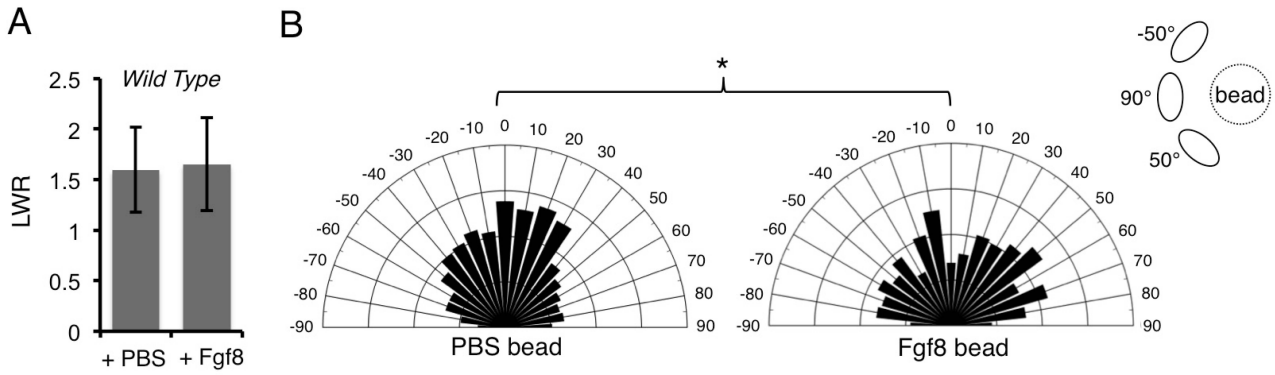

Analysis of Fgf8-regulated cell shape and orientation. (A) Statistical analysis of length-to-width ratio (LWR) of limb chondrocytes implanted with PBS or Fgf8 beads shown in Figure 2A . No significance between PBS and Fgf8 soaked beads (two-tailed *t* test). Error bars are ±SD. Analyzed cells: PBS beads, n=316; Fgf8 beads, n=274. (B) Schematic diagrams summarizing the quantification of cells orientation with implanted PBS or Fgf8 beads. x axis, angle of orientation; y axis, percentage of cells at angle x. kolmogorov smirnov test, *p value=0.0183. The inset show examples of cells surrounding the beads with different angles. Analyzed cells: PBS beads, n=615; Fgf8 beads, n=485.

Figure S7

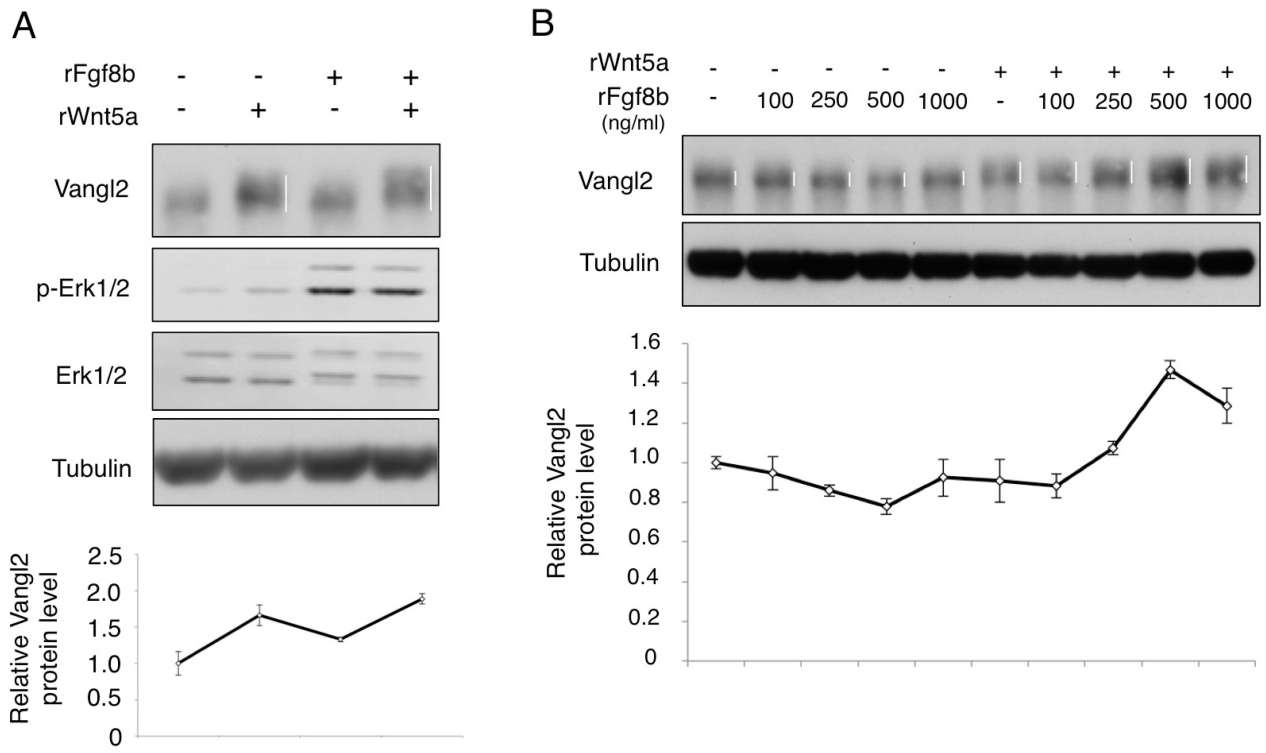

Fgf regulation of Vangl2. Vangl2 phosphorylation and protein level were analyzed in the cultured mesenchymal cells isolated from the E10.5~E11.5 mouse limb buds. Fgf8b recombinant proteins (250ng/ml) appeared to enhance Vangl2 phosphorylation induced by Wnt5a recombinant proteins (500ng/ml) (A) and in a dose-dependent manner (100ng/ml recombinant Wnt5a) (B). The white bars demarcate phosphorylation shift. The relative total Vangl2 protein level was quantified and shown in the lower panel. Fgf8b also enhanced the Vangl2 protein level in the presence of Wnt5a.

Figure S8

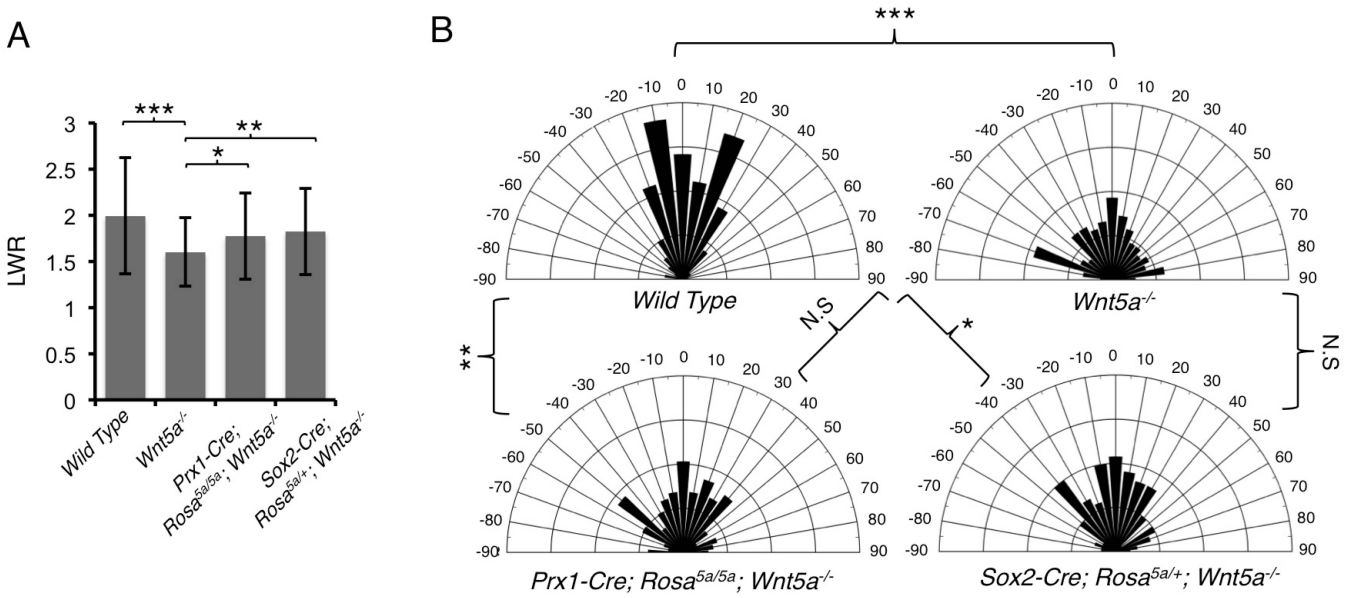

Analysis of cell shape and orientation with non-graded Wnt5a. (A) Statistical analysis of length-to-width ratio (LWR) of distal limb chondrocytes in E13.5 embryos in indicated genotypes. Significances between different genotypes are indicated (two-tailed *t* test, ***p<0.0001; **p=0.00066; *p=0.00576). Error bars are ±SD. Analyzed cells: wild type, n=165; *Wnt5a*$^{-/-}$, n=122; *Prx1-Cre; Rosa*$^{5a/5a}$*; Wnt5a*$^{-/-}$, n=84; *Sox2-Cre; Rosa*$^{5a/+}$*; Wnt5a*$^{-/-}$, n=75. (B) Schematic diagrams summarizing the quantification of cells orientation in each genotype. x axis, angle of orientation; y axis, percentage of cells at angle x. kolmogorov smirnov test, ***p value=0.0025; **p value=0.0144, *p value=0.0422. N.S, no significance (p value>0.05). Analyzed cells: wild type, n=99; *Wnt5a*$^{-/-}$, n=151; *Prx1-Cre; Rosa*$^{5a/5a}$*; Wnt5a*$^{-/-}$, n=175; *Sox2-Cre; Rosa*$^{5a/+}$*; Wnt5a*$^{-/-}$, n=121.

Figure S9

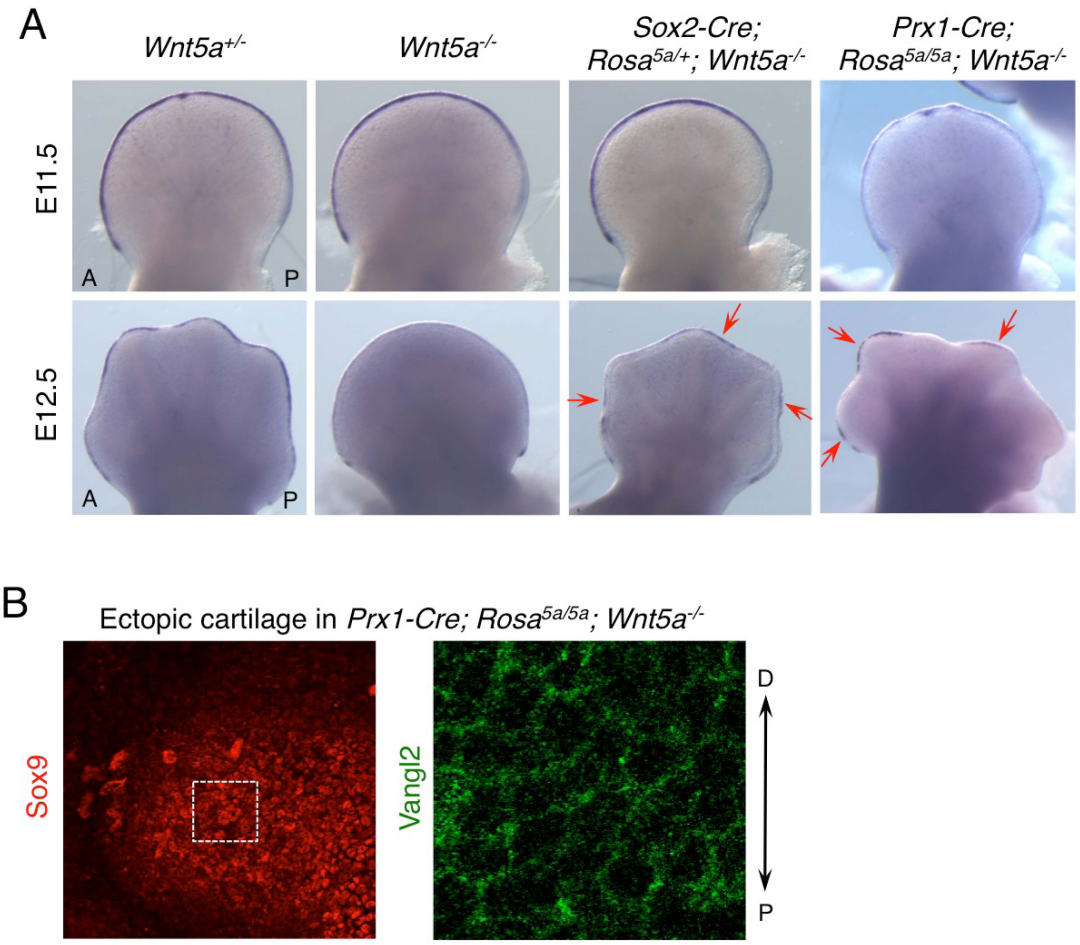

Analysis of mouse models with non-graded *Wnt5a* expression. (A) *Fgf8* expression in *Sox2-Cre;Rosa*$^{5a/+}$*;Wnt5a*$^{-/-}$ and *Prx1-Cre;Rosa*$^{5a/5a}$*;Wnt5a*$^{-/-}$ forelimbs (red arrows). A: anterior; P: posterior. (B) Representative images of fluorescent Immunostaining of Vangl2 (green) and Sox9 (red) in the Wnt5a-induced ectopic cartilage of *Prx1-Cre; Rosa*$^{5a/5a}$*; Wnt5a*$^{-/-}$ limbs. No Vangl2 asymmetric localization was observed. P: proximal; D: distal..

Figure S10

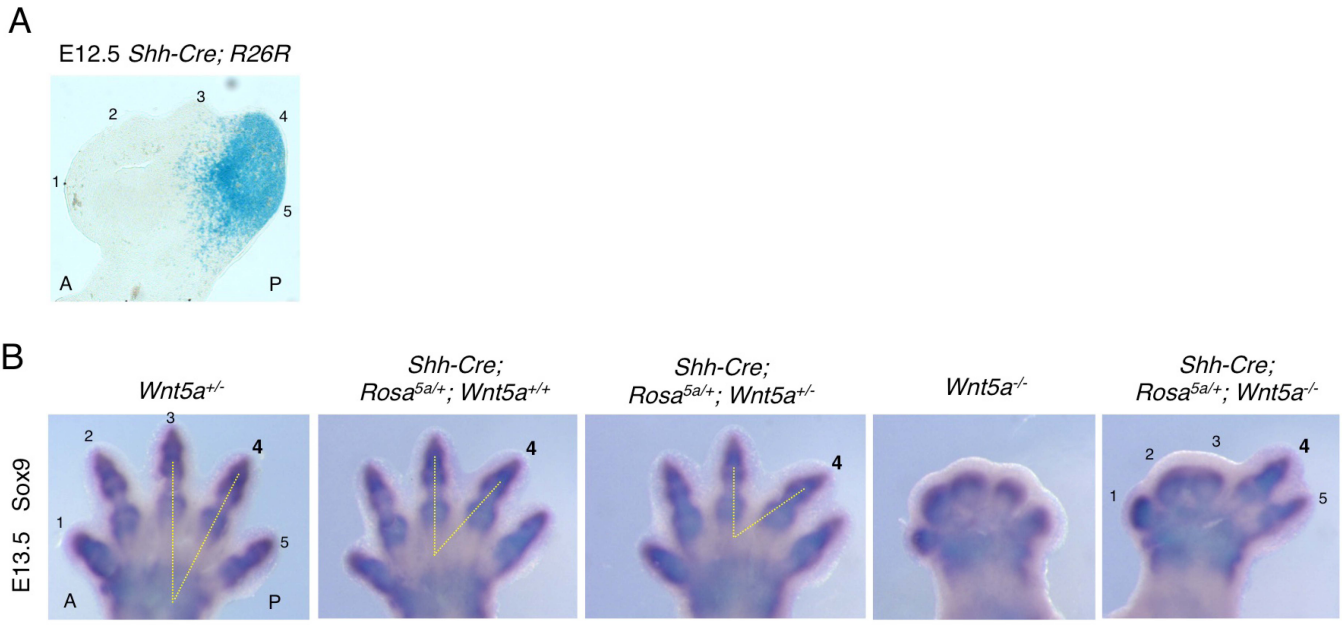

Reoriented *Wnt5a* expression gradient altered digit morphogenesis. (A) The cells derived from *Shh*-expressing cells are shown by X-gal staining of the E12.5 forelimb of the *Shh-Cre; R26R* embryo. Note that digit 3 is partially contributed by X-gal positive cells. (B) *Sox9* whole mount *in situ* hybridization in the mouse E13.5 forelimbs. The angles between longitudinal axes of digit 3 and bending distal part of the digit 4 (yellow dotted lines) were used to indicate the growth direction of digit 4. The increased angles suggest posteriorly biased growth deviation of digit 4 in *Shh Cre; Rosa*$^{5a/+}$*; Wnt5a*$^{+/+}$ and *Shh-Cre; Rosa*$^{5a/+}$*; Wnt5a*$^{+/-}$ compared to that in *Wnt5a*$^{+/-}$ control. Each digit is numbered. A: anterior; P: posterior.

Figure S11

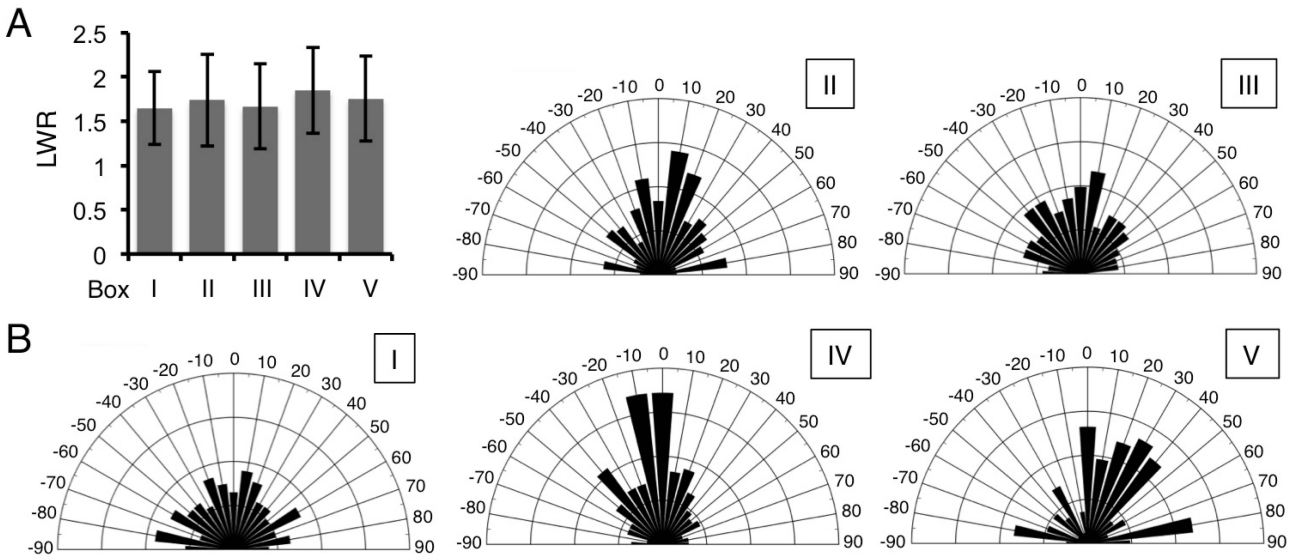

Analysis of cell shape and orientation with reoriented Wnt5a. (A) Length-to-width ratio (LWR) of chondrocytes of E12.5 *Shh-Cre;Rosa*$^{5a/+}$*;Wnt5a*$^{-/-}$ embryos shown in Figure 6A (boxed areas I-V). Error bars are ±SD. Analyzed cells: n=120 for area I; n=191 for area II; n=101 for area III; n=126 for area IV; n=50 for area V. (B) Schematic diagrams summarizing the quantification of cells orientation in each boxed area. x axis, angle of orientation; y axis, percentage of cells at angle x. Analyzed cells: n=251 for area I; n=239 for area II; n=203 for area III; n=211 for area IV; n=104 for area V.

Figure S12

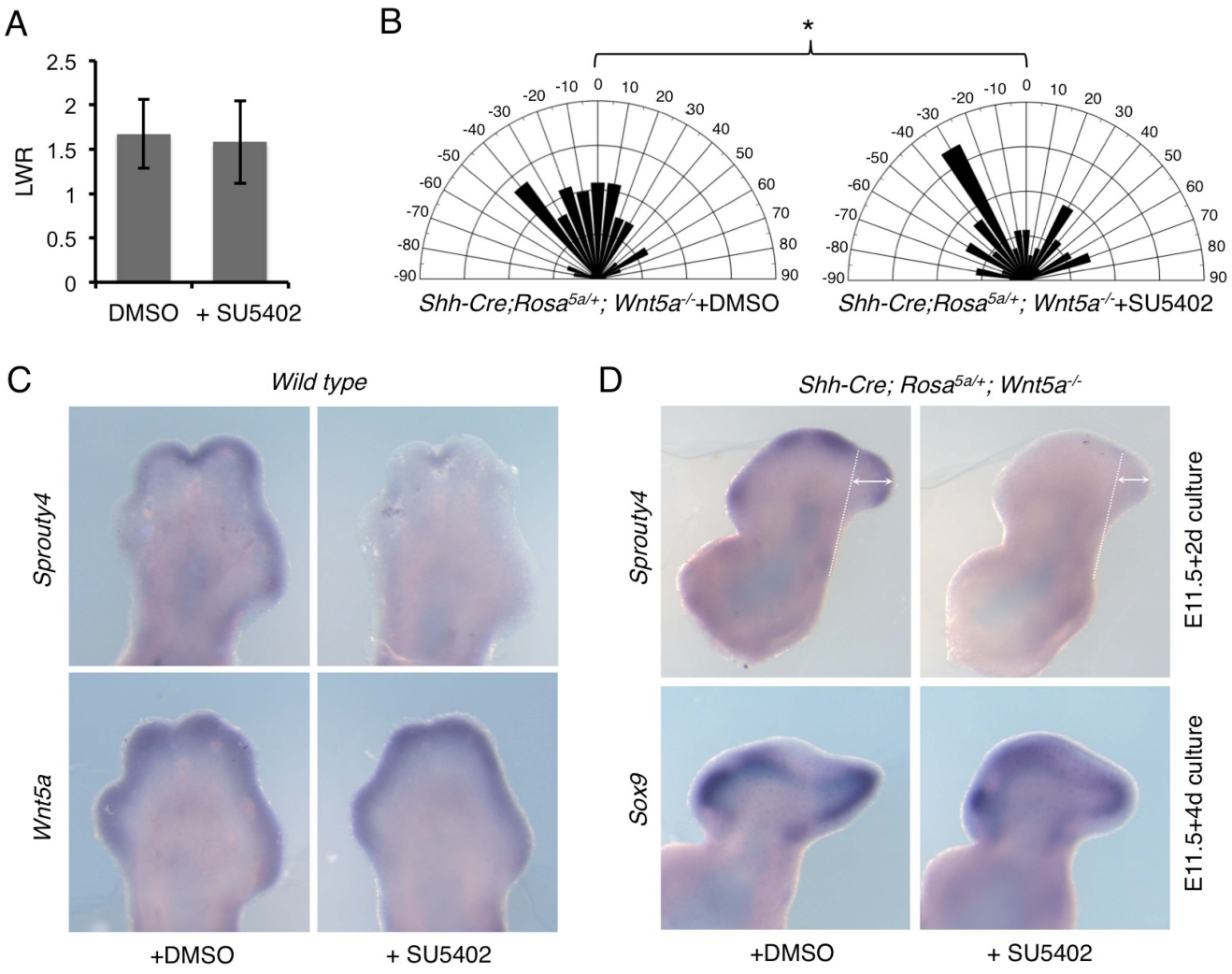

Inhibition of Fgf signaling in cultured limbs. (A) Statistical analysis of length-to-width ratio (LWR) of distal cells in the *Shh-Cre;Rosa*$^{5a/+}$*;Wnt5a*$^{-/-}$ cultured forelimbs with DMSO or SU5402 treatment. Error bars are ±SD. Analyzed cells: DMSO, n=134; SU5402, n=120. (B) Schematic diagrams summarizing the quantification of distal cells orientation in each group. x axis, angle of orientation; y axis, percentage of cells at angle x. kolmogorov smirnov test, *p value=0.0354. Analyzed cells: DMSO, n=111; SU5402, n=106. (C, D) *Sprouty 4, Wnt5a or Sox9* whole mount *in situ* hybridization in cultured limbs. SU5402 inhibited Fgf signaling, but not *Wnt5a* expression. (C) Wild type limb; (D) *Shh-Cre;Rosa*$^{5a/+}$*;Wnt5a*$^{-/-}$ limb. Double-headed arrows indicate the length of digit outgrowth, which was compromised in the *Shh-Cre;Rosa*$^{5a/+}$*;Wnt5a*$^{-/-}$ cultured forelimbs with SU5402 treatment. Dotted lines indicate the baseline of measurement. The difference is more obvious shown by *Sox9* whole mount *in situ* hybridization when the limbs were cultured for 4 days.

Figure S13

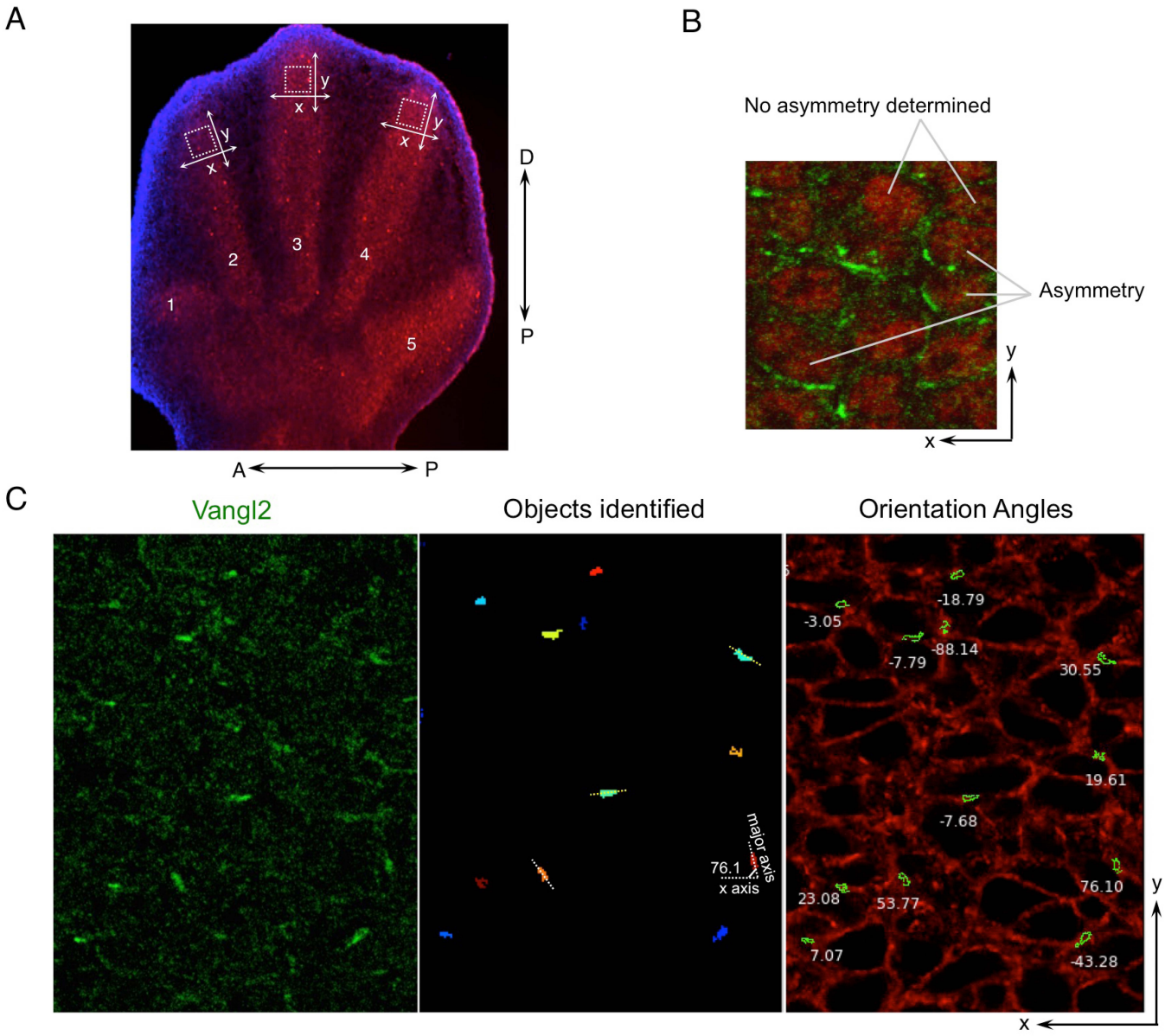

Quantification of Vangl2 orientation. (A) Schematics of vector placement to measure the Vangl2 and cell orientation. The longitudinal axes of the target digits were defined as the y axis. A-P and P-D are anterior-posterior and proximal-distal axis of the whole limb, respectively. The boxed areas were scanned. Digits 1-5 are labeled. (B) Examples of cells with “Asymmetry” or “No asymmetry determined”. “Asymmetry” means a cell has Vangl2 polarized to any direction. “No asymmetry determined” means a cell has no polarized Vangl2. (C) A confocal scanning picture of Vangl2 staining was analyzed by CellProfiler to identify the objects. The orientation was determined by the angle between the x axis and the major axis of the identified object (indicated by dotted lines in the middle picture). The angle was automatically measured by CellProfiler. The angle of each identified object was labeled, and the red signal was co-stained β-catenin to indicate the cell membrane.

Figure S14

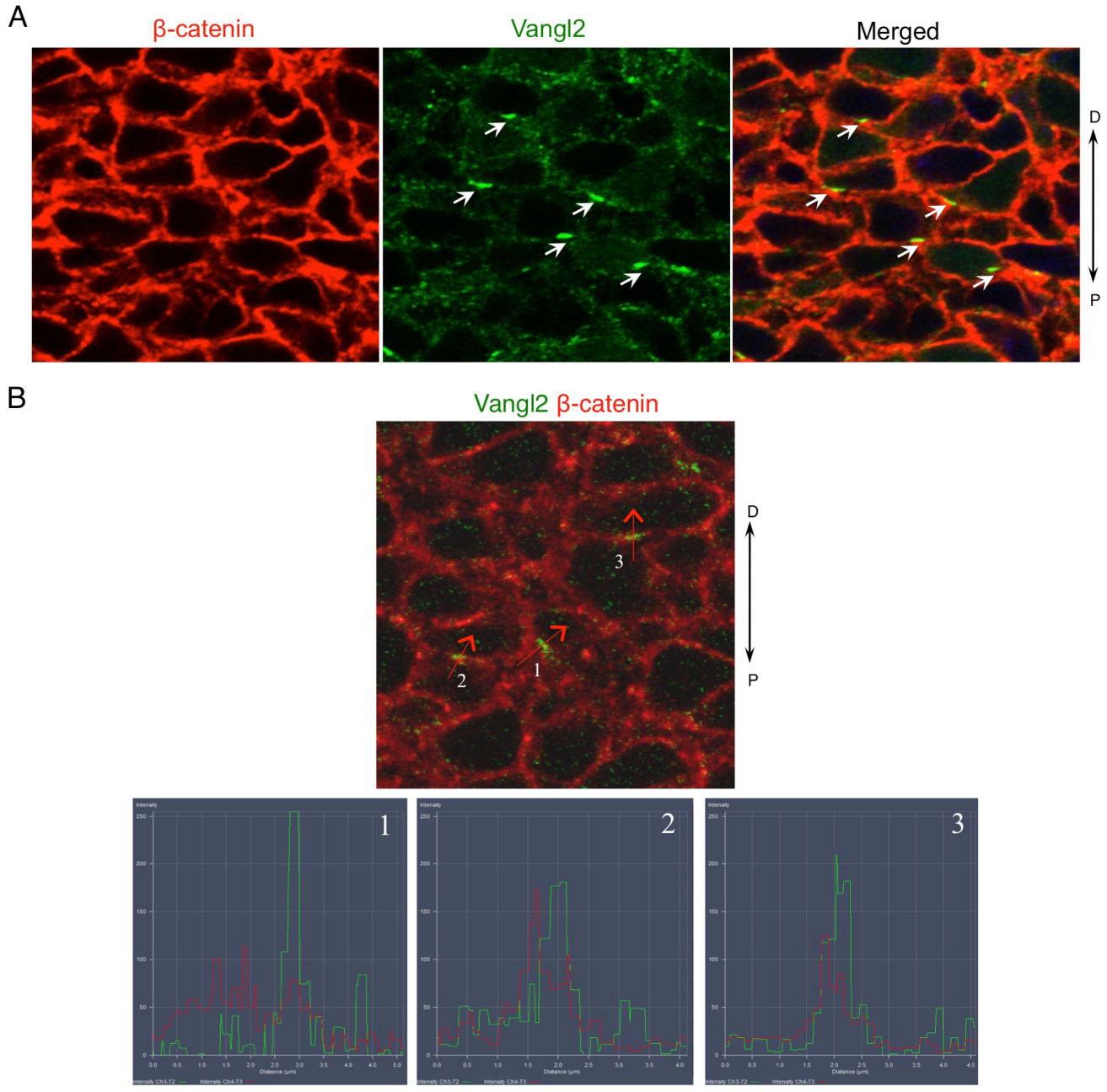

Localization of Vangl2. (A) In the distal limb, the localization of Vangl2 proteins on the membrane (arrows, green) of the cell of interest or its neighbor can be distinguished by its co-localization with β–catenin (red), which marked the cell membrane. (B) Line scan in the indicated proximal to distal direction (red arrows, #1-3) using ZEN 2012. The Vangl2 signal (green) is located to the distal side of the cell boundary shown by β–catenin signals (red), indicating that Vangl2 belongs to the distal cells and located to the proximal side of that distal cell. D-P, distal-proximal axis.

Figure S15

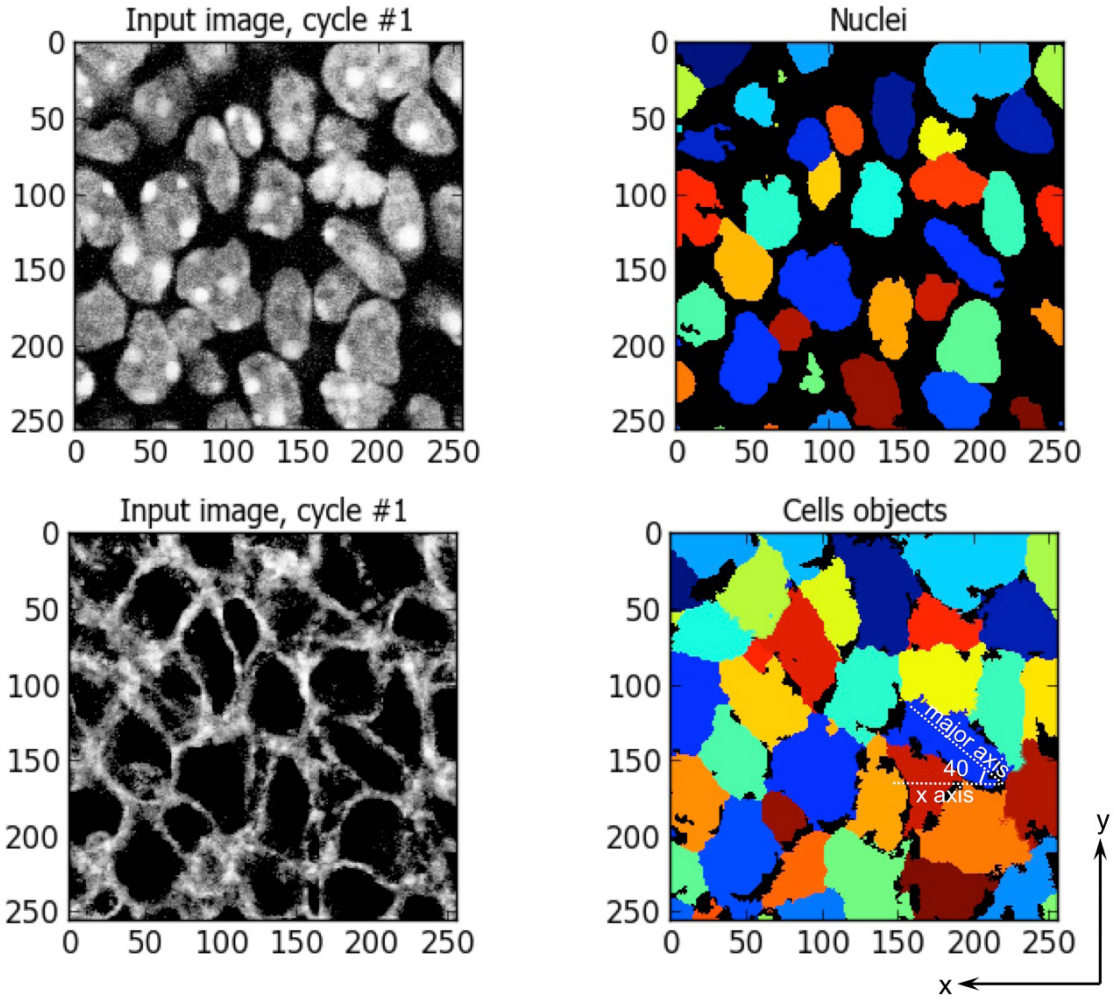

Measurement of cell shape and orientation. Illustration of cell morphology recognized by CellProfiler software. The nucleus of the cell (DAPI or Sox9 staining) was first recognized and imposed to the cell membrane (β-catenin staining) for generation of cell object, which will be subjected to cell shape and orientation analysis by CellProfiler. The orientation is determined by the angle between the x axis and the major axis (indicated by dotted line) of the identified object.